

TURUN YLIOPISTON JULKAISUJA
ANNALES UNIVERSITATIS TURKUENSIS

SARJA - SER. D OSA - TOM. 1030

MEDICA - ODONTOLOGICA

DETECTION OF THE VULNERABLE ATHEROSCLEROTIC PLAQUE

**PRE-CLINICAL EVALUATION OF NOVEL PET IMAGING
PROBES WITH EXPERIMENTAL MODELS**

by

Johanna Silvola née Haukkala

TURUN YLIOPISTO
UNIVERSITY OF TURKU
Turku 2012

From the Department of Clinical Physiology and Nuclear Medicine and Turku PET Centre, University of Turku, Turku, Finland

Supervised by

Professor Juhani Knuuti, MD, PhD
Turku PET Centre
University of Turku
Turku, Finland

and

Professor Anne Roivainen, PhD
Turku PET Centre and Turku Centre for Disease Modelling
University of Turku
Turku, Finland

Reviewed by

Assistant Professor Matthias Nahrendorf, MD, PhD
Massachusetts General Hospital
Center for Systems Biology
Boston, USA

and

Adjunct Professor Kirsi Timonen, PhD
Department of Clinical Physiology and Nuclear Medicine
University of Eastern Finland
Kuopio, Finland

Dissertation opponent

Adjunct Professor Kim Bergström, PhD
Centre for Drug Research
Faculty of Pharmacy
University of Helsinki
Helsinki, Finland

ISBN 978-951-29-5121-5 (PRINT)

ISBN 978-951-29-5122-2 (PDF)

ISSN 0355-9483

Painosalama Oy - Turku, Finland 2012

To Antti and Aida

ABSTRACT

Johanna Silvola née Haukkala

DETECTION OF THE VULNERABLE ATHEROSCLEROTIC PLAQUE

Pre-Clinical Evaluation of Novel PET Imaging Probes With Experimental Models

From the Department of Clinical Physiology and Nuclear Medicine, Turku PET Centre, Turku University Hospital, University of Turku, Turku, Finland

Atherosclerosis is a life-long vascular inflammatory disease and the leading cause of death in Finland and in other western societies. The development of atherosclerotic plaques is progressive and they form when lipids begin to accumulate in the vessel wall. This accumulation triggers the migration of inflammatory cells that is a hallmark of vascular inflammation. Often, this plaque will become unstable and form vulnerable plaque which may rupture causing thrombosis and in the worst case, causing myocardial infarction or stroke. Identification of these vulnerable plaques before they rupture could save lives. At present, in the clinic, there exists no appropriated, non-invasive method for their identification.

The aim of this thesis was to evaluate novel positron emission tomography (PET) probes for the detection of vulnerable atherosclerotic plaques and to characterize, two mouse models of atherosclerosis. These studies were performed by using *ex vivo* and *in vivo* imaging modalities. The vulnerability of atherosclerotic plaques was evaluated as expression of active inflammatory cells, namely macrophages.

Age and the duration of high-fat diet had a drastic impact on the development of atherosclerotic plaques in mice. In imaging of atherosclerosis, 6-month-old mice, kept on high-fat diet for 4 months, showed matured, metabolically active, atherosclerotic plaques. [¹⁸F]FDG and ⁶⁸Ga were accumulated in the areas representative of vulnerable plaques. However, the slow clearance of ⁶⁸Ga limits its use for the plaque imaging. The novel synthesized [⁶⁸Ga]DOTA-RGD and [¹⁸F]EF5 tracers demonstrated efficient uptake in plaques as compared to the healthy vessel wall, but the pharmacokinetic properties of these tracers were not optimal in used models.

In conclusion, these studies resulted in the identification of new strategies for the assessment of plaque stability and mouse models of atherosclerosis which could be used for plaque imaging. In the used probe panel, [¹⁸F]FDG was the best tracer for plaque imaging. However, further studies are warranted to clarify the applicability of [¹⁸F]EF5 and [⁶⁸Ga]DOTA-RGD for imaging of atherosclerosis with other experimental models.

Keywords: atherosclerosis, inflammation, *in vivo* imaging, positron emission tomography (PET)

TIIVISTELMÄ

Johanna Silvola o.s. Haukkala

HAURAAAN ATEROSKLEROOTTISEN PLAKIN HAVAITSEMINEN

Uusien PET-tutkimusaineiden prekliininen testaus

Kliinisen fysiologian ja isotooppilääketieteen oppiaine, Valtakunnallinen PET-keskus, Turun yliopistollinen keskussairaala, Kliininen laitos, Turun yliopisto

Ateroskleroosi on koko eliniän kestävä verisuonten tulehdussairaus ja yleisin kuoliinsy Suomessa ja muuallakin läntisessä yhteiskunnassa. Plakkien kehittyminen on jatkuvaa ja se alkaa rasvan kertymisellä verisuonen sisäpinnalle, mikä aiheuttaa verisuoniin tulehdusta ja valkosolujen kertymistä. Joskus muodostunut plakki kehittyi hauraaksi ja voi repeytyä aiheuttaen verisuonta tukkivan hyytyvän muodostumisen ja pahimmillaan sydän- tai aivoinfarktin. Hauraan plakin havaitseminen ennen sen repeytymistä olisi tärkeää, mutta tällä hetkellä sopivaa ei-kajoavaa menetelmää ole kliinisesti käytössä.

Tämän väitöskirjatutkimuksen tarkoitukseni oli arvioida uusien positroniemissiotomografiassa (PET) käytettävien tutkimusaineiden soveltuvuutta tunnistaa hauraat plakit ja karakterisoida kaksi tutkimuksessa käytettyä ateroskleroottista hiirimallia. Tutkimuksen suoritettiin käyttäen *ex vivo* ja *in vivo* kuvantamistekniikoita. Plakin haurauden mittarina käytettiin aktiivisten tulehdussolujen (makrofagien) esiintymistä plakeissa.

Tutkittavien hiirten iällä ja rasvaisen ruokavalion kestolla oli suuri vaikutus ateroskleroottisten plakkien kehittymiselle. Sopivin malli ateroskleroosin kuvantamiselle on kuusi kuukautta vanha hiiri, joka on ollut rasvaisella ruokavaliolla neljä kuukautta. [¹⁸F]FDG ja ⁶⁸Ga kerääntyivät merkittävästi hauraisiin plakkeihin. ⁶⁸Ga:n erittäin hidas puhdistuma verenkierrosta rajoittaa kuitenkin tämän käyttöä plakkikuvantamisessa. Uudet [⁶⁸Ga]DOTA-RGD ja [¹⁸F]EF5 merkkiaineet kertyivät myös merkittävästi plakkiin verrattaessa kertymää terveeseen verisuonen seinämään, mutta näiden merkkiaineiden farmakokineettiset ominaisuudet kuvantamiselle eivät olleet parhaat mahdolliset tutkituissa malleissa.

Yhteenvedon voidaan todeta, että tutkimuksessa onnistuttiin havaitsemaan kuvantamiselle ideaalinen tilanne hiirimalleissa. Testatuista tutkimusaineista, [¹⁸F]FDG osoittautui soveliaimmaksi plakkikuvantamiseen. [¹⁸F]EF5 ja [⁶⁸Ga]DOTA-RGD tutkimusaineiden testausta muilla ateroskleroosi eläinmalleilla tulisi harkita.

Avainsanat: ateroskleroosi, *in vivo* kuvantaminen, positroniemissiotomografia (PET), tulehdus

TABLE OF CONTENTS

ABSTRACT.....	4
TIIVISTELMÄ	5
TABLE OF CONTENTS.....	6
ABBREVIATIONS	8
LIST OF ORIGINAL PUBLICATIONS	10
1 INTRODUCTION	11
2 REVIEW OF THE LITERATURE.....	12
2.1 Atherosclerosis	12
2.2 Development of atherosclerotic plaque	12
2.3 Molecular imaging of the atherosclerotic plaques	15
2.3.1 Metabolic activity.....	16
2.3.2 Monocytes/macrophages.....	17
2.3.3 LDL, oxLDL and LOX-1	19
2.3.4 Angiogenesis	19
2.3.5 Hypoxia.....	20
2.3.6 Apoptosis.....	20
2.3.7 Matrix degradation	21
2.3.8 Thrombotic markers	21
2.3.9 Other targets	21
2.4 Mouse models of atherosclerosis.....	24
2.4.1 ApoE ^{-/-}	24
2.4.2 LDLR ^{-/-}	24
2.4.3 ApoB ^{100/100}	25
2.4.4 LDLR ^{-/-} ApoB ^{100/100}	25
2.4.5 IGF-II/LDLR ^{-/-} ApoB ^{100/100}	25
3 AIMS OF THE STUDY.....	26
4 MATERIALS AND METHODS.....	27
4.1 General study design	27
4.2 Experimental animals	27
4.3 Radiotracers.....	29
4.4 <i>Ex vivo</i> biodistribution	31
4.5 <i>Ex vivo</i> aorta autoradiography and image analysis.....	32
4.6 Immunohistochemistry	34
4.7 <i>In vivo</i> PET/CT imaging (I, II).....	35
4.8 Statistical analyses.....	36

5	RESULTS	37
5.1	Characterization of atherosclerotic plaques	37
5.1.1	Determination of plaque inflammation and size	37
5.1.2	Verification of plaque hypoxia (IV)	37
5.2	<i>Ex vivo</i> biodistribution of radiotracers in mice.....	38
5.3	<i>In vivo</i> biodistribution of radiotracers in aorta (I, II).....	40
5.4	Digital autoradiography of aortic sections	41
5.4.1	Distribution of radiotracers	41
5.4.2	Co-localization of tracer uptake and plaque inflammation	43
5.4.3	Reproducibility of ARG method (III)	44
6	DISCUSSION	45
6.1	Characterization of the animal models of atherosclerosis	45
6.2	Evaluation of radiotracers for imaging of atherosclerotic plaques.....	46
6.2.1	[¹⁸ F]FDG.....	46
6.2.2	⁶⁸ Ga.....	47
6.2.3	[⁶⁸ Ga]DOTA-RGD.....	48
6.2.4	[¹⁸ F]EF5.....	49
6.3	Potential limitations.....	50
6.4	Future aspects	52
7	SUMMARY AND CONCLUSIONS.....	54
8	ACKNOWLEDGEMENTS	55
9	REFERENCES	57
10	ORIGINAL PUBLICATIONS.....	67

ABBREVIATIONS

%ID/g	Percentage of injected dose per gram of tissue
%IA/g	Percentage of injected radioactivity per gram of tissue (means same as %ID/g)
[¹⁸ F]FDG	2-[¹⁸ F]-Fluoro-2-deoxy-D-glucose
[¹⁸ F]EF5	2-(2-nitro-1H-imidazol-1-yl)-N-(2,2,3,3,3-pentafluoropropyl)-acetamide labelled with ¹⁸ F-fluorine
⁶⁸ Ga	⁶⁸ Gallium
[⁶⁸ Ga]DOTA-RGD	[⁶⁸ Ga]DOTA-(monomeric Arg-Gly-Asp-Dphe-Val-)
ADP	Adenosine diphosphate
AHA	American Heart Association
APOBEC-1	Apolipoprotein B mRNA editing enzyme, catalytic polypeptide-1
ApoB	Apolipoprotein B
ApoE	Apolipoprotein E
ARG	Autoradiography
ASON	Antisense oligonucleotide
ATP	Adenosine triphosphate
CCR-2	C-chemokine receptor type 2
CETP	Cholesterol ester transfer protein
CT	Computed tomography
DOTA	1,4,7,10-tetraazacyclododecane-1,4,7,10-tetraacetic acid
EC	Endothelial cell
ELK3-51	EF5 specific monoclonal antibody
FH	Familial hypercholesterolemia
FR	Folate receptor
G6Pase	Glucose-6-phosphatase
GLUT-1	Glucose transporter 1
HDL	High density lipoprotein
HE	Hematoxylin and eosin
HIF-1	Hypoxia-inducible transcription factor 1
HK	Hexokinase
HPLC	High-performance liquid chromatography
IA	Injected (radio)activity
ICAM-1	Inter-cellular adhesion molecule 1
ID	Injected dose
IDL	Intermediate density lipoprotein
IGF-II	Insulin growth factor II
IGF-II/LDRL ^{-/-} -ApoB ^{100/100}	Genetically engineered mouse deficient for LDLR, expressing only ApoB100-form and over-expressing IGF-II
IL	Interleukin

IMR	Intima-to-media ratio
i.v.	Intravenous(ly)
IVUS	Intravascular ultrasound
LDL	Low density lipoprotein
LDLR	Low density lipoprotein receptor
LDLR ^{-/-} ApoB ^{100/100}	Genetically engineered mouse deficient for LDLR and expressing only ApoB100-form (deficient for ApoB48)
LDLR/ApoB48	same as LDLR ^{-/-} ApoB ^{100/100}
LOX-1	Lectin-like oxidised LDL receptor 1
Mac-3	Mouse cluster of differentiation (CD)107b
MCP-1	Monocyte chemotactic protein 1
MI	Myocardial infarction
MMP	Matrix metalloproteinase
MPI	Matrix metalloproteinase inhibitor
MRI	Magnetic resonance imaging
NO	Nitric oxide
NP	Natriuretic peptide
OCT	Optical coherence tomography
oxLDL	Oxidized low density lipoprotein
PBR	Peripheral benzodiazepine receptor
PET	Positron emission tomography
PS	Phosphatidylserine
RAGE	Receptor for advanced glycation endproducts
PIT	Pathological intima thickening
RGD	Arginine (R), glycine (G), aspartate (D) motif
ROI	Region of interest
PSL/mm ²	Photostimulated luminescence per square millimeter
RT	Room temperature
SD	Standard deviation
SHAPE	Society for Heart Attack Prevention and Eradication
SMC	Smooth muscle cell
SPECT	Single photon emission computed tomography
SR	Scavenger receptor
SSTR ₂	Somatostatin receptor of subtype 2
TNF- α	Tumour necrosis factor alpha
VCAM-1	Vascular cell adhesion molecule 1
VEGF	Vascular endothelial growth factor
VLDL	Very low density lipoprotein

LIST OF ORIGINAL PUBLICATIONS

This dissertation is based on the following original publications which are referred to in the text by the corresponding Roman numerals, I-IV.

- I. Silvola JMU, Saraste A, Laitinen I, Savisto N, Laine VJO, Heinonen SE, Ylä-Herttuala S, Saukko P, Nuutila P, Roivainen A, Knuuti J. Effects of age, diet, and type 2 diabetes on the development and FDG uptake of atherosclerotic plaques. *J Am Coll Cardiol Imaging*. 2011 Dec 4(12): 1294-1301.
- II. Silvola JMU, Laitinen I, Sipilä HJ, Laine VJO, Leppänen P, Ylä-Herttuala S, Knuuti J, Roivainen A. Uptake of ⁶⁸Gallium in atherosclerotic plaques in LDLR^{-/-} ApoB^{100/100} mice. *EJNMMI Res*. 2011 Aug 17;1(1):14.
- III. Haukkala J, Laitinen I, Luoto P, Iveson P, Wilson I, Karlsen H, Cuthbertson A, Laine J, Leppänen P, Ylä-Herttuala S, Knuuti J, Roivainen A. ⁶⁸Ga-DOTA-RGD peptide: biodistribution and binding into atherosclerotic plaques in mice. *Eur J Nucl Med Mol Imaging*. 2009 Jul 36:2058-2067.
- IV. Silvola JMU, Saraste A, Forsback S, Laine VJO, Saukko P, Heinonen SE, Ylä-Herttuala S, Roivainen A, Knuuti J. Detection of hypoxia by [¹⁸F]EF5 in atherosclerotic plaques in mice. *Arterioscler Thromb Vasc Biol*. 2011 May 31(5); 1011-5.

The original publications have been reprinted with the permission of the copyright holders.

1 INTRODUCTION

Atherosclerosis is a vascular inflammation disease which is the major cause of myocardial infarction (MI), stroke, and ischemic gangrene. These result from acute thrombus formation on the surface of a plaque (Hellings et al. 2007). The majority of cardiovascular events occur in asymptomatic subjects classified as low to intermediate risk by current assessment algorithms such as family history, hypercholesterolemia, hypertension, obesity, and smoking. An extensive body of experimental work, as well as a histopathological and clinical data, indicate that immune responses lead to chronic inflammation and this process is integral to the pathogenesis of atherosclerosis. Inflammation modulates lesion initiation, progression, and vulnerability to rupture. (Roger et al. 2012; Packard et al. 2008; Hansson and Libby 2006) Atherosclerotic plaques containing a large number of macrophages are more vulnerable than plaques containing only few macrophages (Narula et al. 2008; Jaffer et al. 2006a). Moreover, hypoxia is considered to be an important factor in plaque rupture (Hulten and Levin 2009). However, the degree of arterial stenosis is weakly correlated to plaque vulnerability (Ambrose et al. 1998). The identification of subjects at risk for cardiovascular events cannot rely solely on the assessment of anatomical severity of vascular stenosis.

Attention should be directed at the evaluation of plaque characteristics and biological processes that determine their vulnerability. Various methods, including ultrasound, multislice computed tomography (CT), magnetic resonance imaging (MRI), single photon emission computed tomography (SPECT), intravascular ultrasound (IVUS), optical coherence tomography (OCT), and others, are being evaluated to detect vulnerable atherosclerotic plaques. However, many of these modalities are invasive or yield inadequate spatial resolution. Non-invasive positron emission tomography (PET) imaging of inflammation or hypoxia in plaques may provide a useful tool to predict risk of plaque rupture and to allow monitoring of anti-atherosclerotic drugs for prevention of the acute cardiovascular events.

Enhanced imaging techniques may detect additional characteristics of plaques and novel predictive models may improve the assessment of plaque vulnerability in patients. To discover these new and improved techniques, experimental animal models are needed. Mouse models of atherosclerosis are criticized because spontaneous plaque rupture is rare. However, the development of mouse plaques has more similarities than differences as compared to humans. The model must be selected according to the nature of plaques which is influenced by many factors such as the age of mouse or the use of high-fat diet, which is generally always used to induce plaque development. The major aim of this thesis was to characterize two mouse models of atherosclerosis for the pre-clinical evaluation of PET imaging agents [^{18}F]FDG, ^{68}Ga , [^{68}Ga]DOTA-RGD, and [^{18}F -EF5] in order to detect vulnerable atherosclerotic plaques.

2 REVIEW OF THE LITERATURE

2.1 Atherosclerosis

Atherosclerosis begins in childhood and develops gradually. Over time, atheromas and advanced atherosclerotic lesions are formed and matured. Atherosclerosis is characterized by inflammation, the thickening of the vascular wall due to the accumulation of lipids in the intima, cell death and fibrosis. (Hansson et al. 2009; Hansson and Libby 2006) In the coronaries, atherosclerosis can lead to myocardial infarction and heart failure, whereas in the arteries that perfuse the brain, it can lead to transient ischemic attacks or stroke. Depending on which arteries atherosclerosis is affecting, it can also result in hypertension, renal impairment, abdominal aortic aneurysms or limb ischemia. (Hansson and Libby 2006)

Plaques in arteries may cause flow-limited stenosis which can lead to clinical complications. However, the most severe clinical events are commonly caused by the rupture of a plaque, exposing the pro-thrombotic material in the plaque to the blood circulation, and causing sudden thrombotic occlusion at the site of artery disruption. This rupture prone plaque is generally called a vulnerable plaque. Typically, such a vulnerable plaque may not cause severe stenosis but it contains a large lipid core and a thin fibrous cap that is often infiltrated by inflammatory cells, particularly at the plaque's shoulder areas. (Hansson and Libby 2006; Davies et al. 1993) Most deaths are caused by thrombotic occlusion of a single plaque. A simultaneous occurrence of two occlusive thrombus is rare but a second vulnerable plaque is common. (Madjid et al. 2004) The thickness of the intimal layer activates the endothelium to express leukocyte adhesion molecules and chemokines that promote recruitment of monocytes and T cells leading to intense immunological activity (Hansson et al. 2009; Hansson and Libby 2006).

2.2 Development of atherosclerotic plaque

Lesion initiation and intimal xanthomata

Atherosclerosis is a progressive disease, which begins in a childhood. Already in the first 6 months of life, about one-half of infants, have signs of atherosclerosis (Stary 2000). Early atherosclerotic lesions, known as intimal xanthomata or initial lesion or fatty streak, consist of subendothelial accumulations of cholesterol-filled macrophages (foam cells). In humans, such lesions are found in the aorta in the first decade, in the coronary arteries in the second decade, and in the cerebral arteries in the third or fourth decades of life (Lusis 2000). Due to differences in blood flow dynamics, curvatures and bifurcations of the arteries are susceptible to increased permeability of cholesterol rich macromolecules, such as low density lipoprotein (LDL) and are preferential sites for lesion formation. The initial events surrounding lipid accumulation is unclear. Elevated

levels of plasma cholesterol, endothelial dysfunction, and inflammation play a role in disease progression. (Lusis 2000; Gimbrone et al. 1999) After LDL accumulates in the intima, it undergoes modifications, like oxidation, lipolysis, proteolysis and aggregation. Oxidized LDL (oxLDL) induces foam cell formation and enhances inflammation by stimulating the overlying endothelial cells (ECs) to produce pro-inflammatory molecules. Oxidized LDL can also inhibit the production of nitric oxide (NO) which is an anti-atherogenic mediator of vasorelaxation. (Lusis 2000) The initial inflammatory reaction at the vessel wall begins when the endothelium expresses adhesion molecules, such as vascular cell adhesion molecule 1 (VCAM-1), P- and E-selectin or inter-cellular adhesion molecule 1 (ICAM-1). These factors recruit leucocytes into the arterial wall. This process is primarily mediated by cytokines like tumour necrosis factor alpha (TNF- α), interleukins (ILs), monocyte chemoattractant protein 1 (MCP-1) which are proteins produced by inflammatory cells, such as macrophages, mast cells, dendritic cells and lymphocytes. (Moore and Tabas 2011; Sun et al. 2007; Stefanadis et al. 2001; Lusis 2000; Li et al. 1993) After internalization, monocytes mature into macrophages and uptake oxidized or otherwise modified LDL particles, leading to foam-cell formation. The most important mediators in this event are scavenger receptors, like SR-A and CD36, which are expressed by macrophages. (Lusis 2000) The lesion in the intima, containing lipid loaded foam cells, is called an intimal xanthomate, fatty streak, or a type I or II lesion as classified by the American Heart Association (Virmani et al. 2000). Fatty streaks are not clinically significant but can progress into mature atherosclerotic plaques or disappear over time (Hansson and Libby 2006).

Pathologic intimal thickening and fibroatheroma

Pathologic intimal thickening (PIT) constitutes the earliest atherosclerotic change and is characterized by the infiltration of smooth muscle cells (SMCs). The entrapment and death of atherosclerotic macrophages is thought to be responsible for the conversion of PIT into an early fibroatheroma. Cytokines produced by internalized leukocytes, promote the release of growth factors which lead to the development of an extracellular matrix, hypertrophy, and hyperplasia of SMCs. SMCs start to produce collagen, elastin and other matrix components and eventually a fibrous cap is formed. The combination of dense macrophage infiltration and apoptosis, together with hypoxia-induced necrosis, promotes the development of mature plaques. Macrophages and other plaque-related cells also release matrix degrading proteases, called matrix metalloproteinases (MMPs), which are pro-inflammatory substances. MMPs initiate the degradation of fibrillar collagen leading to vulnerability of the atherosclerotic plaque. (Stefanadis et al. 2001; Williams and Tabas 1998) In the plaque, apoptotic and necrotic cell death provoke further inflammation. Hypoxic or inflammatory cell infiltration is thought to promote neovascularisation. This permits extravasation of erythrocytes into the plaque further contributing to the enlargement of necrotic core. Moreover, small deposits of calcifications can occur in plaques, similar to bone formation. A fibroatheroma (type III) is a fibrous cap consisting of SMCs and collagen-rich matrix that encloses a lipid-rich core. These types of lesions are common in adolescence and young adulthood. (Virmani et al. 2005; Lusis et al. 2000; Virmani et al. 2000; Fuster et al. 1992)

Thin cap fibroatheroma, plaque rupture, and healing

The thin, fibrous cap is distinguished from the earlier fibroatheroma by the loss of SMCs, extracellular matrix, and inflammatory infiltrate. A significant factor that leads to the progression of fibroatheroma to a thin cap fibroatheroma, also called advanced lesion, vulnerable plaque or type IV lesion, is inflammation. These vulnerable plaques generally have a thin fibrous cap and increased number of inflammatory cells, which produces proteases, and inhibit the production of matrix by SMCs. (Libby and Theroux 2005; Lusis 2000) The development of microvascular channels, as a result of neovascularisation, is also a common feature of this type of plaque. The new blood vessels, which are fragile and are prone to micro-haemorrhage, form a small thrombus in the lesion, and have a nutritive function promoting plaque growth. (Libby 2002; Virmani et al. 2000)

The molecular changes in the plaque and the thickening of a cap, can render it friable and susceptible to rupture. Platelets are activated by thrombin and a thrombus is formed. Plaque ruptures are found in 60% of individuals dying suddenly with luminal thrombi. (Virmani et al. 2000) The pathology of ruptured plaques is markedly heterogenous, but these plaques (type V) typically have a dense core of free cholesterol, necrotic foam cells, cholesterol crystals, hyalinized hemorrhage, calcification, angiogenesis and inflammation (Virmani et al. 2005; Madjid et al. 2004). The classification of atherosclerotic plaques is presented in Table 1 and the progression of an atherosclerotic plaque is presented in Figure 1.

Table 1. Classification of atherosclerotic plaques based on morphological description.

	Description	Thrombosis
Non-atherosclerotic intimal lesions		
Intimal xanthomate (Fatty streak, Type I or II)	Superficial accumulation of foam cells without a necrotic core or fibrous cap	Absent
Progressive atherosclerotic lesions		
Pathological intimal thickening	SMC-rich plaque with proteoglycan-rich matrix and focal accumulation of lipids without necrosis.	Absent
Fibroatheroma (Type III)	Well-formed necrotic core with an overlying fibrous cap.	Absent
Thin cap fibroatheroma (Type IV)	A thin fibrous cap infiltrated by macrophages lymphocytes with rare or absent SMCs and a relatively dense underlying necrotic core. Intraplaque hemorrhage may be presented.	Absent
Plaque rupture (Type V)	Fibroatheroma with fibrous cap disruption. Luminal thrombus communicates with the underlying necrotic core	Occlusive or non-occlusive

Modified from Virmani et al. 2000.

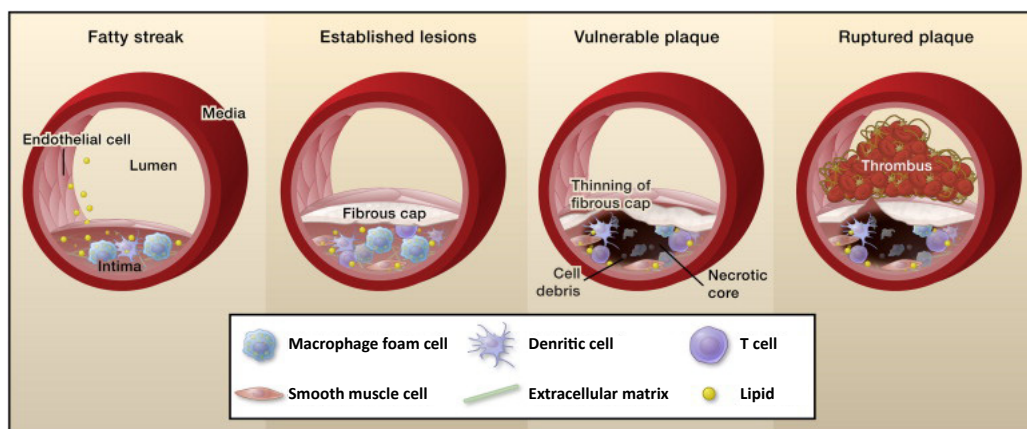


Figure 1. Progression of an atherosclerotic plaque. Early fatty streak lesions are characterized by the accumulation of lipids in the subendothelial space, which incites the recruitment of macrophages, mast cells, dendritic cells and lymphocytes. As the atherosclerotic lesion progresses, smooth muscle cells infiltrate the intima, and lipid retention is amplified. Vulnerable plaques are characterized by the accumulation of macrophages and the lipid-filled necrotic core. A thinning fibrous cap decreases lesion stability, making these atherosclerotic plaques susceptible to rupture and the formation of a thrombus. (Modified from Moore and Tabas 2011)

2.3 Molecular imaging of the atherosclerotic plaques

Traditional imaging of atherosclerotic plaque is based on detection of changes in its morphology and physiological features. Morphological characteristics are related to the anatomical changes of the arterial wall, like lumen diameter, area, and remodeling of vessel wall. For physiological assessment, measurements of blood flow or contractile function are required. However, a technique to assess these are unavailable and typical imaging techniques are invasive. Molecular imaging is a rapidly growing discipline aimed at the non-invasive visualization and characterization of cellular and biomolecular functions. (Saraste et al. 2009; Stefanadis et al. 2001)

PET will play an increasingly important role in early *in vivo* disease detection and improved therapeutic decision making in cardiovascular diseases. Clinical PET scanners have a spatial resolution of 2-4-mm and in a small-animal scanner even below 1-mm. However, the main feature of PET imaging is a very high molecular sensitivity. PET is based on the use of molecular probes or biomarkers in very low concentrations to detect biological processes without disturbing their function. The probe is labelled with a short-living positron emitting radionuclide which can be produced by cyclotron or generator. To achieve images with high target-to-background ratio, the probe should include high binding efficacy, optimal pharmacokinetic properties, and specificity combined with lack of toxicity and feasibility of synthesis. (Saraste et al. 2009) SPECT is based on the use of gamma emitters and is another molecular imaging method used for imaging of vulnerable atherosclerotic plaques. As compared to PET, SPECT has better availability with a large number of clinical scanners but the limited spatial resolution (7-10-mm of clinical scanners) makes this method less attractive for use in small targets such as imaging of

atherosclerotic plaque. (Brindle et al. 2008) A wide range of probes for PET (fluorine-18, ^{18}F ; carbon-11, ^{11}C ; copper-64, ^{64}Cu ; gallium-68, ^{68}Ga) and for SPECT (technetium-99m, $^{99\text{m}}\text{Tc}$; indium-111, ^{111}In ; iodine-125, ^{125}I ; iodine-123, ^{123}I) has been used to detect vulnerable atherosclerotic plaques. The summary of these studies are present in Table 2.

2.3.1 Metabolic activity

Several studies in human or animal atherosclerotic lesions show that inflammatory cells in plaques mainly originate from blood-born monocytes subsequently differentiated into macrophages (Fan and Watanabe 2003). Macrophages express pro-inflammatory and chemotactic molecules thus playing an essential role in the formation, progression, and pathogenicity of atherosclerotic plaques. Macrophage-rich plaques are more vulnerable to rupture than plaques with a few macrophages (Narula et al. 2008; Jaffer et al. 2006a), which make macrophages and their metabolism, a potential target for imaging of plaque vulnerability.

Glucose metabolism

The most widely used PET tracer for targeting the metabolic activity of inflammatory cells, like macrophages, is a ^{18}F -labelled glucose analog 2-fluoro-2-deoxy-D-glucose (^{18}F FDG). ^{18}F FDG is distributed and transported into the cell like glucose but is trapped inside the cell because of the chemical modification of second hydroxyl group. Several studies have proved that, ^{18}F FDG PET is capable to detect inflamed atherosclerotic plaques in human aorta and carotids (Masteling et al. 2011; Menezes et al. 2011; Rudd et al. 2009; Tawakol et al. 2006; Tawakol et al. 2005; Ogawa et al. 2004; Rudd et al. 2002), in experimental model of rabbit (Worthley et al. 2009; Calcagno et al. 2008; Zhang et al. 2006) and in mouse model of atherosclerosis (Zhao et al. 2011; Laitinen et al. 2006). The reduced ^{18}F FDG uptake in atherosclerotic plaque was reported by Laurberg and co-workers (Laurberg et al. 2007) but this study remains controversial. Histological analysis shows that ^{18}F FDG accumulation in atherosclerotic lesions is associated with the degree of macrophage infiltration in humans (Menezes et al. 2011; Tawakol et al. 2006; Rudd et al. 2002) and in experimental models (Zhao et al. 2011; Laitinen et al. 2006). It is accepted that ^{18}F FDG PET carotid imaging is a sensitive and reproducible method to detect plaque inflammation. PET imaging with ^{18}F FDG has also been demonstrated in human coronaries (Wykrzykowska et al. 2009; Alexanderson et al. 2008) but assessment of coronary arteries is challenging because of the myocardial uptake of the ^{18}F FDG and continuous motion of coronary vessels. Recently, we have reported a potential respiratory and cardiac dual-gated method with diet intervention for visualization of focal ^{18}F FDG accumulation in coronary plaques in patients with acute coronary syndromes (Lankinen et al. 2011).

Choline metabolism

Another approach for imaging metabolic activity in atherosclerotic plaques is choline derivatives which are based on increased activity of choline transporters in macrophages. Increased choline uptake occurs in activated macrophages (Boggs et al. 1995). Matter and colleagues have reported choline derivative ^{18}F fluoromethylcholine (^{18}F FCH) uptake in

plaques of apolipoprotein E deficient (ApoE^{-/-}) mice and has correlated this to macrophage content. They also demonstrated greater [¹⁸F]FCH uptake compared to the uptake of [¹⁴C]FDG in the same plaques. However, non-specific [¹⁸F]FCH uptake was detected in metabolically active tissues like liver and myocardium. (Matter et al. 2005) More recently, we have reported uptake of [¹¹C]choline in plaques of LDLR^{-/-}ApoB^{100/100} mice (Laitinen et al. 2010). The clinical feasibility of [¹⁸F]FCH (Bucerius et al. 2008) and [¹¹C]choline (Kato et al. 2009) for detecting atherosclerotic plaques is promising. The uptake of choline and choline derivatives in myocardium is less than that of [¹⁸F]FDG (Kato et al. 2009; Roivainen et al. 2006) but further evidence validating these derivatives are necessary.

2.3.2 Monocytes/macrophages

CCR-2

Activated macrophages can be detected via specific probes. Monocyte chemoattractant protein-1 (MCP-1) is produced by endothelial cells, SMCs, and monocytes/macrophages during atherosclerotic plaque formation. MCP-1 binds to the C-chemokine receptor type 2 (CCR-2) which is expressed on the cellular membrane of monocytes/macrophages. (Kinlay et al. 2001) ^{99m}Tc- and ¹²⁵I-labelled MCP-1 was evaluated for molecular imaging in a rabbit model of atherosclerosis (Hartung et al. 2007; Ohtsuki et al. 2001). It seems that MCP-1 is a potential target for imaging of plaque vulnerability.

PBR/TSPO

Activated macrophages express peripheral benzodiazepine receptors (PBR) (Jones et al. 2002), also called 18 kDa translocator protein (TSPO). The PBR/TSPO targeted PET tracer [¹¹C]PK11195 has been tested for imaging atherosclerotic macrophages in LDLR^{-/-}ApoB^{100/100} mice (Laitinen et al. 2008), and in human carotid plaques (Gaemperli et al. 2011; Pugliese et al. 2010; Hoppela et al. 2007). [¹¹C]PK11195 enables non-invasive imaging of vascular inflammation. However, significant binding occurs in the healthy vessel wall corresponding with PBR/TSPO expression. The longer-lived radiotracers targeting peripheral benzodiazepine receptors are being tested for clinical applications (Pugliese et al. 2010).

RAGE

The receptor for advanced glycation endproducts (RAGE) is implicated in the development and progression of atherosclerosis. The ^{99m}Tc-labelled anti-RAGE F(ab')₂ probe is used to image atherosclerotic lesions in ApoE^{-/-} mice. These data demonstrate the feasibility of non-invasively imaging of RAGE in atherosclerotic lesions in a murine model and confirm to levels of RAGE expression sufficient to allow detection via *in vivo* imaging. (Tekabe et al. 2008)

FR

A folate receptor (FR) is expressed on the surface of activated macrophages but is absent from other immune cells and resting macrophages. FR-targeted imaging agents are

used in the imaging of inflammation in a variety of diseases, in animals and humans. (Xia et al. 2009; Matteson et al. 2009; Turk et al. 2002) Recently, a folate-targeted radiopharmaceutical, [^{99m}Tc]EC20, is compatible for imaging murine atherosclerotic lesions at the sites of macrophage accumulation (Ayala-López et al. 2010).

IL-2

Interleukin-2 (IL-2) is a cytokine, which binds to its receptor (IL2R), expressed mainly on activated T-cells and macrophages. Recently, Opalinska and co-workers (Opalinska et al. 2012) tested [^{99m}Tc]-HYNIC-IL-2 to detect vulnerable atherosclerotic plaques in humans and found a correlation between tracer uptake in carotid plaques and serum concentration of cardiovascular risk markers. Annovazzi and co-workers investigated [^{99m}Tc]IL-2 uptake in atherosclerotic plaques in humans and found the correlation between the tracer accumulation in plaques and the amount of IL2R-positive cells. However, IL2Rs is also expressed by SMCs, which may limit the use of [^{99m}Tc]IL-2 in plaque imaging. (Annovazzi et al. 2006)

SSTR₂

Somatostatin receptor of subtype 2 (SSTR₂) is expressed by macrophages (Armani et al. 2007). Rominger and co-workers evaluated the PET ligand targeting SSTR₂ [^{68}Ga]-[1,4,7,10-tetrazacyclododecane-*N,N,N'',N'''*-tetraacetic acid) - D - Phe¹, Tyr³-octreotate (DOTATATE) to detect atherosclerotic plaques in the human coronary arteries. As result, the [^{68}Ga]DOTATATE uptake was significantly correlated with plaque calcification. (Rominger et al. 2010)

Phagocytosis

A variety of labelled carbohydrate and nanoparticles can be used to detect macrophages based on their active internalization and intracellular trapping into phagocytic cells (Jaffer et al. 2006b; Ruehm et al. 2001; Schmitz et al. 2000). *In vivo* PET imaging of macrophages with a ^{64}Cu -labelled trireporter nanoparticle ([^{64}Cu]TNP) can detect inflammation in atherosclerotic aortas of ApoE^{-/-} mice (Nahrendorf et al. 2008). Also, PET-CT imaging with ^{18}F -labelled nanoparticles can quantitate macrophage content in mouse model of aortic aneurysms (Nahrendorf et al. 2011). Further studies for imaging plaque vulnerability are warranted.

Trafficking

Kircher and co-workers injected, *in vitro* prepared [^{111}In]Oxine monocytes into atherosclerotic ApoE^{-/-} mice to track plaque specific macrophages by *in vivo* imaging. The focal hotspot in the aorta was detected with an excellent correlation between the *in vivo* signal and the macrophage content. This demonstrates an effective approach to detect vulnerable atherosclerotic plaques. (Kircher et al. 2008)

VCAM-1

Vascular cell adhesion molecule-1 (VCAM-1) has a major role in the recruitment of inflammatory cells in developing atherosclerotic plaques (Ley and Huo 2001). [^{123}I]

B2702-p and [^{99m}Tc]B2702-p peptides targeting VCAM-1 were tested in experimental atherosclerotic rabbit models. These tracers have potential for molecular imaging of VCAM-1 in atherosclerosis, but *in vivo* studies are needed to prove that these tracers are specific and detect vulnerable plaques. (Broisat et al. 2007) The [^{18}F]4V peptide can be used to *in vivo* image VCAM-1 in ApoE $^{-/-}$ mice and correlates with VCAM-1 and CD68, a macrophage marker, expression levels (Nahrendorf et al. 2009).

2.3.3 LDL, oxLDL and LOX-1

Native LDLs and oxidized LDLs play an important role in the pathogenesis of development of atherosclerotic plaques. Direct radiolabelling of LDLs with ^{99m}Tc , ^{123}I , and ^{111}In (Bozóky et al. 2004; Rosen et al. 1990; Lees et al. 1988; Lees et al. 1983) can be synthesized. The inherent slow kinetics of LDL accumulation in arteries and blood clearance limits the use of LDL as a molecular vehicle for radiotracers. Several oxLDL targeted tracers were tested to detect vulnerable atherosclerotic plaques in animals and humans. [^{99m}Tc]oxLDLs has demonstrated improved tissue accumulation and more favorable blood clearance than radiolabelled native LDL in humans (Iuliano et al. 1996). Hardoff and colleagues performed *in vivo* and *ex vivo* imaging of plaques with a rabbit model by ^{123}I - and ^{125}I -labelled synthetic oligopeptide fragment of apolipoprotein B, SP-4 (Hardoff et al. 1993). The SP-4 was located in aortic lesions but the level of inflammation was not investigated. A few years later, the same group prepared a ^{99m}Tc -labelled form of the SP-4 peptide ([^{99m}Tc]P199) and found that [^{99m}Tc]P199 is better for *in vivo* imaging than [^{123}I]SP4 (Hardoff et al. 1995). Several studies have been carried out to image atherosclerotic plaques with a specific radiolabelled antibody against malondialdehyde-lysine epitopes (MDA-2), present on oxLDL and other oxidatively modified proteins but not on native LDL (Torzewski et al. 2004; Shaw et al. 2001a; Tsimikas et al. 2000, Tsimikas et al. 1999). Even though these probes seem to have the ability to detect atherosclerotic plaques, the slow blood clearance may limit their use in the clinic. Lectin-like, oxidized low density lipoprotein receptor 1 (LOX-1) is a cell surface receptor for oxLDL and may function in vascular cell dysfunction related to plaque instability (Sawamura et al. 1997). Two studies have demonstrated *in vivo* imaging of atherosclerotic plaques by LOX-1 antibodies in experimental atherosclerotic models. (Li et al. 2010; Ishino et al. 2008) Both studies showed that LOX-1 can be used as a target for molecular imaging of atherosclerotic plaques and may be useful for predicting atheromas with high risk to rupture.

2.3.4 Angiogenesis

A potential marker for the targeting of angiogenesis in atherosclerotic lesions is alpha-v-beta-3 ($\alpha_v\beta_3$) integrin, a cell surface glycoprotein receptor, highly expressed by macrophages, medial and some intimal SMCs, and endothelial cells (Waldeck et al. 2008; Winter et al. 2003; Hoshiga et al. 1995). Expression of $\alpha_v\beta_3$ integrin is found in the shoulder of advanced plaques and in the necrotic core of human atherosclerotic lesions (Antonov et al. 2004). In addition to $\alpha_v\beta_3$ integrin, $\alpha_v\beta_5$ is also expressed in the intima of human atherosclerotic plaques, but for *in vivo* imaging purposes, the integrin $\alpha_v\beta_3$ is the most extensively examined marker of angiogenesis (Beer et al. 2008; Dufourcq et

al. 1998). Natural ligands of $\alpha_v\beta_3$ integrins bind via a RGD (arginine (R), glycine (G), aspartate (D)) motif. ^{68}Ga - (Decristoforo et al. 2008; Jeong et al. 2008; Li et al. 2008), ^{64}Cu - (Li et al. 2007) and ^{18}F - (Gaertner et al. 2012) labelled RGD peptides have potential for PET imaging for angiogenesis and therapy of $\alpha_v\beta_3$ integrin-positive tumours. To date, the [^{18}F]galacto-RGD is the only tested RGD-based PET tracer to detect vascular inflammation (Laitinen et al. 2009). They showed novel evidence that [^{18}F]galacto-RGD detects advanced atherosclerotic plaques in mouse models of atherosclerosis. The $\alpha_v\beta_3$ integrin specific tracer [^{111}In]RP748 localizes into the atherosclerotic lesions in ApoE^{-/-} mice *ex vivo* (Sadeghi et al. 2004).

2.3.5 Hypoxia

A remarkable feature of various inflamed tissues, including atherosclerotic plaques, is the presence of hypoxia. In such hypoxic sites, macrophages accumulate and respond rapidly by altering their expression of many genes. Hypoxia may play an important role in the progression of vulnerable atherosclerotic lesions by promoting lipid accumulation, increased inflammation, adenosine triphosphate (ATP) depletion, and angiogenesis (Hulten and Levin 2009; Murdoch et al. 2005). Microvessels in lesions are likely stimulated by plaque hypoxia, reactive oxygen species, and hypoxia-inducible factor (HIF) signaling. The presence of plaque hypoxia is primarily determined by the extent of plaque inflammation - mostly increasing oxygen demand together with insufficient oxygen supply in macrophage-rich areas inside the lesions. (Hulten and Levin 2009; Sluimer and Daemen 2009) Hypoxic areas are known to be present in human atherosclerotic lesions (Hulten and Levin 2009; Sluimer et al. 2008), in experimental hypercholesterolemic, balloon-injured rabbit models (Zemplenyi et al. 1989, Jurrus and Weiss 1977; Björnheden et al. 1999), in ApoE^{-/-} (Parathath et al. 2011), and LDLR^{-/-} (Sluimer and Daemen 2009) mice. Hypoxia correlates with angiogenesis (Hulten and Levin 2009), the amount of macrophages, and the expression of HIF and vascular endothelial growth factor (VEGF) (Sluimer et al. 2008). Molecular imaging of hypoxia may have a potential to assess the plaque vulnerability but this technical approach demands validation.

2.3.6 Apoptosis

Apoptosis, a programmed death of cells including inflammatory cells and SMCs, has a role in plaque vulnerability. The thinning of the fibrous cap, the development of necrotic core, and positive vessel remodeling are linked to apoptosis. (Laufer et al. 2009; Virmani et al. 2007) Visualization of apoptosis in atherosclerotic lesions may help to identify rupture prone plaques. During apoptosis, phosphatidylserine (PS) is externalized to the outer membrane of the cell (van Engeland et al. 1998; Koopman et al. 1994). Annexin A5 is a ligand for PS and is a routinely used probe for molecular imaging of apoptosis. [$^{99\text{m}}\text{Tc}$]Annexin A5 detects apoptosis and inflammation in experimental rabbit models of atherosclerosis (Ishino et al. 2007; Sarai et al. 2007; Hartung et al. 2005; Kolodgie et al. 2003), in ApoE^{-/-}, and LDLR^{-/-} mice (Tekabe et al. 2010; Zhao et al. 2007; Isobe et al. 2006), in swine models of coronary atherosclerosis (Johnson et al. 2005), and in clinical settings (Kietselaer et al. 2004). Haider et al. demonstrated the correlation of macrophage content and the uptake of [^{111}In]Annexin A5 in atherosclerotic plaques (Haider et al. 2009).

However, Annexin A5 is not specific for apoptosis and it binds secondary to necrotic cells (Dumont et al. 2000). This has led to development of other probes targeting apoptosis. Several research groups have developed ^{18}F - and ^{64}Cu - (Cauchon et al. 2007; Keen et al. 2005; Murakami et al. 2004; Toretsky et al. 2004) labelled PET tracers of apoptosis but presently, these tracers have not been validated to detect atherosclerotic inflammation or apoptosis. Recently, Zhao and co-workers performed dual molecular imaging with [^{14}C] FDG and [$^{99\text{m}}\text{Tc}$]Annexin A5 in experimental models. Based on their results, it can be reasoned that [^{18}F]FDG may give greater sensitivity for detecting atherosclerotic plaques as compared to [$^{99\text{m}}\text{Tc}$]Annexin A5. (Zhao et al. 2011)

2.3.7 Matrix degradation

Matrix metalloproteinases are expressed in atherosclerotic plaques and play important roles in plaque instability. To date, various research groups have introduced three approaches for *in vivo* assessment of MMPs activity in atherosclerotic lesions by using radiolabelled MMP inhibitors (Tekabe et al. 2010; Haider et al. 2009; Ohshima et al. 2009; Fujimoto et al. 2008; Schäfers et al. 2004), MMP substrates (Razavian et al. 2011) or monoclonal antibody for membrane type 1 matrix metalloproteinase (MT1-MMP) (Kuge et al. 2010). Based on these studies, molecular imaging of MMPs can detect unstable atherosclerotic plaques, non-invasively. However, the techniques using antibodies cannot differentiate between active and inactive MMPs and are not optimal to detect active MMPs (Schäfers et al. 2010). Recently, Tekabe and co-workers investigated aorta and carotid uptake of [$^{99\text{m}}\text{Tc}$]MPI (matrix metalloproteinase inhibitor) in atherosclerotic ApoE^{-/-} mice and compared it to the apoptosis tracer uptake, [$^{99\text{m}}\text{Tc}$]Annexin A5, in the same animals. They showed that the expression of MMP-2 and MMP-9 increases more rapidly than apoptosis during atherosclerosis progression in ApoE^{-/-} mice and MPI may be a better imaging agent for more advanced disease than Annexin A5. (Tekabe et al. 2010)

2.3.8 Thrombotic markers

Thrombogenicity is a central feature of plaque vulnerability and the imaging of cells participating in thrombus formation, coagulation factors, or the visualization of exposed subendothelial matrices may be relevant strategies to assess vulnerability. Initially, radionuclide-labelled platelets (Moriwaki et al. 1995; Minar et al. 1989; Davis et al. 1978) or radiolabelled purine analogs were used as competitive inhibitors of adenosine diphosphate (ADP) in platelet aggregation to image plaque vulnerability. In a rabbit model, derivatives of diadenosine oligophosphate, [$^{99\text{m}}\text{Tc}$]AppCHClppA, and [^{18}F] AppCHFppA demonstrated rapid accumulation into the atherosclerotic aorta with optimal target-to-background ratio and correlations with plaque macrophage density (Elmaleh et al. 2006; Elmaleh et al. 1998).

2.3.9 Other targets

Different signaling pathways and various cell transcription factors, including proto-oncogenes such as c-fos and c-myc, are activated during the early stage of

atherosclerotic process. Qin and co-workers used ^{99m}Tc -radiolabelled antisense oligonucleotides (ASONS) to detect atherosclerotic plaques in experimental models. The tracer accumulated in the areas of artery lesions. (Qin et al. 2005) However, the non-specific myocardium uptake limits the use of this tracer to detect plaques in coronaries.

The expression of natriuretic peptide (NP) clearance receptor (NPR-Cs) is up-regulated in human atherosclerotic plaques (Casco et al. 2002). Finally, a recent study demonstrated a novel approach to image plaque vulnerability with ^{64}Cu -labelled NP targeting NPR-Cs in rabbit model of atherosclerosis. With a blood clearance of a few minutes, [^{64}Cu]DOTA-C-ANF was effective as a PET tracer for *in vivo* imaging of atherosclerotic plaques. (Liu et al. 2010)

Table 2. Summary of the studies to image vulnerable atherosclerotic plaques with PET and SPECT probes.

Target	Tracer/probe	Nature of tracer	Experimental setting	Imaging assessment of tracer uptake	Reference(s)
Metabolic activity					
Glucose metabolism	[^{18}F]FDG	Carbohydrate	Human carotid	<i>In vivo</i>	Rudd 2002, Ogawa 2004, Tawakol 2005, Tawakol 2006, Rudd 2009, Menezes 2011, Masteling 2011
	[^{18}F]FDG	Carbohydrate	Human coronary	<i>In vivo</i>	Alexanderson 2008, Wykrzykowska 2009, Lankinen 2011
	[^{18}F]FDG	Carbohydrate	Rabbit aorta	<i>In vivo</i>	Zhang 2006, Calcagno 2008, Worthley 2009
	[^{18}F]FDG	Carbohydrate	Mouse aorta (ApoE $^{-/-}$)	<i>In vivo</i>	Laurberg 2007
	[^{18}F]FDG	Carbohydrate	Mouse aorta (LDLR $^{-/-}$ -ApoB $^{100/100}$)	<i>Ex vivo</i>	Laitinen 2006
	[^{14}C]FDG	Carbohydrate	Mouse aorta (ApoE $^{-/-}$)	<i>Ex vivo</i>	Zhao 2011, Matter 2005
Choline metabolism	[^{18}F]FCH	Amino alcohol	Human aorta	<i>In vivo</i>	Bucerius 2008
	[^{18}F]FCH	Amino alcohol	Mouse aorta (ApoE $^{+/+}$)	<i>Ex vivo</i>	Matter 2005
	[^{11}C]choline	Amino alcohol	Human aorta and carotid	<i>In vivo</i>	Kato 2009
	[^{11}C]choline	Amino alcohol	Mouse aorta (LDLR $^{-/-}$ -ApoB $^{100/100}$)	<i>Ex vivo</i>	Laitinen 2010
Monocytes/Macrophages					
CCR-2	[^{99m}Tc]MCP-1	Peptide	Rabbit aorta	<i>In vivo</i>	Hartung 2007
	[^{111}In]MCP-1	Peptide	Rabbit aorta	<i>Ex vivo</i>	Ohtsuki 2001
PBR/TSPO	[^{11}C]PK11195	Peptide	Human carotid	<i>In vivo</i>	Hoppela 2007, Pugliese 2010, Gaemperli 2011
	[^{11}C]PK11195	Peptide	Mouse aorta (LDLR $^{-/-}$ -ApoB $^{100/100}$)	<i>Ex vivo</i>	Laitinen 2008
RAGE	[^{99m}Tc]anti-RAGE F(ab) $'_2$	Antibody	Mouse aorta (ApoE $^{+/+}$)	<i>In vivo</i>	Tekabe 2008
FR	[^{99m}Tc]EC20	Peptide	Mouse aorta (ApoE $^{+/+}$)	<i>In vivo</i>	Ayala-López 2010
IL-2	[^{99m}Tc]IL2	Sytokine	Human carotid	<i>In vivo</i>	Annovazzi 2006
	[^{99m}Tc]HYNIC-IL-2	Sytokine	Human carotid	<i>In vivo</i>	Opalinska 2012
SSTR $_2$ Phagocytosis	[^{68}Ga]DOTATATE	Peptide	Human coronary	<i>In vivo</i>	Rominger 2010
	[^{64}Cu]TNP	Nanoparticle	Mouse aorta (ApoE $^{-/-}$)	<i>In vivo</i>	Nahrendorf 2008
Trafficking	[^{111}In]oxine	Cells	Mouse aorta (ApoE $^{+/+}$)	<i>In vivo</i>	Kircher 2008

Adhesion molecule					
VCAM-1	[¹⁸ F]4V	Peptide	Mouse aorta (ApoE ^{-/-})	<i>In vivo</i>	Nahrendorf 2009
	[^{99m} Tc]B2702-p	Peptide	Rabbit aorta	<i>Ex vivo</i>	Broisat 2007
	[¹²³ I]B2702-p	Peptide	Rabbit aorta	<i>Ex vivo</i>	Broisat 2007
Lipoproteins					
LDL	[¹²³ I]LDL	Lipoprotein	Human carotid	<i>In vivo</i>	Lees 1983
	[^{99m} Tc]LDL	Lipoprotein	Human carotid, iliac, femoral	<i>In vivo</i>	Lees 1988
	[^{99m} Tc]LDL	Lipoprotein	Rabbit aorta, carotid	<i>In vivo</i>	Bozóky 2004
OxLDL	[¹¹¹ In]LDL	Lipoprotein	Rabbit aorta	<i>In vivo</i>	Rosen 1990
	[^{99m} Tc]oxLDL	Lipoprotein	Human carotid	<i>In vivo</i>	Iuliano 1996
	[¹²³ I]SP4	Oligopeptide	Rabbit aorta	<i>In vivo</i>	Hardoff 1993
	[^{99m} Tc]P199	Oligopeptide	Rabbit aorta, carotid	<i>In vivo</i>	Hardoff 1995
	[¹²⁵ I]MDA2	Antibody	Rabbit aorta	<i>Ex vivo</i>	Tsimikas 1999, Tsimikas 2000, Torzewski 2004
	[¹²⁵ I]MDA2	Antibody	Mouse aorta (LDLR ^{-/-})	<i>Ex vivo</i>	Torzewski 2004
	[¹²⁵ I]MDA2	Antibody	Mouse aorta (LDLR ^{-/-} and ApoE ^{-/-})	<i>Ex vivo</i>	Tsimikas 2000
LOX-1	[^{99m} Tc]LOX1-mab	Antibody	Rabbit aorta	<i>In vivo</i>	Ishino 2008
	[¹¹¹ In]LOX-1	Antibody	Mouse aorta (ApoE ^{-/-} and LDLR ^{-/-})	<i>In vivo</i>	Li 2010
	[^{99m} Tc]MDA2	Antibody	Rabbit aorta	<i>In vivo</i>	Tsimikas 1999
[¹²⁵ I]IK17	Antibody	Mouse aorta (LDLR ^{-/-})	<i>Ex vivo</i>	Shaw 2001a	
Angiogenesis					
$\alpha_v\beta_3$ integrin	[¹⁸ F]galacto-RGD	Peptide	Mouse aorta (LDLR ^{-/-} ApoB ^{100/100})	<i>In vivo</i>	Laitinen 2009
	[¹¹¹ In]RP748	Peptide	Mouse aorta (ApoE ^{-/-})	<i>Ex vivo</i>	Sadeghi 2004
Apoptosis					
Phosphatidyl-serine	[^{99m} Tc]Annexin A5	Protein	Human carotid	<i>In vivo</i>	Kietselaer 2004
	[^{99m} Tc]Annexin A5	Protein	Swine coronary	<i>In vivo</i>	Johnson 2005
	[^{99m} Tc]Annexin A5	Protein	Rabbit aorta	<i>In vivo</i>	Kolodgie 2003, Hartung 2005, Ishino 2007, Sarai 2007
	[^{99m} Tc]Annexin A5	Protein	Mouse aorta (ApoE ^{-/-})	<i>Ex vivo</i>	Zhao 2007, Tekabe 2010, Zhao 2011
	[^{99m} Tc]Annexin A5	Protein	Mouse aorta (ApoE ^{-/-} and LDLR ^{-/-})	<i>In vivo</i>	Isobe 2006
[¹¹¹ In]Annexin A5	Protein	Rabbit aorta	<i>In vivo</i>	Haider 2009	
Matrix degradation					
MMP inhibition	[^{99m} Tc]MPI	Hydroxamate der.	Rabbit aorta	<i>In vivo</i>	Haider 2009, Fujimoto 2008
	[^{99m} Tc]MPI	Hydroxamate der.	Mouse aorta (ApoE ^{-/-})	<i>Ex vivo</i>	Tekabe 2010
	[^{99m} Tc]MPI	Hydroxamate der.	Mouse aorta (ApoE ^{-/-} and LDLR ^{-/-})	<i>In vivo</i>	Ohshima 2009
	[¹²³ I]HO-CGS 27023A	Hydroxamate der.	Mouse aorta (ApoE ^{-/-} *)	<i>In vivo</i>	Schäfers 2004
MMP activation	[¹¹¹ In]RP782	Substrate	Mouse aorta (ApoE ^{-/-})	<i>In vivo</i>	Razavian 2011
MT1-MMP	[^{99m} Tc]MT1-MMP mAb	Antibody	Rabbit aorta	<i>Ex vivo</i>	Kuge 2010
Thrombosis					
Platelets	[¹¹¹ In]platelets	Cells	Human carotid	<i>In vivo</i>	Davis 1978, Minar 1989, Moriwaki 1995
ADP inhibitor	[¹⁸ F]AppCHFppA	Purine analog	Rabbit aorta	<i>In vivo</i>	Elmaleh 2006
	[^{99m} Tc]AppCHClppA	Purine analog	Rabbit aorta	<i>In vivo</i>	Elmaleh 1998
Additional targets					
NP	[⁶⁴ Cu]DOTA-C-ANF	Peptide	Rabbit aorta	<i>In vivo</i>	Liu 2010
Oncogene activation	[^{99m} Tc]ASONS	Antisense nucleotide	Rabbit aorta	<i>In vivo</i>	Qin 2005

*Carotid ligation model

2.4 Mouse models of atherosclerosis

Human atherosclerosis research is challenging because lesion development matures slowly. In small animal models, atherosclerosis can be induced in weeks to months which make them useful for research purposes. Mouse models of atherosclerosis, have many advantages: the relatively low cost, easy access and rapid fertility. Further, atherosclerosis can be induced via genetic modifications and dietary manipulations. (Tannock and King 2010) Although mouse models have many advantageous features, there are several limitations. Firstly, mice do not express cholesterol ester transfer protein (CETP) which has a significant role in human lipoprotein metabolisms. Secondly, mice carry their cholesterol predominantly in HDL particles. (Tannock and King 2010) Thirdly, lesion development starts above the endothelium instead of in the thickening intima (Calara et al. 2001). Fourthly, spontaneous plaque ruptures are rare in mice (Tannock and King 2010). One potential reason for the lack of plaque rupture in mice may be the small diameter of the aorta. As the diameter of vessel decreases, the surface tension increases exponentially which may then become markedly higher for plaque rupture. However, plaque rupture occurs in ApoE^{-/-}, LDLR^{-/-} mice but the exact nature of this is unclear. (Calara et al. 2001; Rosenfeld et al. 2000)

2.4.1 ApoE^{-/-}

The first mouse model of atherosclerosis, the apolipoprotein E (ApoE)-deficient mouse, was developed in 1992 (Piedrahita et al. 1992; Plump et al. 1992). ApoE exists on the surface of several lipoproteins, including chylomicrons, very low density lipoprotein (VLDL) and high density lipoprotein (HDL) particles and it has a key protective role in atherosclerosis. It is an important modulator of lipoprotein interactions and clearance with several receptors like low-density lipoprotein receptor (LDLR). (Curtiss 2000; Krieger et al. 1994) The ApoE^{-/-} mice has 4-5 times greater plasma total cholesterol value than the C57BL/6 mice fed with normal chow. Baseline hypercholesterolemia can be elevated with a high fat diet to result in massive hypercholesterolemia and atherosclerosis. (Reddick et al. 1994) Lesions start with an initial fatty streak, which progresses to complex lesions with a fibrous cap and later calcified lesions develop. Advanced atherosclerotic plaques are formed throughout the aorta and in the carotid arteries (Nakashima et al. 1994). The spontaneous plaque rupture of high-fat fed ApoE^{-/-} mice has been reported (Calara et al. 2001). Although the ApoE^{-/-} is the most widely used mouse model of atherosclerosis research, the absence of ApoE in humans is rare and the lipoprotein profile of the ApoE-deficient mice resembles poorly human profiles. (Nakashima et al. 1994)

2.4.2 LDLR^{-/-}

The LDLR^{-/-} mouse model was developed by Ishibashi and co-workers (Ishibashi et al. 1993) and it closely resembles the conditions of human familial hypercholesterolemia (FH). They develop moderate hypercholesterolemia and atherosclerosis due the delayed clearance of VLDL, intermediate density lipoprotein (IDL), and LDL from the plasma. Total plasma cholesterol levels are 2 times higher than C57BL/6 mice on normal chow. The lipoprotein profile resembles those of humans and the development of lesions is similar than untreated

FH in humans. LDLR^{-/-} mice develop fatty streaks without the diet, and advanced lesions with a fibrous cap and calcification can be induced by high fat diet. The spontaneous plaque rupture of high-fat fed LDLR^{-/-} mice has been reported. LDLR^{-/-} mice fed with a high fat diet, also develop itchy skin lesions, xanthomas, the same kind of lesions as described in FH patients. (Calara et al. 2001; Powell-Braxton et al. 1998; Ishibashi et al. 1994)

2.4.3 ApoB^{100/100}

The full-length Apolipoprotein B (ApoB100) is a structural component of VLDL, IDL, and LDL (Young et al. 1990). After post-transcriptional modification by the APOBEC-1 (apolipoprotein B mRNA editing enzyme, catalytic polypeptide-1) enzyme, ApoB also exists in the ApoB48 form and it is required for the assembly of chylomicrons in the intestine (Véniant et al. 1998; Kane 1983). The ApoB^{100/100} model is made by targeted mutagenesis towards the ApoB gene, resulting in the disruption of APOBEC-1 enzyme (Farese et al. 1996). The ApoB^{100/100} mice have mild hypercholesterolemia and hypertriglyceridemia and they do not develop atherosclerotic plaques when fed with chow. However, plaque development can be induced by a high fat diet responding moderate hypercholesterolemia and atherosclerosis. (Véniant et al. 1998; Purcell-Huynh et al. 1995)

2.4.4 LDLR^{-/-}ApoB^{100/100}

LDLR-deficient mice, which are able to synthesize only ApoB100 (LDLR^{-/-}ApoB^{100/100}, also known as LDLR^{-/-}ApoB48-knockout mice), was created by Powell-Braxton and co-workers (Powell-Braxton et al. 1998) by cross-breeding the LDLR^{-/-} and ApoB^{100/100} mice. LDLR^{-/-}ApoB^{100/100} mice represent a model of hypercholesterolemia with elevated levels of LDL cholesterol and expression of only ApoB100. Extensive atherosclerosis is developed with chow and can be elevated by a high fat diet which causes advanced lesions with a fibrous cap and calcification. The lipid profile of these mice resembles the type commonly seen in FH patients and in humans in general. This makes these mice better than any other mouse model currently available to study atherosclerosis. (Heinonen et al. 2007; Goldstein et al. 1989) Therefore, LDLR^{-/-}ApoB^{100/100} mice are appropriate model for atherosclerosis imaging.

2.4.5 IGF-II/LDLR^{-/-}ApoB^{100/100}

The insulin-like growth factor-II (IGF-II)/LDLR^{-/-}ApoB^{100/100} mouse model was created by Heinonen and colleagues (Heinonen et al. 2007) by crossing the LDLR^{-/-}ApoB^{100/100} mice with transgenic mice in which type 2 diabetes is caused by over-expressing IGF-II in pancreatic beta cells (Devedjian et al. 2000). IGF-II/LDLR^{-/-}ApoB^{100/100} mice are characterized by insulin resistance, hyperglycemia, and mild hyperinsulinemia. Aged IGF-II/LDLR^{-/-}ApoB^{100/100} mice display significantly increased lesion calcification compared to those of LDLR^{-/-}ApoB^{100/100} mice. This calcification is dependent on insulin resistance rather than glucose levels. Also, a significantly greater baseline expression in aorta of several genes related to calcification and inflammation are elevated. Despite of this diabetic phenotype, lipid levels of IGF-II/LDLR^{-/-}ApoB^{100/100} and LDLR^{-/-}ApoB^{100/100} mice are similar. (Heinonen et al. 2007)

3 AIMS OF THE STUDY

The purpose of this study was to investigate the development and the metabolic activity of plaques using two mouse models of atherosclerosis combined with PET imaging. Three novel PET tracer targeting inflammation (^{68}Ga), angiogenesis (^{68}Ga]DOTA-RGD) and hypoxia (^{18}F]EF5) were tested for the imaging of vulnerable atherosclerotic plaques in mice. Furthermore, the ^{18}F]FDG was used as a reference tracer.

The specific aims of the study were:

1. To characterize atherosclerotic plaques of $\text{LDLR}^{-/-}\text{ApoB}^{100/100}$ and $\text{IGF-II/LDLR}^{-/-}\text{ApoB}^{100/100}$ mouse models for PET imaging and to investigate plaque inflammation with ^{18}F]FDG
2. To investigate plaque inflammation with ^{68}Ga
3. To investigate plaque angiogenesis with ^{68}Ga]DOTA-RGD
4. To investigate plaque hypoxia with ^{18}F]EF5

4 MATERIALS AND METHODS

4.1 General study design

In study I, we reported the effects of age, duration of a high-fat diet, and type 2 diabetes on atherosclerotic plaque composition and metabolic activity assessed by [^{18}F]FDG uptake in LDLR^{-/-}ApoB^{100/100} and IGF-II/LDLR^{-/-}ApoB^{100/100} mice. In studies II-IV, we performed animal studies to explore the feasibility of novel PET tracers to identify inflammation, angiogenesis, and hypoxia in atherosclerotic plaques. We compared tracer uptake with the plaque histology and macrophage content by autoradiography. The biodistribution of radioactivity after intravenous (i.v.) tracer injection in atherosclerotic and control mice were studied by gamma counting of excised tissue samples. The general study design is shown in Figure 2. The four different radiotracers used in these studies were produced in-house using generator-produced ^{68}Ga (a physical half-life of 68 min) or cyclotron-produced ^{18}F (a physical half-life of 110 min).

4.2 Experimental animals

Atherosclerotic LDLR^{-/-}ApoB^{100/100} (Jackson Laboratory, Bar Harbor, ME, strain #003000) as well as atherosclerotic and diabetic IGF-II/LDLR^{-/-}ApoB^{100/100} (A. I. Virtanen Institute for Molecular Sciences, University of Eastern Finland, Kuopio, Finland) were used as the animal models. Atherosclerotic mice were fed with a Western-type diet (0.2% total cholesterol, TD 88137, Harlan Teklad, Harlan Laboratories, Madison, Wisconsin), starting at the varying ages until imaging (Table 3). In studies II and III, the LDLR^{-/-}ApoB^{100/100} mice were bred in the University of Eastern Finland and transferred to Turku. The C57BL/6N controls used in studies I-IV and atherosclerotic mice used in studies III and IV were bred in University of Turku. The C57BL/6N mice were used as the controls since the LDLR^{-/-}ApoB^{100/100} and IGF-II/LDLR^{-/-}ApoB^{100/100} strains were cross-bred to C57BL/6N background. The C57BL/6N mice were fed with regular chow for the whole study period. All mice were maintained under standard conditions on a 12 h light/dark cycle. In study I, mice were fasted with ad libitum access to water for 4 h before the [^{18}F]FDG injection to obtain equal blood glucose levels. In studies II-IV mice had free access to food and water. All animal experiments were reviewed and approved by the Lab-Animal Care & Use Committee of the State Provincial Office of Southern Finland.

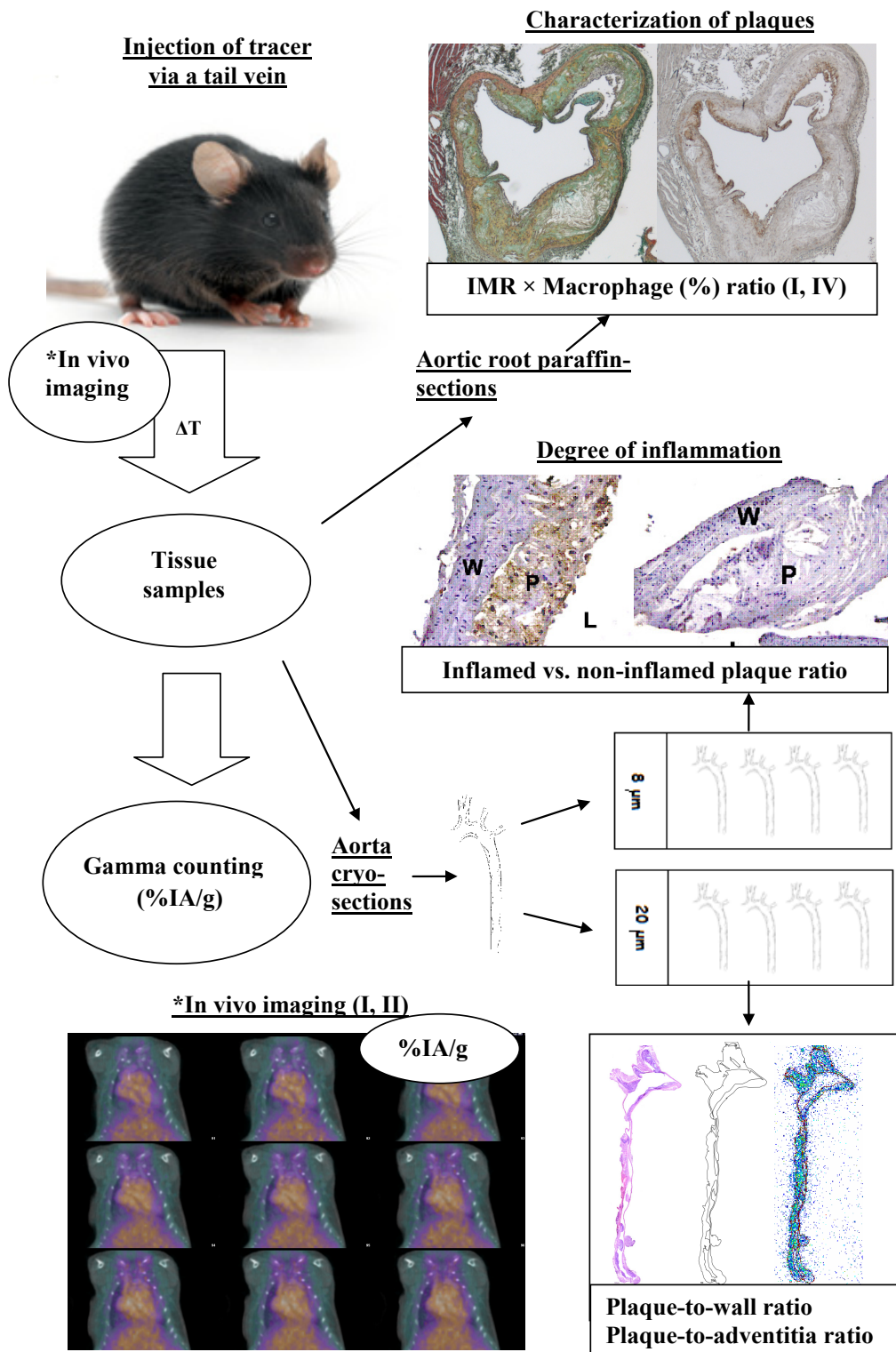


Figure 2. General study design. ΔT = investigated time point, L = lumen, P = plaque, W = wall.

Table 3. Characteristics of study animals.

Study	No. of animals (F+M)	Age, months	High-fat diet, months	Weight, gram
LDLR^{-/-}ApoB^{100/100}				
I a*	7 (7/0)	4	2	23 ± 2
I b*	10 (1/9)	6	4	39 ± 7
I c*	13 (2/11)	12-17	3-4	41 ± 7
II a **	9 (0/9)	10-11	3-4	35 ± 5
II b **	3 (3/0)	14-15	5-6	36 ± 10
III	6 (0/6)	11-12	5	39 ± 6
IV a ***	6 (3/3)	8-9	3-4	28 ± 2
IV b ***	4 (3/1)	7-8	3-4	37 ± 9
IGF-II/LDLR^{-/-}ApoB^{100/100}				
I a	9 (7/2)	4	2	25 ± 6
I b	9 (6/3)	6	4	32 ± 8
I c	11 (5/6)	12-15	3	38 ± 4
IV a ***	6 (5/1)	8-13	3-4	39 ± 6
C57BL/6N				
I	15 (0/15)	7-14	-	38 ± 4
II	6 (0/6)	14	-	41 ± 4
III	6 (0/6)	2.5	-	28 ± 1
IV a ***	6 (0/6)	6-9	-	43 ± 3

* Study I a: 4-month old, I b: 6-month old, I c: 12-month old or older.

**Study II a: Animals used in biodistribution and ARG experiments, II b: Animals used only for PET/CT imaging.

***Study IV a: Sacrifice time of 90 min, IV b: Sacrifice time of 180 min.

F = female, M = male.

4.3 Radiotracers

Synthesis of [¹⁸F]FDG (I)

[¹⁸F]FDG was synthesized, as a previously described by Hamacher et al. 1986, at the Radiopharmaceutical Chemistry Laboratory of the University of Turku (Turku PET Centre, Turku, Finland). The specific radioactivity at the end of synthesis was more than 75 MBq/nmol, and radiochemical purity exceeded 98%. The structure of [¹⁸F]FDG is shown in Figure 3a.

Production of ionic ⁶⁸Ga (II)

⁶⁸Ga was obtained in the form of ⁶⁸GaCl₃ from a ⁶⁸Ge/⁶⁸Ga generator (Cyclotron Co., Obninsk, Russia) by elution of 0.1 M HCl at the Laboratory of Turku PET Centre. The elution of the generator was monitored on-line with a positron-sensitive photodiode detector (Hamamatsu S5591, Hamamatsu Photonics K.K. Solid State Division, Japan). The radioactive elution peak was collected and the ⁶⁸GaCl₃ was neutralized with 1 M NaOH to give pH 7, as earlier described by Ujula et al. 2010. The final ⁶⁸Ga product

contained 13% of colloidal forms of ^{68}Ga as measured by the activity retained on the 0.2- μm ultrafilter.

Syntheses of [^{68}Ga]DOTA-RGD (III)

The 1,4,7,10-tetraazacyclododecane-1,4,7,10-tetraacetic acid (DOTA) chelated RGD peptide (Figure 3b) was obtained from GE Healthcare (Oslo, Norway). The synthesis of DOTA-RGD peptide has been described by Indrevoll et al. 2006. The *in vitro* affinity of the DOTA-RGD peptide for $\alpha_v\beta_3/\alpha_v\beta_5$ integrin is 3.2 nM (Indrevoll et al. 2006). The $^{68}\text{GaCl}_3$ was obtained as described above. The $^{68}\text{GaCl}_3$ eluate was mixed with 4-(2-hydroxyethyl)-1-piperazineethanesulfonic acid (HEPES, Sigma-Aldrich Chemie, Germany) and DOTA-RGD and the mixture was incubated at 100°C for 20 min. No further purification was needed. The radiochemical purity was determined by reversed-phase radio-HPLC (high-performance liquid chromatography). The compounds in the samples were separated by comparing the retention times of unlabelled peptide and authentic standards [^{68}Ga]DOTA and $^{68}\text{Ga}^{3+}$. The radio-HPLC system consisted of LaChrom instruments (Hitachi; Merck, Darmstadt, Germany) including pump L7100, UV detector L-7400 and interface D-7000; an on-line radioactivity detector (Radiomatic 150 TR, Packard, Meriden, CT); and a computerized data acquisition system. The specific radioactivity at the end of synthesis was 8.7 ± 1.1 MBq/nmol, and radiochemical purity was $97 \pm 2\%$.

Synthesis of [^{18}F]EF5 (IV)

[^{18}F]EF5 (Figure 3c) was synthesized from 2-(2-nitro-1H-imidazol-1-yl)-N-(2,3,3-trifluoroallyl)-acetamide as described previously (Bergman et al. 1997). The specific radioactivity of [^{18}F]EF5 was always >3.7 MBq/nmol and the radiochemical purity was $>98.5\%$ throughout the study.

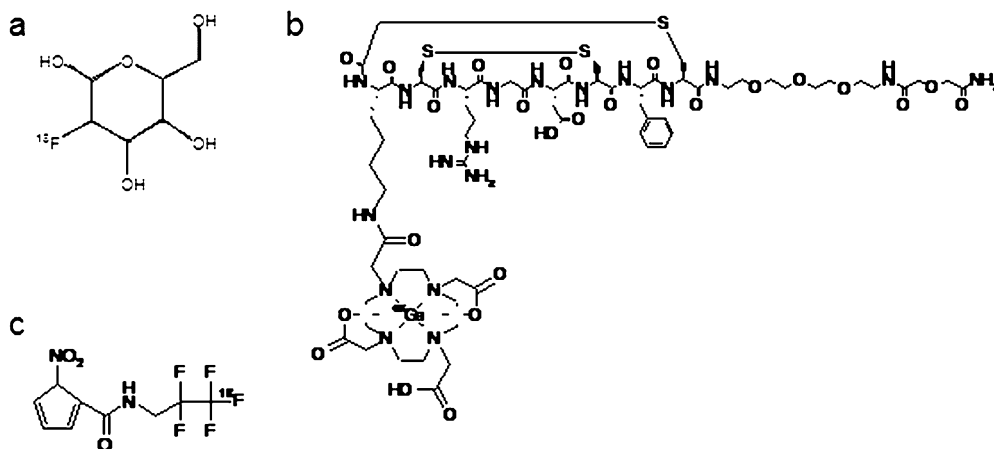


Figure 3. Molecular structures of the tracers. a) [^{18}F]FDG, b) [^{68}Ga]DOTA-RGD, c) [^{18}F]EF5.

4.4 *Ex vivo* biodistribution

Radiotracers were i.v. injected directly (II, III) or via a catheter (I, IV) into tail vein and allowed to distribute for a specified time before the animals were sacrificed by a cervical dislocation under isoflurane-anaesthesia. In studies II and III, the tracer was administered in non-anaesthetised mice, while in studies I and IV mice were anaesthetised throughout the study. In study I, the blood glucose levels were measured from the femoral vein with a glucometer (One Touch, UltraEasy, LifeScan, Inc., Milpitas, California), before the tracer injection.

After sacrifice, arterial blood was collected by cardiac puncture, samples of various tissues and organs were immediately dissected, weighed, and radioactivity was measured using a automatic (in studies II and III, 1480 Wizard 3[™] Gamma Counter; EG & G Wallac, Turku, Finland) or a well type gamma counter (in studies I and IV, Triathler 3[™], Hidex, Turku, Finland) cross-calibrated with a dose calibrator (VDC-202, Veenstra Instruments, Joure, The Netherlands). All measured data were corrected for background radioactivity. The injected radioactivity dose and radioactivity of the tissue samples were decay-corrected to the time of injection and the radioactivity dose remaining in the tail was compensated. The amount of radioactivity that had accumulated in the tissue samples or blood over the distribution period was expressed as a percentage of the injected radioactivity dose per gram of tissue (%ID/g or %IA/g). The main methodological differences among the studies are presented in Table 4. In studies I and IV, the hearts were collected and preserved in formalin for further studies.

In vivo stability of [⁶⁸Ga]DOTA-RDG (III)

The *in vivo* stability of [⁶⁸Ga]DOTA-RDG peptide was measured from a blood sample (six LDLR^{-/-}ApoB^{100/100} mice, six C57BL/6N mice) and a urine sample (five LDLR^{-/-}ApoB^{100/100} mice, two C57BL/6N mice) 60 min after intravenous injection of tracer in study III. The plasma was separated by centrifugation (2.118 × g for 5 min) at +4°C. Proteins of plasma and urine were precipitated using 10% sulfosalicylic acid. A supernatant obtained after centrifugation followed by filtration through syringe filter (0.45-μm, Waters Corporation, USA) was analyzed by radio-HPLC.

Table 4. Methodological details in different studies. Euthanasia was performed under isoflurane-anaesthesia by a cervical dislocation in all studies.

Study	Tracer	Injected radioactivity (MBq)	Injected mass (*ng, **μg)	Injection	Sacrifice time (min)
I	[¹⁸ F]FDG	12 ± 3	*0.2 ± 0.04	isoflurane anaest.	90
II	⁶⁸ Ga	17 ± 2	-	awake	180
III	[⁶⁸ Ga]DOTA-RGD	17 ± 4	**3.0 ± 0.5	awake	60
IV a	[¹⁸ F]EF5	11 ± 2	*3.1 ± 0.5	isoflurane anaest.	90
IV b	[¹⁸ F]EF5			isoflurane anaest.	180

4.5 *Ex vivo* aorta autoradiography and image analysis

The regional distribution of the radioactivity in the mouse aortic tissue (I-IV) and muscle (II and III) was determined using an autoradiography (ARG) method. The muscle was used as an internal control from the same animal in studies II and III. In studies I and IV, the autoradiography of muscle tissue was not performed, but results from each mouse were normalized for injected radioactivity and decay.

After dissection, aorta and muscle tissues were measured with a gamma counter as described in section 4.4 and thereafter immediately frozen. Sequential longitudinal 8- and 20- μm sections were cut with a cryomicrotome at -15°C , thaw-mounted onto microscope slides. The sections were air dried for 5 min and applied to an imaging plate (Fuji Imaging Plate BAS-TR2025, Fuji Photo Film Co., Ltd., Japan). After a pre-specified exposure time of at least two half lives of tracer the imaging plates were scanned with Fuji Analyser BAS-5000 (Fuji Tokyo, Japan; internal resolution 25 μm). The 20- μm sections were stained with hematoxylin and eosin (HE), and 8- μm sections with anti-Mac-3 antibody (see section 4.6). After careful co-registration of the autoradiographs and images of HE-stained 20- μm sections and examination of section morphology under a light microscope, data was interpreted. The radioactivities of ^{68}Ga (II, III) or ^{18}F (I, IV) were measured in the following regions of interest (ROIs): (1) non-calcified plaque (excluding media), (2) calcified area in plaque (excluding media), (3) normal vessel wall (no lesion formation), (4) adventitia (including adjacent fat) and given as photostimulated luminescence per square millimeter (PSL/ mm^2). The background was subtracted from the image data and the results from each mouse were normalized against internal control (II and III) or for injected radioactivity and decay (I and IV). An example of the ARG analysis is shown Figure 4.

Reliability of ARG method was tested in study III by two independent observers (authors Haukkala and Laitinen). Reproducibility of the autoradiography results was evaluated by calculating the coefficient of variation (CV%), mean difference and intra-class factor. A CV of $\leq 10\%$ is considered acceptable. The average of various ROIs was calculated for each animal from the other observer's analyses.

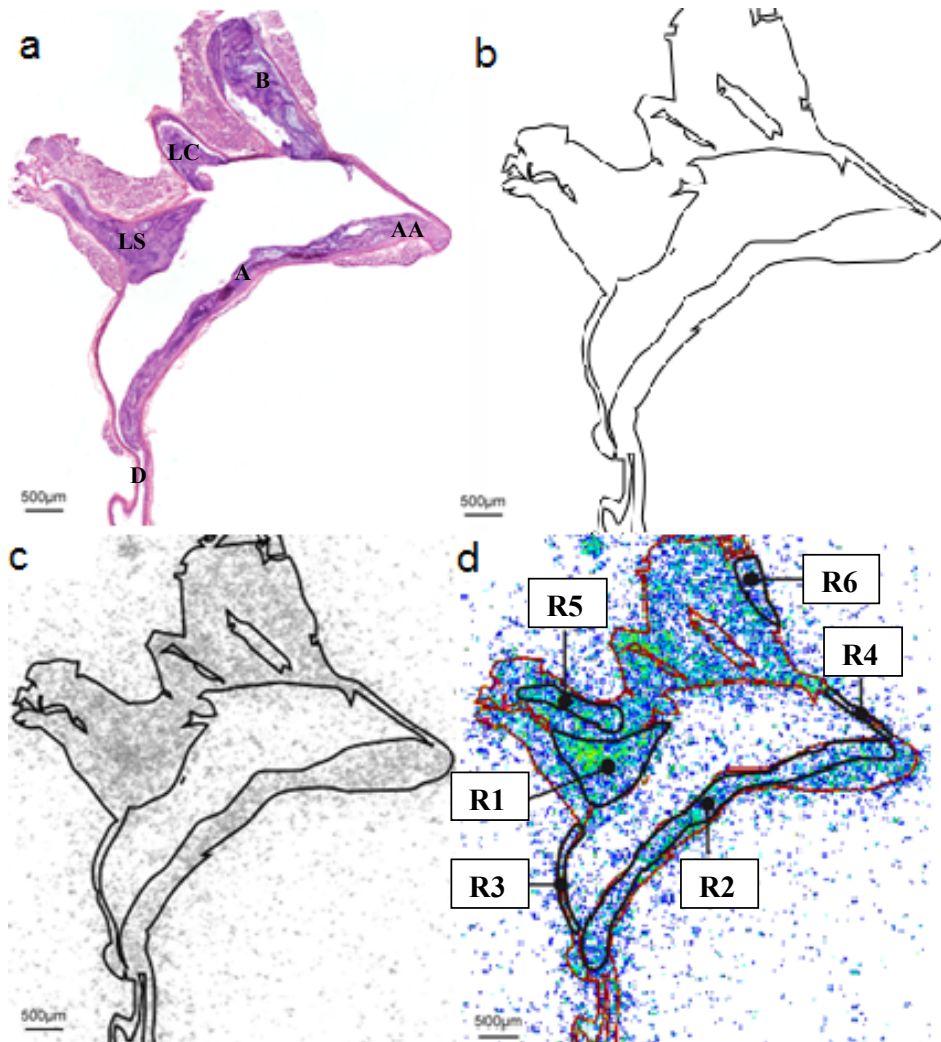


Figure 4. An example of autoradiography analysis. a) Haematoxylin-eosin staining. b) Patch image made from image a. c) Patch image superimposed to the autoradiography image. d) Co-registered autoradiograph and haematoxylin-eosin and eosin image (red lines represent the borders from the image a. R1 and R2 = regions of interest (ROIs) in plaque (non-calcified); R3 and R4 = ROIs in healthy vessel wall; R5 and R6 = ROI in adventitia. A = arch; AA = ascending aorta; B = brachiocephalic artery; D = descending thoracic aorta; LC = left common carotid artery; LS = left subclavian artery.

4.6 Immunohistochemistry

The degree of inflammation in the plaques (I-IV)

The 8- μ m cryosections were stained with anti-mouse Mac-3 (mouse cluster of differentiation (CD)107b, antibody for mouse macrophages) to compare the tracer uptake (measured by ARG) and density of macrophages in atherosclerotic plaques. In studies I, III-IV, the plaques were visually graded under a light microscope as (1) non-inflamed (none or occasional Mac-3 positive macrophages) or (2) inflamed (groups of macrophages or abundant infiltration of macrophages). In study II, the plaques were categorized as: (1) no inflammation = no macrophages, (2) mild inflammation = occasional macrophages, (3) moderate inflammation = occasional and some groups of macrophages, (4) severe inflammation = abundant infiltration of macrophages.

For Mac-3 staining, 8- μ m cryosections were stored at -70°C , melted and fixed in formaldehyde. Mac-3 antigen was uncovered by boiling in hot citrate buffer. Then the sections were incubated with primary rat anti-mouse Mac-3 antibody (Clone M3/84, BD Pharmingen, USA) and endogenous peroxidase was blocked (DakoCytomation, Denmark). Thereafter, the sections were incubated with polyclonal rabbit anti-rat antibody (Dako, Denmark) and with tertiary EnVision+ System- HRP-labelled goat anti-rabbit antibody (DakoCytomation, Denmark). Finally, Mayer's haematoxylin was used for counterstaining.

To detect endothelial cells in the plaques (III)

In study III, the anti-CD31 antibody was used to detect endothelial cells from 8- μ m cryosections. The sections were stored at -70°C , melted, fixed in ice cold acetone, and air dried. Endogenous peroxidase was blocked (DakoCytomation, Denmark). The sections were incubated with primary rat anti-mouse CD31 antibody (Clone 390, AB Serotec, Oxford UK) and with secondary biotinylated mouse anti-rat antibody (BD Pharmingen, USA). The sections were inspected under light microscope.

Determination of plaque inflammation and size (I, IV)

In studies I and IV, mouse hearts were collected for further studies. The serial 5- μ m sections of formalin-fixed and paraffin embedded hearts were cut at the level of the aortic root and stained with anti-Mac-3 or modified Movat's pentachrome stain. The high-resolution digital photomicrographs were captured and the areas of intima and media were constrained by using image editing software (Adobe Photoshop cp, Adobe Systems, San Jose, California). The intima-to-media ratios (IMRs) were calculated from the Movat-stained sections and the proportion of macrophages in the intima (Macrophage %) was determined from the anti-Mac-3-stained sections by using automated image analysis software (Image-Pro Plus 5.0, Media Cybernetics, Silver Spring, Maryland). Furthermore, the $\text{IMR} \times \text{macrophage } (\%)$ factor was used to describe the amount of macrophages compared with plaque size.

Verification of hypoxia in the plaques (IV)

Plaque hypoxia in LDLR^{-/-}ApoB^{100/100} and IGF II/LDLR^{-/-}ApoB^{100/100} mice was verified through the detection of EF5 adducts and with injection of pimonidazole.

Four additional non-anaesthetized (2 LDLR^{-/-}ApoB^{100/100} and 2 IGF II/LDLR^{-/-}ApoB^{100/100}) mice were i.v. administered with a high dose of non-labelled EF5 (10 mM in 0.9% saline, 0.01 ml/g body weight, kindly provided by C. J. Koch) 3 h before the mice were sacrificed. Frozen 8- μ m aorta sections were fixed in paraformaldehyde and the sections were blocked. Then, the sections were stained overnight in +4°C with Cy-3 conjugated ELK3-51 monoclonal antibody (University of Pennsylvania, Philadelphia, USA) and stored in PBS until image acquisition. After imaging on a fluorescent microscopy, the sections were counterstained with HE. Aorta sections from mice not injected with EF5 were also stained and used as negative controls in order to assess the non-specific binding of the antibody.

Furthermore, plaque hypoxia was confirmed by the staining of aorta sections after injection of 50 mM pimonidazole (HypoxyprobeTM-1, Natural Pharmacia International, Inc, Burlington, USA) in 0.9% saline in two additional (1 LDLR^{-/-}ApoB^{100/100} and 1 IGF-II/LDLR^{-/-}ApoB^{100/100}) mice. Pimonidazole (0.06 ml/g body weight) was injected 1 h before sacrifice, followed by aorta preparation, formalin-fixing and embedding in paraffin. Serial 4- μ m cross sections of aorta were cut and stained using the HypoxyprobeTM-1 kit (Natural Pharmacia International). The sections were blocked and stained overnight in +4°C with fluorescein isothiocyanate-conjugated antipimonidazole (1:50, HypoxyprobeTM-1), and then immediately imaged. Adjacent sections were stained with HE. Aorta sections from mice not injected with pimonidazole were also stained and used as negative controls in order to assess the non-specific binding of the antibody.

4.7 *In vivo* PET/CT imaging (I, II)

A dedicated, small animal PET/CT scanner with a resolution of 1.5 mm (Siemens Medical Solutions, Knoxville, TN, USA) was used for *in vivo* imaging. In study I, a subset of animals (n = 34) were imaged, 50 min after injection of 13 ± 4 MBq [¹⁸F]FDG. PET images were acquired for 20 min, followed by CT angiography (20 min). To obtain vascular contrast, an iodinated intravascular contrast agent (Fenestra VC, Art Advanced Research Technologies Inc., Montreal, Quebec, Canada) was injected (0.2 ml) via a tail vein catheter without moving the animal.

In study II, three additional LDLR^{-/-}ApoB^{100/100} mice were imaged at 3 h after injection of ⁶⁸Ga (16 ± 3 MBq). PET images were acquired for 15 min, followed by CT angiography (10 min) without moving the animal. To obtain vascular contrast, 0.2 ml of iodinated intravascular contrast agent eXIATM160XL (Binitio Biomedical Inc, Ottawa, ON, Canada) was injected.

In both studies, mice were kept fully sedated with 1.5% isoflurane during imaging. Co-registration of PET and CT images was done using an automatic weighted mutual information algorithm and confirmed visually on the basis of anatomical landmarks.

Quantitative PET analysis was performed by drawing ROIs of the same size in the left ventricle (blood pool), aortic arch, and brachiocephalic artery as identified on the basis of the CT angiography by using the Inveon Research Workplace software (Siemens Medical Solutions, Knoxville, TN, USA). Radioactivity concentrations were corrected for injected radioactivity, and the results were expressed as %IA/g, assuming 1 mL equals 1 g.

4.8 Statistical analyses

All results are expressed as mean \pm SD values. The limit for statistical significance was set at $p < 0.05$. Normality tests were performed using the Shapiro-Wilkins method. In biodistribution studies, comparisons of non-paired data between 2 groups, *t* test and one-way ANOVA were used. Comparisons between multiple groups were made using ANOVA with the Tukey correction. The paired *t* test was used for comparing paired data between 2 groups. *T* test with a mixed Dunnett's model was applied to correct *p* values of the biodistribution of aortic uptake versus different tissue uptakes in the same animal.

5 RESULTS

5.1 Characterization of atherosclerotic plaques

5.1.1 Determination of plaque inflammation and size

In study I, the effects of age, diet, and diabetes were determined in the development of atherosclerotic plaques. The LDLR^{-/-}ApoB^{100/100} and IGF-II/LDLR^{-/-}ApoB^{100/100} mice showed extensive atherosclerotic plaques. The plaque size, given as the IMR, was comparable between the LDLR^{-/-}ApoB^{100/100} and IGF-II/LDLR^{-/-}ApoB^{100/100} mice, and it increased from 4 months to 6 and ≥ 12 months in both strains (Figure 5a). Macrophage density was greatest at 4 and 6 months of age and decreased by ≥ 12 months of age (Figure 5b). As a result, the indicator of the total plaque macrophage number calculated as the IMR \times macrophage (%) factor (Figure 5c) was greatest at 6 month of age in IGF-II/LDLR^{-/-}ApoB^{100/100} mice and at both 6 and ≥ 12 month of age in LDLR^{-/-}ApoB^{100/100} mice. Calcified plaques existed in all mice, 12 months and older (21% of analyzed plaques in ARG) and in 11 of 19 mice aged 6 months (6% of analyzed plaques in ARG), but only in 1 LDLR^{-/-}ApoB^{100/100} mouse aged 4 months (2% of analyzed plaques in ARG).

In study IV, the extent of Mac-3 positive areas in the plaques from the aortic root was greatest in IGF-II/LDLR^{-/-}ApoB^{100/100} mice ($55 \pm 2\%$) compared to LDLR^{-/-}ApoB^{100/100} mice ($36 \pm 2\%$, $P < 0.09$). The IMR was significantly greater in LDLR^{-/-}ApoB^{100/100} mice (3.6 ± 1.3) than IGF-II/ LDLR^{-/-}ApoB^{100/100} (0.9 ± 0.2 , $P < 0.001$). The duration of high-fat diet was similar in all atherosclerotic mice.

5.1.2 Verification of plaque hypoxia (IV)

The presence of hypoxia was verified in the deep layers of plaques by fluorescent microscopy using Cy-3-conjugated ELK3-51 antibody after the injection of non-labelled EF5 in LDLR^{-/-}ApoB^{100/100} and IGF-II/LDLR^{-/-}ApoB^{100/100} mice. Plaque hypoxia was determined also by anti-pimonidazole antibody after i.v. injection of pimonidazole in both atherosclerotic models. Hypoxia immunoreactivity was not detected in adventitia, wall areas, or in the plaques of the mice not injected with EF5 and pimonidazole.

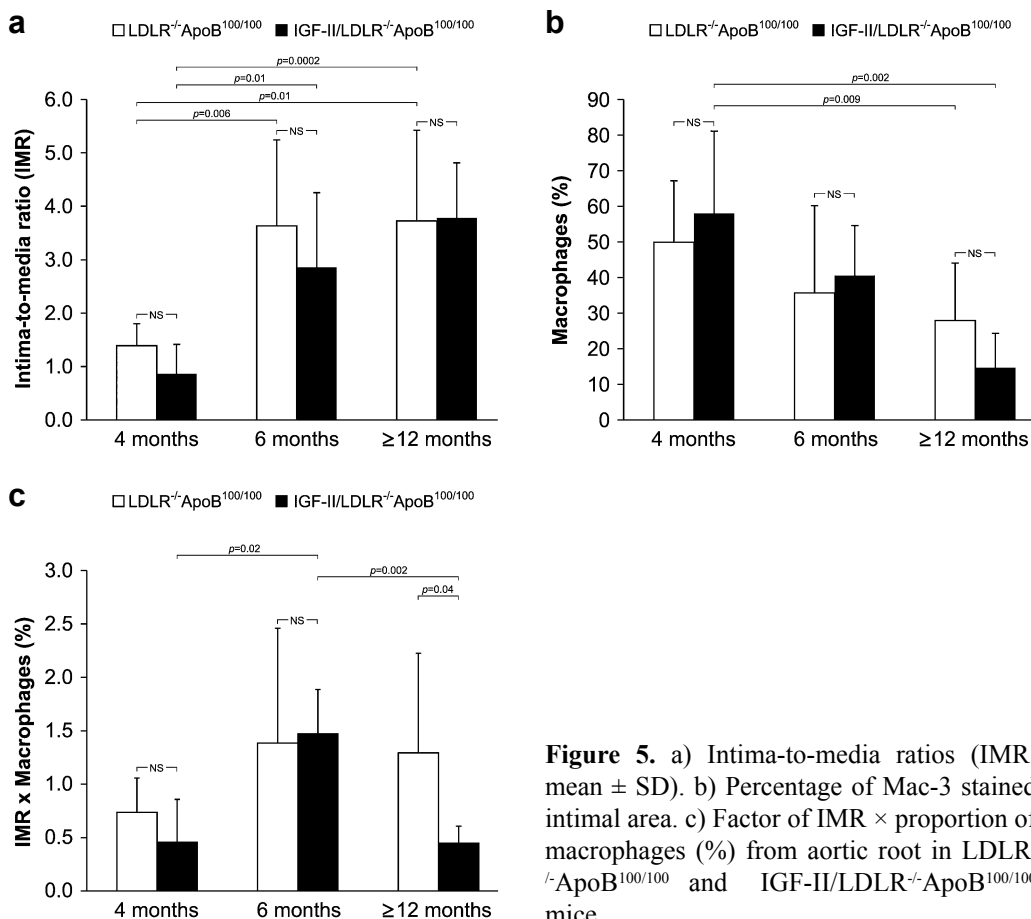


Figure 5. a) Intima-to-media ratios (IMR, mean \pm SD). b) Percentage of Mac-3 stained intimal area. c) Factor of IMR \times proportion of macrophages (%) from aortic root in LDLR^{-/-}ApoB^{100/100} and IGF-II/LDLR^{-/-}ApoB^{100/100} mice.

5.2 *Ex vivo* biodistribution of radiotracers in mice

In study I, only the uptake of [¹⁸F]FDG in blood was studied. The [¹⁸F]FDG radioactivity in blood was at the same level between LDLR^{-/-}ApoB^{100/100} and IGF-II/LDLR^{-/-}ApoB^{100/100} mice, and comparatively with C57BL/6N controls. No significant differences were observed in blood glucose values between the LDLR^{-/-}ApoB^{100/100} (7.2 ± 1.5 mmol/l), IGF-II/LDLR^{-/-}ApoB^{100/100} (6.9 ± 1.6 mmol/l) or C57BL/6N control (7.8 ± 1.8 mmol/l) mice after a 4-h fast.

In study II, the uptake of ⁶⁸Ga was greater in atherosclerotic mice than in controls but the difference was not statistically significant. The densest level of ⁶⁸Ga-radioactivity was found in the blood in both mouse strains. The aorta-to-heart and aorta-to-blood uptake ratios were comparable among LDLR^{-/-}ApoB^{100/100} and control mice. The measured radioactivities in the bone and liver of atherosclerotic mice were significantly lower than in the control mice.

In study III, the uptake of [⁶⁸Ga]DOTA-RGD was greatest in atherosclerotic mice than in controls but the difference was not statistically significant. The greatest level of [⁶⁸Ga]DOTA-RGD uptake was found in the kidneys in LDLR^{-/-}ApoB^{100/100} and control mice.

The levels of uptake in the liver and intestine were significantly lower in comparison to the kidneys, indicating the predominance of the renal excretion route and minor hepatobiliary excretion in atherosclerotic and control mice. The uptakes in heart and blood were the same between LDLR^{-/-}ApoB^{100/100} and control mice but the aorta-to-heart aorta-to-blood uptake ratios were significantly higher in LDLR^{-/-}ApoB^{100/100} than control mice. The radio-HPLC analysis of the mouse-plasma samples from LDLR^{-/-}ApoB^{100/100} mice and control mice showed $70.3 \pm 5.2\%$ and $65.9 \pm 5.2\%$ of unchanged [⁶⁸Ga] DOTA-RGD peptide, respectively, at 1 h after injection. In the urine, the percentages of unchanged peptide were $3.3 \pm 1.0\%$ for LDLR^{-/-}ApoB^{100/100} mice and $2.8 \pm 1.0\%$ for control mice at 1 h after injection.

In study IV, the uptake of [¹⁸F]EF5 was significantly greater in the aorta of LDLR^{-/-}ApoB^{100/100} mice than C57BL/6N controls 90 minutes after the tracer injection. In all atherosclerotic and control mice, the greatest levels of [¹⁸F]EF5 were found in tissues involved in the processes of EF5 clearance and excretion via the urinary system. At 180 minutes postinjection, the blood uptake of [¹⁸F]EF5 remained at $1.95 \pm 0.26\%$ IA/g in LDLR^{-/-}ApoB^{100/100} mice, revealing a slow blood clearance of [¹⁸F]EF5. The aorta-to-heart and aorta-to-blood ratios were comparable among LDLR^{-/-}ApoB^{100/100}, IGF-II/LDLR^{-/-}ApoB^{100/100}, and C57BL/6N mice at both 90 and 180 minutes after injection. The *ex vivo* aorta, aorta-to-heart and aorta-to-blood biodistribution of tracers are shown in Table 5.

Table 5. *Ex vivo* aorta, aorta-to-heart and aorta-to-blood biodistribution of radiotracers in studies II-IV.

Study	Animal	ΔT (min)	Aorta	Aorta-to-heart	Aorta-to-blood
II ⁶⁸ Ga	LDLR ^{-/-} ApoB ^{100/100}	180	1.99 ± 0.73 (p = NS*)	1.6 ± 0.7 (p = NS*)	0.2 ± 0.1 (p = NS*)
	C57BL/6N	180	1.52 ± 0.40	1.2 ± 0.2	0.2 ± 0.1
III [⁶⁸ Ga] DOTA-RGD	LDLR ^{-/-} ApoB ^{100/100}	60	0.91 ± 0.21 (p = NS*)	1.8 ± 0.4 (p = 0.01*)	1.1 ± 0.2 (p = 0.02*)
	C57BL/6N	60	0.70 ± 0.20	1.3 ± 0.1	0.8 ± 0.1
IV [¹⁸ F]EF5	LDLR ^{-/-} ApoB ^{100/100}	90	1.88 ± 0.35 (p=0.0002*)	0.8 ± 0.2 (p = NS*)	0.6 ± 0.1 (p = NS*)
	C57BL/6N	90	1.10 ± 0.23	0.6 ± 0.1	0.6 ± 0.1
	IGF-II/LDLR ^{-/-} ApoB ^{100/100}	90	1.18 ± 0.17 (p = NS**)	0.9 ± 0.3 (p = NS**)	0.7 ± 0.1 (p = NS**)
	LDLR ^{-/-} ApoB ^{100/100}	180	1.19 ± 0.19 (p = NS*)	0.8 ± 0.2 (p = NS*)	0.6 ± 0.1 (p = NS*)

Results are expressed as %IA/g (mean ± SD).

NS = not significant. ΔT = investigated time point.

*Difference between LDLR^{-/-}ApoB^{100/100} and control C57BL/6N mice

**Difference between IGF-II/LDLR^{-/-}ApoB^{100/100} and control C57BL/6N mice

5.3 *In vivo* biodistribution of radiotracers in aorta (I and II)

In vivo biodistribution of [^{18}F]FDG (I) and ^{68}Ga (II) was determined in areas of an aortic arch and a brachiocephalic artery by small animal PET/CT. The *in vivo* [^{18}F]FDG uptake in the aortic arch and brachiocephalic artery was significantly greater in the LDLR $^{-/-}$ ApoB $^{100/100}$ mice at the age of 6 months (3.0 ± 1.2 and 2.7 ± 0.5 %IA/g, respectively) in the IGF-II/LDLR $^{-/-}$ ApoB $^{100/100}$ mice at the age of 4 months (3.5 ± 1.7 and 2.7 ± 1.1 %IA/g, respectively), and 6 months (3.6 ± 0.4 and 3.1 ± 0.1 %IA/g, respectively) compared to healthy control mice (1.0 ± 0.1 and 1.0 ± 0.2 %IA/g, respectively). There were no significant differences in [^{18}F]FDG uptake between the LDLR $^{-/-}$ ApoB $^{100/100}$ and IGF-II/LDLR $^{-/-}$ ApoB $^{100/100}$ mice in any age group (Figure 6).

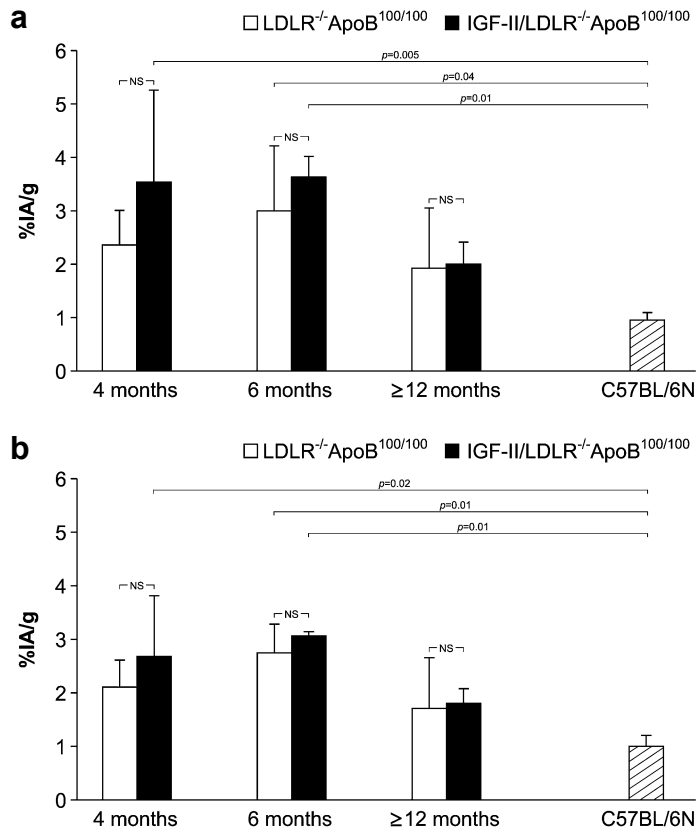


Figure 6. Average uptake of [^{18}F]FDG measured in the a) aortic arch and b) brachiocephalic artery in LDLR $^{-/-}$ ApoB $^{100/100}$, IGF-II/LDLR $^{-/-}$ ApoB $^{100/100}$ and C57BL/6N mice expressed as percentage of injected radioactivity per gram of tissue (%IA/g) (mean \pm SD).

Elevated ^{68}Ga -radioactivity in the blood pool (8.1 ± 2.2 %IA/g) was detected in LDLR $^{-/-}$ ApoB $^{100/100}$ mouse even after 3 h post-injection. The *in vivo* uptake of ^{68}Ga -radioactivity in the aortic arch and brachiocephalic artery was 6.4 ± 3.0 and 5.8 ± 2.5 %IA/g, respectively (Figure 7).

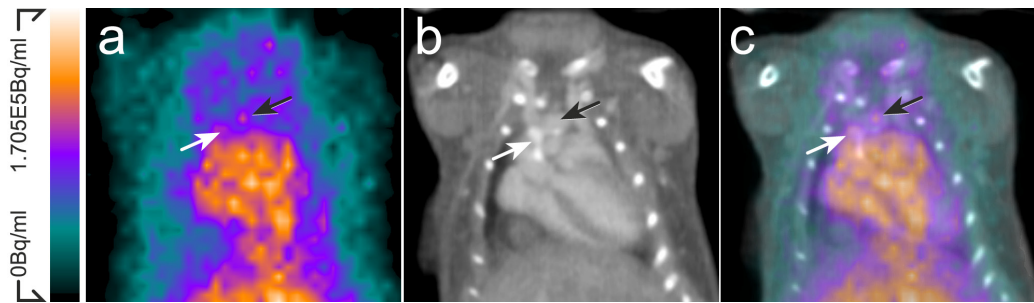


Figure 7. *In vivo* imaging of ^{68}Ga . a) *In vivo* PET, b) CT angiography, and c) fused PET/CT images demonstrate elevated ^{68}Ga signal in the blood pool as seen in the aorta and heart. Calcified (white arrows) and non-calcified (black arrows), aortic arch and aortic root can be seen in contrast enhanced CT angiography.

5.4 Digital autoradiography of aortic sections

5.4.1 Distribution of radiotracers

Autoradiography analysis was performed in the longitudinal sections of aorta at the sites of atherosclerotic plaque, healthy vessel wall, and adventitia. The number of analyzed sections and regions are shown in Table 6. The count densities of background radiation were subtracted from the actual ROI data and the results for each mouse were normalized against the internal control tissue muscle (II and III) or for injected radioactivity and decay (I and IV). To avoid the confounding variability caused by the injected radioactivity dose, decay and scanning protocol, the data were represented as plaque-to-wall and plaque-to-adventitia ratios for each study (Table 7).

Table 6. Numbers of analyzed plaque, wall, adventitia and muscle ROIs in different studies from 20- μm sections for ARG analyses. The numbers of animals represents both atherosclerotic and control mice.

Study	Sections/mouse	No. of animals	Plaque	Wall	Adventitia	Muscle
I	8-10	74	2469	1975	1240	-
II	8-12	14	384	396	406	56
III	8-13	12	414	334	513	48
IV	8-10	22	523	555	427	-
	Total	122	3790	3260	2586	104

In study I, the uptake of [^{18}F]FDG was 2 to 2.4 times greater in atherosclerotic plaques than in the healthy vessel wall ($p < 0.0001$) in all groups of atherosclerotic mice. No differences in [^{18}F]FDG uptakes were observed between non-calcified plaques and calcified areas inside of plaques and therefore these data were pooled. Furthermore, the uptake levels of [^{18}F]FDG in plaques and healthy vessel walls were comparable between the LDLR $^{-/-}$ ApoB $^{100/100}$ and IGF-II/LDLR $^{-/-}$ ApoB $^{100/100}$ mouse strains and at different ages in both atherosclerotic strains. No differences were found in the uptake of [^{18}F]FDG in the healthy vessel wall or adventitia between the atherosclerotic and control mice. Plaque uptake was consistently greater as adventitia uptake in all mice and a statistical significance was found in 4-month old IGF-II/LDLR $^{-/-}$ ApoB $^{100/100}$ mice and both 6-month-old LDLR $^{-/-}$ ApoB $^{100/100}$ and IGF-II/LDLR $^{-/-}$ ApoB $^{100/100}$ mice.

In study II, a significantly greater uptake of ^{68}Ga -radioactivity in plaques compared with healthy vessel wall (plaque-to-wall ratio 1.8 ± 0.2 , $p = 0.0002$) and adventitia (plaque-to-adventitia ratio 1.3 ± 0.2 , $p = 0.001$) was detected in LDLR $^{-/-}$ ApoB $^{100/100}$ mice. The difference between the adventitia and the healthy vessel wall was not statistically significant in either of the mouse strains. A relatively elevated uptake of ^{68}Ga -radioactivity was detected in the calcified areas ($n = 55$ from the total number of analyzed 384 plaque ROIs) of atherosclerotic plaques vs. healthy vessel wall (ratio 2.1 ± 0.6 , $p = 0.001$). No statistically significant difference was detected in calcified areas of plaques vs. non-calcified plaques and therefore these data were pooled.

In study III, the uptake of [^{68}Ga]DOTA-RGD was 1.4 ± 0.1 -fold greater in the plaques compared to the healthy vessel wall ($p = 0.0004$) and 1.6 ± 0.1 -fold greater in the plaques compared to the adventitia ($p = 0.0002$) in LDLR $^{-/-}$ ApoB $^{100/100}$ mice. The accumulation of ^{68}Ga -radioactivity in the adventitia as compared to the healthy vessel wall was statistically significant in LDLR $^{-/-}$ ApoB $^{100/100}$ mice ($p = 0.01$) and in control mice ($p = 0.003$).

In study IV, the uptake of [^{18}F]EF5 was significantly greater in the atherosclerotic plaques than in adjacent healthy vessel wall at 90 and 180 minutes after injection (plaque-to-healthy vessel wall ratios of 1.9 to 2.2 in LDLR $^{-/-}$ ApoB $^{100/100}$ and IGF-II/LDLR $^{-/-}$ ApoB $^{100/100}$ mice). No differences were observed between non-calcified and calcified regions. In addition to plaques, the adventitia immediately adjacent to aorta showed [^{18}F]EF5 uptake in both atherosclerotic mouse strains and controls (the average plaque-to-adventitia ratio between atherosclerotic and control mice was 1.0 ± 0.2 , $p = \text{NS}$). The [^{18}F]EF5 uptake in the healthy vessel wall was similar between the atherosclerotic strains and control mice.

Table 7. The results of autoradiography analysis (I-IV) presented as ratios.

Study	Animal	Age in months in study I, ΔT (min) in study IV	Plaque-to-wall	Plaque-to-adventitia	Non-inflamed-to-inflamed		
I [¹⁸ F]FDG	LDLR ^{-/-} ApoB ^{100/100}	4	2.0 ± 0.3 (p < 0.0006)	1.6 ± 0.6 (p = NS)	ND		
	IGF-II/LDLR ^{-/-} ApoB ^{100/100}	4	2.2 ± 0.4 (p < 0.0002)	1.9 ± 0.6 (p = 0.006)	ND		
	LDLR ^{-/-} ApoB ^{100/100}	6	2.3 ± 0.5 (p < 0.0002)	1.9 ± 0.7 (p = 0.02)	*1.7 ± 0.5 (p < 0.0001)		
	IGF-II/LDLR ^{-/-} ApoB ^{100/100}	6	2.4 ± 0.4 (p < 0.0003)	2.3 ± 0.4 (p = 0.0006)			
	LDLR ^{-/-} ApoB ^{100/100}	≥12	2.3 ± 0.5 (p < 0.0001)	1.6 ± 0.8 (p = NS)			
	IGF-II/LDLR ^{-/-} ApoB ^{100/100}	≥12	2.4 ± 0.6 (p < 0.0003)	1.8 ± 0.7 (p = NS)			
	II ⁶⁸ Ga	LDLR ^{-/-} ApoB ^{100/100}	-	1.8 ± 0.2 (p = 0.0002)		1.3 ± 0.2 (p = 0.001)	See Table 8.
	III [⁶⁸ Ga]DOTA-RGD	LDLR ^{-/-} ApoB ^{100/100}	-	1.4 ± 0.1 (p = 0.0004)		1.6 ± 0.1 (p = 0.0002)	1.1 ± 0.2 (p = NS)
IV [¹⁸ F]EF5	LDLR ^{-/-} ApoB ^{100/100}	90	2.2 ± 0.2 (p = 0.0001)	*1.0 ± 0.2 (p = NS)	*1.1 ± 0.4 (p = NS)		
	IGF-II/LDLR ^{-/-} ApoB ^{100/100}	90	1.9 ± 0.2 (p = 0.0004)				
	LDLR ^{-/-} ApoB ^{100/100}	180	1.9 ± 0.2 (p = 0.01)				

*pooled data, NS not significant, ND not determined

5.4.2 Co-localization of tracer uptake and plaque inflammation

The degree of inflammation in the plaques was semiquantitatively assessed by using 4-6 Mac-3-stained aortic sections of each mouse. ¹⁸F or ⁶⁸Ga-radioactivity uptake and the macrophage contents in the plaques were analyzed from two-categorized (non-inflamed or inflamed) or four-categorized (no-inflamed, mild, moderate or severe inflamed) plaque regions from atherosclerotic mice autoradiographs.

The uptake of [¹⁸F]FDG was 1.7 ± 0.5-fold greater in inflamed than non-inflamed plaques (p < 0.0001; pooled data from 6 months and 12 months and older LDLR^{-/-}ApoB^{100/100} and IGF-II/LDLR^{-/-}ApoB^{100/100} mice). The 4 months mice were not included in the analysis because of lack of non-inflamed plaques in these groups.

The uptake of ⁶⁸Ga-radioactivity was 3.3 ± 1.5-fold greater in severe inflamed plaque than non-inflamed plaques. ⁶⁸Ga-radioactivity was co-localized with the degree of inflammation as shown in Table 8.

No difference was found in comparing [^{68}Ga]DOTA-RGD and [^{18}F]EF5 uptake between non-inflamed and inflamed plaque regions (ratio 1.1 ± 0.2 and 1.1 ± 0.4 , respectively).

Table 8. Uptake of ^{68}Ga -radioactivity in non-inflamed to various degrees of inflamed plaques based on the Mac-3 autoradiography analysis.

	Non-inflamed (n = 16)	p value
Mild (n=38)	1.4 ± 0.4	0.01
Moderate (n = 89)	2.6 ± 0.9	0.03
Severe (n = 41)	3.3 ± 1.5	0.02

n = number of analysed plaques

5.4.3 Reproducibility of ARG method (III)

The CV% for the ROI analyses of adventitia, plaque, healthy vessel wall and muscle was 4.5% (range 3.5 - 5.8%). The mean differences between two analyzers for plaque versus adventitia, plaque versus healthy vessel wall, and plaque versus muscle were statistically insignificant ($p > 0.05$ for all). The corresponding intra-class factors ranged between 0.90 - 0.97 ($p = \text{NS}$).

6 DISCUSSION

6.1 Characterization of the animal models of atherosclerosis

Two mouse models of atherosclerosis were used in this thesis, namely the LDLR^{-/-}ApoB^{100/100} and the diabetic IGF-II/LDLR^{-/-}ApoB^{100/100} mouse strains. The LDLR^{-/-}ApoB^{100/100} mice were chosen as our model to study atherosclerosis because these mice share a similar lipoprotein profile to humans and their lipid phenotype closely resembles human familial hypercholesterolemia (Powell-Braxton et al. 1998). Moreover, when fed a high fat diet, LDLR^{-/-}ApoB^{100/100} mice develop complex atherosclerotic lesions. The novel diabetic IGF-II/LDLR^{-/-}ApoB^{100/100} mouse is a promising model for studies of macrovascular complications in type 2 diabetes with insulin resistance, hyperglycemia, and mild hyperinsulinemia with a hypercholesterolemic background (Heinonen et al. 2007). We used this mouse model because these mice may show greater amounts of complex, developed lesions compared to LDLR^{-/-}ApoB^{100/100}.

The age at the start of a high-fat diet and the duration of the diet may have drastic effects on the development and composition of plaques in mouse models (Heinonen et al. 2007). Therefore, the first aim of this thesis was to determine the optimal time point for studying the metabolic activity of atherosclerotic plaques for imaging purposes. This was done by determining the size and the inflammatory level of plaques from the level of aortic root. Furthermore, the metabolic activity in plaques was determined by *ex vivo* and *in vivo* imaging with [¹⁸F]FDG. After 2 months on high-fat diet, both 4-month-old LDLR^{-/-}ApoB^{100/100} and IGF-II/LDLR^{-/-}ApoB^{100/100} mice demonstrated an extremely dense infiltration of macrophages in plaques. However, at this stage, the plaques are underdeveloped, which limits the use of these young groups of mice for atherosclerotic research. The plaques in mice at 12-month and older were characterized by large areas of calcification, a necrotic core, and low content of macrophages. Therefore, these kinds of mice are not recommended for studies which would require developed areas of plaque inflammation. However, the 6-month-old mice had the greatest IMR × macrophage (%) ratio demonstrating the most advanced and largest atherosclerotic plaques. The results revealed that both the duration of high-fat diet and the age of mice at the onset of the diet are crucial for the development of the advanced atherosclerotic plaques when using these two mouse strains. Regarding plaque development, no apparent differences were found between LDLR^{-/-}ApoB^{100/100} and IGF-II/LDLR^{-/-}ApoB^{100/100} mice. The 6-month-old LDLR^{-/-}ApoB^{100/100} and IGF-II/LDLR^{-/-}ApoB^{100/100} mice were optimal (*e.g.* for the evaluation of new imaging agents). This was also confirmed by *in vivo* [¹⁸F]FDG imaging. The greatest [¹⁸F]FDG signal in the aortic arch and brachiocephalic artery was detected in the 6-month-old LDLR^{-/-}ApoB^{100/100} and IGF-II/LDLR^{-/-}ApoB^{100/100} mice. After a four hour fasting period, LDLR^{-/-}ApoB^{100/100}, IGF-II/LDLR^{-/-}ApoB^{100/100} and control mice had equal blood glucose values in [¹⁸F]FDG studies.

6.2 Evaluation of radiotracers for imaging of atherosclerotic plaques

6.2.1 [¹⁸F]FDG

[¹⁸F]FDG competes with glucose for uptake into metabolically active cells such as macrophages (Langer et al. 2008). Several [¹⁸F]FDG-based studies have been shown that [¹⁸F]FDG PET is potential method for detection of vulnerable atherosclerotic plaques and that the uptake of [¹⁸F]FDG correlates with the amount of macrophages in plaques (Tawakol et al. 2006; Rudd et al. 2002). However, the factors that determine [¹⁸F]FDG uptake in atherosclerotic plaques still remain unclear (Sheikine et al. 2010). A recent study suggests that hexokinase activity is responsible for the [¹⁸F]FDG uptake by vulnerable atherosclerotic plaques. In contrast, changes in glucose-6-phosphatase (G6Pase) activity and glucose transporter 1 (GLUT-1) expression did not parallel [¹⁸F]FDG uptake *in vitro*. It appears that [¹⁸F]FDG detects the early stages in foam cell formation and is therefore a suitable tracer for imaging of vulnerable plaques (Ogawa et al. 2012).

Hypoxia exposed macrophages and foam cells have increased glucose uptake *in vitro*. Hypoxia induces greater protein expression of hexokinase-2 (HK-2) in human macrophages than GLUT-1 (Folco et al. 2011). However, these results conflict with a study showing that hypoxia induces GLUT-1 expression in plaques (Burke et al. 2003). Thus, the complete understanding of the mechanism by which hypoxia increases glucose uptake in macrophages demands further clarification because GLUT protein expression may not correlate with the GLUT activity.

[¹⁸F]FDG tracer uptake and the metabolic pathways it follows, in atherosclerotic plaques, remains unclear. In atherosclerosis-focused studies, [¹⁸F]FDG is not flawless because it can also be internalized by myocardium which limits its use to detect metabolically active atherosclerotic lesions, in coronaries. The high-fat, low carbohydrate diet has been reported to suppress myocardium [¹⁸F]FDG uptake (Williams and Kolodny 2008), but sometimes this might be difficult to achieve in many patients. The cardiac-respiratory dual gating PET/CT is a potential method for imaging of coronary plaques with [¹⁸F]FDG (Lankinen et al. 2011; Teräs et al. 2010). The first clinical studies were encouraging and further studies in larger clinical populations are under process. Despite its limits, to date [¹⁸F]FDG-PET/CT is the most commonly used non-invasive method for detection of metabolically active vulnerable atherosclerotic plaques and therefore it was used as a reference tracer.

In study I, [¹⁸F]FDG was used to investigate the metabolic activity of atherosclerotic plaques in atherosclerotic LDLR^{-/-}ApoB^{100/100} and diabetic as well as atherosclerotic IGF-II/LDLR^{-/-}ApoB^{100/100} mice. There were no major differences in the vascular [¹⁸F]FDG uptake and plaque development between the LDLR^{-/-}ApoB^{100/100} and IGF-II/LDLR^{-/-}ApoB^{100/100} mouse strains. The greatest *in vivo* [¹⁸F]FDG signal (%IA/g) in the aortic arch and brachiocephalic artery was detected in 6-month-old LDLR^{-/-}ApoB^{100/100} and IGF-II/LDLR^{-/-}ApoB^{100/100} mice, in which histology and immunohistochemical assessments also demonstrated the highest IMR × macrophage (%) factor. Kim and co-workers compared the intima-to-media thickness in patients with impaired glucose tolerance (IGT) or type 2 diabetes (T2DM) with patients with normal glucose tolerance and found no difference.

They also demonstrated by [^{18}F]FDG-PET/CT, that patients with IGT, as well as T2DM, had greater target-to-background (TBR) levels, reflecting greater vascular inflammation than subjects in the normal glucose tolerance group (Kim et al. 2010). In the present study, no difference was found in the uptake of [^{18}F]FDG in plaques between LDLR^{-/-}ApoB^{100/100} and IGF-II/LDLR^{-/-}ApoB^{100/100} mice. This suggests that, in these models that showed markedly elevated plasma cholesterol values, due to the a high-fat diet, drove plaque development.

Based on the autoradiography analyze, [^{18}F]FDG uptake in the plaque was significantly greater as compared to the healthy vessel wall or adventitia. Furthermore, the plaque-to-wall ratio was the greatest in all tested tracers. However, the plaque-to-wall ratio was the same between atherosclerotic mice and was not influenced by age, duration of high fat diet, or type 2 diabetes. Thorough analyses, based on the anti-Mac-3 stained section, demonstrated that [^{18}F]FDG was significantly co-localized in inflamed plaques. This is consistent with previous studies indicating that the greatest uptake of [^{18}F]FDG is seen in the plaques with the heaviest macrophage density (Zhao et al. 2011).

In the present study, no differences were observed in the uptake of [^{18}F]FDG in the plaques areas with or without calcification. The majority of [^{18}F]FDG-PET studies reported that the intensity of [^{18}F]FDG uptake rarely co-localized with the vascular calcification (Rudd et al. 2009; Dunphy et al. 2005; Ben-Haim et al. 2004; Tatsumi et al. 2003). These findings may indicate that the calcification and [^{18}F]FDG uptake reflect different stages of atherosclerosis. However, in some cases vascular calcification may non-specifically trap [^{18}F]FDG (Laitinen et al. 2006).

6.2.2 ^{68}Ga

In study II, ^{68}Ga was used to detect plaque macrophages. Macrophages play an important role in the progression and development of atherosclerosis from early fatty-streak lesions to advanced atherosclerotic plaques (Saha et al. 2009). Therefore, the contents of macrophages may be an effective imaging biomarker reflecting the vulnerability of atherosclerotic plaques. The hypothesis that ^{68}Ga could target plaque inflammation and therefore affect vulnerability was based on the fact that ^{67}Ga (Gallium (^{67}Ga)) is traditionally used as a SPECT tracer of inflammation. Since ^{68}Ga owns the same chemical characteristics as ^{67}Ga , it is assumed that ionic ^{68}Ga could accumulate in the inflammatory lesions. Moreover, ^{68}Ga has been reported to accumulate at the area of inflammation in osteomyelitis rat model (Mäkinen et al. 2005) and in pancreatic adenocarcinoma xenografts in rats (Ujula et al. 2010).

^{68}Ga -radionuclide is readily available by elution from a $^{68}\text{Ge}/^{68}\text{Ga}$ generator which is an advantage as compared to the cyclotron produced radionuclides. ^{68}Ga is obtained in the form of ^{68}Ga -chloride due the eluted solution of hydrochloric acid. ^{68}Ga -chloride is hydrolyzed after neutralization with NaOH *in situ* or after administration *in vivo*. In general, in aqueous solution, ionic $^{68}\text{Ga}^{3+}$ is in the form of soluble anion called gallate, $^{68}\text{Ga}(\text{OH})^+$, and/or insoluble colloidal particles $^{68}\text{Ga}(\text{OH})_3$. The uptake mechanisms of radiolabelled gallium into areas of inflammation are not fully understood but it is known that uncharged gallium hydroxide or gallium nanoparticles are capable of penetrating

the cell, and under the lower pH conditions, inside the cell, the material ionizes and becomes bound. (Mäkinen et al. 2005; Hnatowich et al. 1977) In atherosclerotic plaques, the majority of ^{68}Ga diffuses through arterial tissue to sites of inflammation. The greatest deposits of ^{68}Ga was seen in the calcified areas of atherosclerotic plaques, which may be explained by the competitive binding of gallium ions to the Ca^{2+} and Mg^{2+} binding sites. (Ando et al. 1987) In blood, ^{68}Ga can migrate as a free $^{68}\text{Ga}^{3+}$, mimic ferric ions, and bind to transferrin, ferritin, and lactoferrin. This may explain its elevated uptake in the blood. One way to facilitate the solubilization of ^{68}Ga may be its chelation with citrate. For SPECT imaging, ^{67}Ga is usually administrated as citrate to avoid protein binding. But since citrate is a weak chelator *in vivo*, ^{67}Ga is rapidly released, hydrolyzed, and bound to transferrin and other iron-binding proteins. (Oyen et al. 1996; Green et al. 1989; Hoffer et al. 1980; Hnatowich et al. 1977)

In the present study, ^{68}Ga accumulated in severely inflamed atherosclerotic plaques, as compared to the non-inflamed plaques, healthy vessel wall or adventitia, but also in the areas of calcification in the plaques. According to the *ex vivo* biodistribution results, the uptake of ^{68}Ga -radioactivity was elevated in aortas of $\text{LDLR}^{-/-}\text{ApoB}^{100/100}$ mice as compared to the control mice, but the difference was not significant. The heightened blood uptake values of ^{68}Ga , even after 180 minutes post-injection, was observed, which limits the use of ^{68}Ga to detect vulnerable atherosclerotic plaques. Based on earlier observations, [^{18}F]FDG seems to be more promising PET tracer for imaging of atherosclerotic plaques than ^{68}Ga .

6.2.3 [^{68}Ga]DOTA-RGD

Both $\alpha_v\beta_3$ and $\alpha_v\beta_5$ integrins are up-regulated in activated endothelial cells during angiogenesis, thus modulating cell survival and migration (Dijkgraaf et al. 2007; Paulhe et al. 2001). In the human atherosclerotic intima, both $\alpha_v\beta_3$ and $\alpha_v\beta_5$ integrins are expressed by endothelial cells (Antonov et al. 2004; Dufourcq et al. 1998). Furthermore, the expression of $\alpha_v\beta_3$ in macrophages is up-regulated by oxLDL in early and advanced atherosclerotic lesions (Antonov et al. 2004). Therefore, the imaging of atherosclerotic plaques with $\alpha_v\beta_3$ and $\alpha_v\beta_5$ integrins with radiolabelled RGD-peptides is of particular interest. The *in vitro* affinity of the DOTA-RGD peptide used in study III has been evaluated for both $\alpha_v\beta_3$ and $\alpha_v\beta_5$ integrins and it is practical for *in vivo* imaging (Indrevoll et al. 2006). The monomeric DOTA-RGD peptide was successfully labelled with ^{68}Ga with a moderate specific radioactivity and showed *in vivo* stability. The fact that [^{68}Ga]DOTA-RGD binds to both $\alpha_v\beta_3$ and $\alpha_v\beta_5$ integrins can be an advantage for *in vivo* imaging since both of these integrins are expressed in human atherosclerotic plaques. The expression of $\alpha_v\beta_5$ integrin in $\text{LDLR}^{-/-}\text{ApoB}^{100/100}$ mice plaques is unknown and was not studied due to the lack of corresponding anti-mouse antibodies.

In the present study, anti-CD31 immunostaining was used to detect endothelial cells but inside the plaque, no positive staining was observed. Endothelial cells in human intraplaque microvessels do not always express CD31 and CD31 is absent in inflammatory states (Shaw et al. 2001; Jeziorska et al. 1999). The lack of microvessels in mouse plaques could also be another explanation for the negative CD31 immunostaining.

To the best of our knowledge, this was the first time that the ^{68}Ga -labelled RGD peptide was used for imaging atherosclerotic plaques and showed novel evidence that [^{68}Ga]DOTA-RGD peptide is accumulated in atherosclerotic plaques in the LDLR^{-/-}ApoB^{100/100} mice. The autoradiography analysis demonstrated significantly greater [^{68}Ga]DOTA-RGD uptake in the atherosclerotic plaques than in the healthy vessel wall and in the adventitia. However, the plaque-to-wall ratio was the lowest in all tested tracers in this thesis. The aortic uptake of [^{68}Ga]DOTA-RGD was greater in atherosclerotic LDLR^{-/-}ApoB^{100/100} mice as compared with the control mice, but the difference was not statistical significant. The relatively great [^{68}Ga]DOTA-RGD radioactivity in the blood, 60 minutes after the tracer injection was observed with both the investigated mouse strains and this limits its use for *in vivo* imaging. Creation of a later time point, for example to two hours, may improve the biodistribution of [^{68}Ga]DOTA-RGD tracer.

Only one PET study with RGD ligand, namely [^{18}F]galacto-RGD, has been published to image atherosclerotic plaques (Laitinen et al. 2009). They showed a plaque-to-wall ratio of 1.4 in LDLR^{-/-}ApoB^{100/100} mice and a correlation between plaque uptake and nuclear density in plaques. Mouse plaques are extremely dense in macrophages which possibly explains the [^{18}F]galacto-RGD signal in plaques. However, the uptake of [^{68}Ga]DOTA-RGD was not co-localized with the density of macrophages, based on the analysis of Mac-3 positive cells, indicating that the primary mechanism of [^{68}Ga]DOTA-RGD uptake is not inflammation. In contrast to previously studies (Laitinen et al. 2009; Heinonen et al. 2007), we found no evidence of angiogenesis within the plaques of LDLR^{-/-}ApoB^{100/100} mice based on inspection of HE-stained sections and anti-CD31 immunostaining. Furthermore, limited intraplaque neovascularization has been reported also in ApoE^{-/-} mice (Moulton et al. 2003). In terms of pharmacokinetics, some additional improvements are expected to be achieved through the use of multimeric peptides (Beer et al. 2008). It is also expected that other ligands recognizing the RGD motif, with stronger affinity and/or better selectivity for $\alpha_v\beta_3$, may make this approach feasible.

6.2.4 [^{18}F]EF5

The *ex vivo* biodistribution results demonstrated a significantly greater aorta uptake of [^{18}F]EF5 in LDLR^{-/-}ApoB^{100/100} mice than in the control mice. The plaques of LDLR^{-/-}ApoB^{100/100} mice were dense in macrophages (up to 60% of plaque area) and much larger than the plaques in IGF-II/LDLR^{-/-}ApoB^{100/100} as verified by the calculation of intima-to-media ratio in the aortic root. The observation that aortic [^{18}F]EF5 uptake of diabetic IGF-II/LDLR^{-/-}ApoB^{100/100} mice was comparable to that of control mice is likely explained by the small size of plaques. Thus, our results suggest that hypoxia is consistently present in advanced and large atherosclerotic plaques in investigated atherosclerotic mice.

Hypoxic areas exist in advanced human atherosclerotic lesions (Hulten et al. 2009; Sluimer et al. 2008), in rabbit models of atherosclerosis (Björnheden et al. 1999), and more recently in mouse models of atherosclerosis, namely the LDLR^{-/-} (Sluimer et al. 2009), and ApoE^{-/-} strains (Parathath et al. 2011). Until recently, it has been controversial whether mouse atherosclerotic plaques are hypoxic because of mouse plaque thickness is generally smaller than the depth at which severe hypoxia is seen in human and rabbit

plaques (100-250 μm). However, it was recently reported by Sluimer and co-workers that the plaques in the carotid artery in LDLR^{-/-} mice are more hypoxic (4.4-55.2% of plaque hypoxia) compared with the plaques in the carotid arteries of symptomatic patients (0.4-23.5%) as detected by pimonidazole. They also showed that plaques in LDLR^{-/-} mice were extremely macrophage-rich (47-73% of plaque macrophages of all cells) compared to human plaques (11-44%) which might be a reason for mouse plaque hypoxia (Sluimer et al. 2009). Even more recently Parathath et al. showed hypoxia in plaques of ApoE^{-/-} mice with the anti-HIF-1 α staining. They noted that HIF-1 α was prominently expressed in the central region of plaques and significantly co-localized with CD68-positive macrophages (Parathath et al. 2011). This is compatible with human studies demonstrating hypoxia is present in the center of an advanced plaque and co-localizes with CD68-positive macrophages (Sluimer et al. 2008).

In the present study, no difference was observed in the uptake of [¹⁸F]EF5 in inflamed and non-inflamed plaques based on autoradiography studies with anti-Mac-3 stained sections. However, it is important to note that the content of macrophages in plaques is heterogeneous and macrophages can express different antigens (Wilson et al. 2009). Expression of Mac-3 antigen is up-regulated during differentiation of monocytes into activated macrophages. This can be detected by anti-Mac-3 antibody immunohistochemical staining in the cap area and in the shoulder regions of the plaques. In human advanced carotid atherosclerotic plaques, the cap region shows mild or no hypoxia while the shoulder segment of the plaque is not hypoxic, irrespective of the infiltration of macrophages (Sluimer et al. 2008). In the present study, this may explain the difference in the [¹⁸F]EF5 uptake and Mac-3 positive macrophages.

Autoradiography analyze showed consistent, focally greater uptake of [¹⁸F]EF5 in atherosclerotic plaques, as compared with the vessel wall in the same animals. Further, hypoxia in plaques was verified by antibody staining of EF5 adducts and pimonidazole. However, the slow blood clearance suggests that [¹⁸F]EF5 is strongly bound to the plasma proteins, even after 180 minutes post-injection. The circulatory half-life of EF5 is approximately 40 minutes in mice (Laughlin et al. 1996) and approximately 12 hours in humans (Koch et al. 2001). This is problematic for PET imaging because the physical half-life of [¹⁸F] is only 110 minutes. Also a greater, non-specific uptake of [¹⁸F]EF5 in adventitia is problematic for plaque imaging. The adventitial uptake of [¹⁸F]EF5 is probably due to the presence of blood in the adventitial microvessels and is not specific, based on the absence of EF5 adducts in the adventitia. The pharmacokinetic properties of [¹⁸F]EF5 are not favorable for plaque imaging due to slow blood clearance in used mouse models.

6.3 Potential limitations

Autoradiography analysis of mouse aorta is challenging because of the size of aorta and therefore multiple, consecutive section analysis were performed. Another limitation was that the number of mice used in the studies was, but this was compensated by the exact analyses of entire aorta with a large number of analyzed regions interest (in total approximately 9700 ROIs were analyzed in studies I-IV). The PSL/mm² has a wide

dynamic range, but the detection of microstructures existing in a healthy vessel wall, may give variation in the results. In addition, technically, the section may break during the staining and result in varying thicknesses and an area of artifact. This is a one reason why each section should be carefully examined under light microscopy. Another limitation is that autoradiography is also affected by the decay of radioactivity. In studies II and III, decay compensation was not performed and therefore the muscle was used as an internal control to compare calculated mean values between animals in the study. However, this does not allow for the comparison of mice from the different studies and therefore the plaque-to-wall ratio was used for this comparison. In studies I and IV, the decay compensation formula was created and PSL/mm² values can be directly compared between different animals. However, the comparable data sets were lacking in studies II and III and therefore the plaque-to-wall ratio was used to represent ARG result in this thesis. It must also be noted that the PSL/mm² unit does not accurately describe the true distribution of the tracer because it measures the total radioactivity of the samples, including the potential radiometabolites. This stays true also in *ex vivo* gamma counting and the unit of %IA/g. The reliability of autoradiography analysis was performed in study III and it showed consistent reproducibility (mean CV% was 4.5%) between analyzers. With regards to the healthy vessel wall, the CV% was greater but within an acceptable range (5.8%). This can be expected because of the smaller size of the healthy wall and the potential interference from other nearby tissues, such as fat.

The absolute assessment of the injected radioactivity is important. This assessment aims to give approximately the same dose per gram of weight to mouse as in human. However, in experimental studies, the dose should be high enough so that after the radioactivity decay and preparation time there remains enough radioactivity for the gamma counting and the autoradiography. This means that the injected radioactivity and amount of the compound in micrograms in mice is much higher than in humans and these might have influence in the biodistributions of tracers. One important reason why no statistical differences were observed in aorta biodistribution between atherosclerotic and control mice is the processing of the tissues. The preparation of control mice aortas are much more challenging than in atherosclerotic mice and usually it contains more nearby tissue, mainly fat, which may distort the biodistribution result. Meticulous cleaning of aortas may improve this result in the future.

Inter-animal variation in the extent of atherosclerosis existing in LDLR^{-/-}ApoB^{100/100} and IGF-II/LDLR^{-/-}ApoB^{100/100} mice (as well as other atherosclerosis prone mice) existed in study IV, where the IGF-II/LDLR^{-/-}ApoB^{100/100} mice showed surprisingly smaller plaques than LDLR^{-/-}ApoB^{100/100} mice. This variation increases the number of animals needed to ensure sufficient statistical power. This variation could be reduced by doing serial, non-invasive measurements on the same animal. However, creating PET/CT images, with PET tracers, owing to the relatively long half-life of radionuclide, is not a possible to perform in the same animal. Furthermore, the main evaluation of atherosclerosis in mice is conducted *post mortem* and repeat measurements are not possible. However, one option is to use dual tracer imaging with a gamma emitting radionuclide, such as tritium and to perform another autoradiography image after the first, short half-life radionuclide, has been delayed. With this method, the radioactivity uptake from two different tracers in same plaques can be determined and uptake rates are directly compared.

In this thesis, only minor methodological differences existed between sub-studies. In studies II and III, the tracers were injected via the tail vein and some animals had to be removed from these studies because of the high dose of tracer which remained in the tail vein. After these studies, cannulation of the mouse tail vein was developed and in studies I and IV, no mouse radioactivity data was invalid because of remaining tail radioactivity. In all studies, the radioactivity remained in the tail and was reduced from the total injected radioactivity.

6.4 Future aspects

The histology of atherosclerotic plaque development in mice and humans has more similarities than differences, and comparative genetics show that many mechanisms of murine and human atherogenesis are shared (Bentzon et al. 2010). However, the rupture of lesion occurs rarely in mouse plaques and therefore the selection of an alternative animal model for investigations into plaque vulnerability is warranted. Several research groups have used rabbit models of atherosclerosis to image plaque vulnerability. The development of plaque can be induced by high-fat diet and/or by surgery. High-fat diet induced atherosclerosis in rabbit models are better for plaque imaging than surgical models because the wound itself may create an artifact. The pig models of atherosclerosis are very interesting, since the size, anatomy and physiology are most related to humans. However, the maintenance of these models is uneconomical and inconvenient. It must be also noted that rabbits and pigs are much more sensitive to handling than mice and long-term studies, like the follow-up and treatment response studies, may induce stress. For studies that demand a large number of experiments and animals, the mouse models are ideal. As already mentioned, several mouse models of atherosclerosis have been created and an important aspect to consider is to choose the most appropriate model for the experiment. As reported, not only the strain but also the age and duration of high-fat diet have crucial effects on the development of plaques. In present studies, the LDLR^{-/-}ApoB^{100/100} mice were selected based on similarities to lipoprotein profiles present in man. However, as these mice are deficient of LDL receptor it is assumed that they do not respond to the 3-hydroxy-3-methyl-glutaryl-CoA reductase inhibitors, the most commonly used cholesterol lowering drugs. For intervention studies with statins, an alternate model could be useful.

The potential of atherosclerotic plaques to rupture depends on their structural components and metabolic activation which are difficult to assess using anatomical imaging modalities. Recent studies suggest that functional imaging has the potential to assess plaque metabolism and to predict vascular risk. For several years, [¹⁸F]FDG has been the most useful PET tracer for the imaging of vulnerable atherosclerotic plaques. [¹⁸F]FDG accumulates in macrophage-rich areas of plaques (Ogawa et al. 2012) and is then a potent tracer for imaging of plaque vulnerability. Moreover, the uptake of [¹⁸F]FDG in vessels is a stable parameter to identify when [¹⁸F]FDG is used for diagnostic purposes and for the assessment of treatment efficacy (Sheikine et al. 2010). However, as previously discussed, [¹⁸F]FDG has limitations and therefore more specific tracers are needed. Since [¹⁸F]FDG is clinically used, its availability is plenty and it detects plaque

inflammation therefore it is a suitable reference tracer for the discovery of new and better probes.

Radiotracer molecular size influences its pharmacokinetics. When imaging atherosclerotic plaques, small molecules or peptides are selected over larger molecular structures like antibodies. Recently, ^{18}F -labelled nanoparticles (^{18}F]CLIO) showed both specific quantification of macrophage content in a mouse model of aortic aneurysm and optimal target-to-blood activity ratio emerging 10 to 12 hours post-injection (Nahrendorf et al. 2011). Slow blood clearance rates are important because these limit the availability of tested radiotracers used for plaque imaging. As discussed in study II, free ^{68}Ga binds avidly to plasma proteins. In case of ^{68}Ga]DOTA-RGD, free ^{68}Ga ions may also be responsible for the tracer's slow blood clearance rates. In blood, ^{18}F]EF5 also circulated in large amounts. Recently, a study suggested that mice metabolize extensively ^{18}F]EF5 as compared to rats or humans. After 2 hours of post-injection, approximately 60% of the radioactivity in plasma represents radioactive metabolites of ^{18}F]EF5. (Eskola et al. 2012) To detect atherosclerotic plaques with ^{18}F]EF5, further studies in different animal models are warranted.

To detect plaque vulnerability, PET and SPECT are two commonly used nuclear imaging modalities. Despite the fact that the majority of studies published used SPECT probes, the leading molecular imaging modality is PET for imaging of atherosclerotic plaques. PET is popular because it acquires data with sharper spatial resolution than SPECT (2-4- vs. 7-10-mm with clinical scanners).

Nuclear imaging modalities are effective tools because of their high sensitivity and the availability for synthesis of a diverse array of targeted, radioactively labelled tracers. However, the exposure to ionizing radiation may be a major limitation to screening asymptomatic individuals or follow-up imaging and the radiation burden is a potential drawback of PET, SPECT, and also CT scanning modalities. MRI does not use an ionizing radiation source and could constitute a valid alternative providing also a method to study intraplaque haemorrhage. However, the hybrid imaging would combine specific strengths of single modalities while compensating their individual weakness. In their spatial resolution, sensitivity, and detection range for imaging disease, PET/CT or PET/MRI are powerful tools for the clinical detection of atherosclerotic plaque vulnerability in future.

7 SUMMARY AND CONCLUSIONS

1. A major aim of this work was to characterize two mouse models of atherosclerosis for potential use in molecular imaging for plaque vulnerability. This was done to determine optimal conditions to test new imaging probes in appropriate mouse models of atherosclerosis. The best ages in the models of LDLR^{-/-}ApoB^{100/100} and IGF-II/LDLR^{-/-}ApoB^{100/100} was a six month old mouse maintained on high fat diet for 4 months. At this age, these mice had the largest and the most inflamed lesions and showed the greatest uptake of [¹⁸F]FDG in atherosclerotic plaques. These mouse strains did not exhibit thrombosed or thrombus-prone lesion. In general, it is debatable whether the findings in mice can be applied to human atherosclerotic plaque vulnerability. However, in the evaluation of different tracers, the LDLR^{-/-}ApoB^{100/100} and IGF-II/LDLR^{-/-}ApoB^{100/100} mouse models are suitable since they develop large plaques with metabolically active inflammation. In plaque development, no differences were observed between the two tested mice models and gender of these mice.
2. ⁶⁸Ga uptake was greatest in severely inflamed plaques, but non-specific binding to plasma proteins limits the use of ⁶⁸Ga for plaque imaging *in vivo*.
3. The novel DOTA-RGD peptide was successfully labelled with ⁶⁸Ga. The [⁶⁸Ga]DOTA-RGD peptide was internalized by the atherosclerotic plaques but its colocalization with macrophages was not detected. Further, the pharmacokinetic properties of [⁶⁸Ga]DOTA-RGD were not optimal for the plaque *in vivo* imaging in used animal model.
4. Hypoxia was confirmed in LDLR^{-/-}ApoB^{100/100} and IGF-II/LDLR^{-/-}ApoB^{100/100} mouse atherosclerotic plaques by a specific EF5 antibody and by pimonidazole. The specific hypoxia tracer [¹⁸F]EF5 showed plaque uptake by comparing its rate in the healthy vessel wall. However, the slow blood clearance and the elevated adventitial uptake may limit the value of [¹⁸F]EF5 for *in vivo* imaging of atherosclerosis. Further testing in other animal models and humans are warranted.

In summary, novel tracers demonstrated potentially optimal properties for the imaging of atherosclerotic plaques. All had specific limitations which makes their use for *in vivo* plaque imaging challenging. Of the tested tracers, [¹⁸F]FDG was clearly the best in imaging for plaque vulnerability. The uptake of [¹⁸F]FDG by myocardium is a limitation which necessitates the discovery of new, specific tracers that map plaque vulnerability.

8 ACKNOWLEDGEMENTS

This study was carried out in the Turku PET Centre, Institute of Clinical Medicine, Department of Clinical Physiology and Nuclear Medicine during the years 2008-2012. I wish to express my appreciation to Professor Juhani Knuuti, the director of the Turku PET Centre and Professor Jaakko Hartiala, the head of the Department of Clinical Physiology and Nuclear Medicine, for providing such excellent research facilities.

I owe my deepest gratitude to my supervisors, Professor Juhani Knuuti and Professor Anne Roivainen. I could not have asked for better mentors. Juhani, you have always had so valuable advices and comments. It is such admirable how you have been able to hold the office of director and at the same time been able to be a clinician and follow scientific projects in many fields. I want to also thank you for sharing with me several other projects that had broadened my understanding of cardiology and nuclear medicine. Anne, you have always been such supported and thoughtful. You always have new ideas and thoughts and you are always around when needed. It is so amazing how fast you are able to reply for e-mails, sometimes even before the e-mail has been sent at the first time. Anne is thanked for always have time to go through manuscripts with me. Juhani and Anne thank you both for being such a great supervisors!

The official reviewers of this thesis, Assistant Professor Matthias Nahrendorf and Adjunct Professor Kirsi Timonen are warmly acknowledged for their valuable and constructive comments. I also wish to thank Dr. Robert Badeau for the language editing (and even more) of this thesis.

In addition to Juhani and Anne, I want to also thank my other supervisory board members Professor Matti Poutanen and Dr. Minnamaija Lintunen for their support. The director of the FinPharma Doctoral Program Drug Discovery Section, (previously called as DDGS), Professor Mika Scheinin and the coordinator of the program Dr. Eeva Valve, are acknowledged for all the support they have provided for me during the past years. I also want to thank Docent Ulla-Marjut Jaakkola, Director of the Animal Facility of the University of Turku, and personnel for their services.

I would like to express my gratitude to my co-authors and collaborators during these years. I especially want to thank Dr. Iina Laitinen for all the teaching in several theoretical and practical issues and your precious advices. You have been such a great role model of a young female scientist to me! You are also an excellent photographer, thanks for the memorialized the important days of my life. Docent Antti Saraste is specially acknowledged for his intellectual research work. It has been really pleasure to work with you. Thank you also for the sharing with me other interesting projects. The first lady of the CoE, Professor Pirjo Nuutila, is warmly acknowledged and also thanked for the financial support by the SUMMIT project. The team in Eastern Finland, Professor Seppo Ylä-Herttua, Dr. Suvi Heinonen and Dr. Pia Leppänen, are sincere thanked for the collaboration during these years. I also wish to thank the experts of pathology Docent Jukka Laine and Professor Pekka Saukko for all their help. The team of GE Dr's Peter Ivesor, Ian Willson, Hege Karlsen and Alan Cuthbertson are warmly acknowledgement

for the collaboration concerning the study III. The radiochemistry experts Pauliina Luoto, Henri Sipilä, Sarita Forsback and Nina Savisto are sincere thanked. Sarita is also thanked for creating Figure 3c of this thesis.

I want also thank Erica Nyman for the cutting of aortic sections and the histological stainings (you are really an amazing); Erja Mäntysalo for the all technical help (you really taught me a lot of practical issues); Irina Lisinen and Ville Aalto for the statistical help; and Liisa Lempiäinen for the cutting of the aortic roots. Without you all, I would have had some serious troubles! I am grateful to all of the personnel in PET Centre providing me such an enjoyable and inspiring atmosphere to work in. Especially, I want to thank for Sanna Suominen, Eija Nirhamo and Emilia Puhakka from the lab always being willing to help me in so many times. Minna Aatsinki and Tarja Keskitalo are thanked for their help with scheduling and taking care of dosimeters. Leena Tokoi-Eklund is sincere thanked for the handling of small animal PET/CT camera and being a great help during studies in Biocity. Marko Tirri is thanked for his help with cameras and reconstructions. Tuula Tolvanen, Mika Teräs and Hannu Sipilä are thanked for all the physics and chemistries related matters. For secretarial matters Mirja Jyrkinen and Laura Jaakkola are acknowledged. Rami Mikkola and Marko Tättäläinen are warmly acknowledged for all the help with information technology. All the members of CoE are sincere acknowledged for interest meetings (official or informals) during the past years. I am grateful for Iina, Anu, Sanna, Tipi, Pauliina, Tiina, Heidi, Helena, Miikka, Max, Henkka, Jarkko and Aake for all the discussions and laughter we have shared in different fields of life or science. Anu, thank you for sharing your experience in life and work in so many times!

I owe my deepest gratitude to my family for their support. My husband Antti, my parents Marke and Hemmo, my brother Jani and his family, and also my parents-in-law Tuula and Jukka made this possible with their never ending support and child-care help. My one and half-year-old daughter Aida, has been my precious sunshine.

This study was conducted within the Finnish Centre of Excellence in Molecular Imaging in Cardiovascular and Metabolic Research supported by the Academy of Finland, the University of Turku, the Turku University Hospital and the Åbo Akademi University. The research leading to these results has also received funding from the European Union's Seventh Framework Program (FP7/2007-2013) for the Innovative Medicine Initiative under grant agreement No. IMI/115006 (the SUMMIT consortium), the Instrumentarium Foundation, the Finnish Cultural Foundation, the Finnish Foundation for Cardiovascular Research, the Aarne Koskelo Foundation, the Ida Montine Foundation, the Finnish-Norwegian Medical Foundation, the Siiri Suominen Foundation of Heart Disease (University of Turku), and from the EVO-grants of the Hospital District of Southwest Finland.

Turku, October 2012



Johanna Silvola

9 REFERENCES

- Alexanderson, E., Slomka, P., Cheng, V., Meave, A., Saldana, Y., Garcia-Rojas, L. et al. (2008). Fusion of positron emission tomography and coronary computed tomographic angiography identifies fluorine 18 fluorodeoxyglucose uptake in the left main coronary artery soft plaque. *J. Nucl. Cardiol.*, *15*, 841-843.
- Ambrose, J. A. & Fuster, V. (1998). The risk of coronary occlusion is not proportional to the prior severity of coronary stenoses. *Heart*, *79*, 3-4.
- Ando, A., Nitta, K., Ando, I., Katsuda, S., Tonami, N., Hiraki, T. et al. (1987). Ga-67 Accumulation in Inflammatory Lesion and Its Mechanism - Comparison with Malignant-Tumor. *Eur. J. Nucl. Med.*, *12*, 560-566.
- Annovazzi, A., Bonanno, E., Arca, M., D'Alessandria, C., Marcoccia, A., Spagnoli, L. G. et al. (2006). 99mTc-interleukin-2 scintigraphy for the in vivo imaging of vulnerable atherosclerotic plaques. *Eur. J. Nucl. Med. Mol. Imaging*, *33*, 117-126.
- Antonov, A. S., Kolodgie, F. D., Munn, D. H., & Gerrity, R. G. (2004). Regulation of macrophage foam cell formation by alpha V beta 3 integrin - Potential role in human atherosclerosis. *Am. J. Pathol.*, *165*, 247-258.
- Armani, C., Catalani, E., Balbarini, A., Bagnoli, P., & Cervia, D. (2007). Expression, pharmacology, and functional role of somatostatin receptor subtypes 1 and 2 in human macrophages. *J. Leukoc. Biol.*, *81*, 845-855.
- Ayala-López, W., Xia, W., Varghese, B., & Low, P. S. (2010). Imaging of atherosclerosis in apolipoprotein e knockout mice: targeting of a folate-conjugated radiopharmaceutical to activated macrophages. *J. Nucl. Med.*, *51*, 768-774.
- Bergman, J. & Solin, O. (1997). Fluorine-18-labeled fluorine gas for synthesis of tracer molecules. *Nucl. Med. Biol.*, *24*, 677-683.
- Beer, A. J. & Schwaiger, M. (2008). Imaging of integrin alphavbeta3 expression. *Cancer Metastasis Rev.*, *27*, 631-644.
- Ben-Haim, S., Kupzov, E., Tamir, A., & Israel, O. (2004). Evaluation of 18F-FDG uptake and arterial wall calcifications using 18F-FDG PET/CT. *J. Nucl. Med.*, *45*, 1816-1821.
- Bentzon, J. F. & Falk, E. (2010). Atherosclerotic lesions in mouse and man: is it the same disease? *Curr. Opin. Lipidol.*, *21*, 434-440.
- Björnheden, T., Levin, M., Evaldsson, M., & Wiklund, O. (1999). Evidence of hypoxic areas within the arterial wall in vivo. *Arterioscler. Thromb. Vasc. Biol.*, *19*, 870-876.
- Boggs, K. P., Rock, C. O., & Jackowski, S. (1995). Lysophosphatidylcholine and 1-O-octadecyl-2-O-methyl-rac-glycero-3-phosphocholine inhibit the CDP-choline pathway of phosphatidylcholine synthesis at the CTP:phosphocholine cytidylyltransferase step. *J. Biol. Chem.*, *270*, 7757-7764.
- Bozóky, Z., Balogh, L., Máthé, D., Fülöp, L., Bertók, L., & Jánoki, G. A. (2004). Preparation and investigation of 99m technetium-labeled low-density lipoproteins in rabbits with experimentally induced hypercholesterolemia. *Eur. Biophys. J.*, *33*, 140-145.
- Brindle, K. (2008). New approaches for imaging tumour responses to treatment. *Nat. Rev. Cancer*, *8*, 94-107.
- Broisat, A., Riou, L. M., Ardisson, V., Boturyn, D., Dumy, P., Fagret, D. et al. (2007). Molecular imaging of vascular cell adhesion molecule-1 expression in experimental atherosclerotic plaques with radiolabelled B2702-p. *Eur. J. Nucl. Med. Mol. Imaging*, *34*, 830-840.
- Bucerius, J., Schmaljohann, J., Bohm, I., Palmedo, H., Guhlke, S., Tiemann, K. et al. (2008). Feasibility of 18F-fluoromethylcholine PET/CT for imaging of vessel wall alterations in humans--first results. *Eur. J. Nucl. Med. Mol. Imaging*, *35*, 815-820.
- Burke, B., Giannoudis, A., Corke, K. P., Gill, D., Wells, M., Ziegler-Heitbrock, L. et al. (2003). Hypoxia-induced gene expression in human macrophages: implications for ischemic tissues and hypoxia-regulated gene therapy. *Am. J. Pathol.*, *163*, 1233-1243.
- Calara, F., Silvestre, M., Casanada, F., Yuan, N., Napoli, C., & Palinski, W. (2001). Spontaneous plaque rupture and secondary thrombosis in apolipoprotein E-deficient and LDL receptor-deficient mice. *J. Pathol.*, *195*, 257-263.
- Calcagno, C., Cornily, J. C., Hyafil, F., Rudd, J. H., Briley-Saebo, K. C., Mani, V. et al. (2008). Detection of neovessels in atherosclerotic plaques of rabbits using dynamic contrast enhanced MRI and 18F-FDG PET. *Arterioscler. Thromb. Vasc. Biol.*, *28*, 1311-1317.
- Casco, V. H., Veinot, J. P., Kuroski de Bold, M. L., Masters, R. G., Stevenson, M. M., & de Bold, A. J.

- (2002). Natriuretic peptide system gene expression in human coronary arteries. *J. Histochem. Cytochem.*, *50*, 799-809.
- Cauchon, N., Langlois, R., Rousseau, J. A., Tessier, G., Cadorette, J., Lecomte, R. et al. (2007). PET imaging of apoptosis with (64)Cu-labeled streptavidin following pretargeting of phosphatidylserine with biotinylated annexin-V. *Eur. J. Nucl. Med. Mol. Imaging*, *34*, 247-258.
- Curtiss, L. K. (2000). ApoE in atherosclerosis : a protein with multiple hats. *Arterioscler. Thromb. Vasc. Biol.*, *20*, 1852-1853.
- Davies, M. J., Richardson, P. D., Woolf, N., Katz, D. R., & Mann, J. (1993). Risk of Thrombosis in Human Atherosclerotic Plaques - Role of Extracellular Lipid, Macrophage, and Smooth-Muscle Cell Content. *Br. Heart J.*, *69*, 377-381.
- Davis, H. H., Heaton, W. A., Siegel, B. A., Mathias, C. J., Joist, J. H., Sherman, L. A. et al. (1978). Scintigraphic detection of atherosclerotic lesions and venous thrombi in man by indium-111-labelled autologous platelets. *Lancet*, *1*, 1185-1187.
- Decristoforo, C., Hernandez, G., I, Carlsen, J., Rupprich, M., Huisman, M., Virgolini, I. et al. (2008). (68)Ga- and (111)In-labelled DOTA-RGD peptides for imaging of alphavbeta3 integrin expression. *Eur. J. Nucl. Med. Mol. Imaging*, *35*, 1507-1515.
- Devedjian, J. C., George, M., Casellas, A., Pujol, A., Visa, J., Pelegrin, M. et al. (2000). Transgenic mice overexpressing insulin-like growth factor-II in beta cells develop type 2 diabetes. *J. Clin. Invest.*, *105*, 731-740.
- Dijkgraaf, I., Kruijtzter, J. A., Liu, S., Soede, A. C., Oyen, W. J., Corstens, F. H. et al. (2007). Improved targeting of the alpha(v)beta (3) integrin by multimerisation of RGD peptides. *Eur. J. Nucl. Med. Mol. Imaging*, *34*, 267-273.
- Dufourcq, P., Louis, H., Moreau, C., Daret, D., Boisseau, M. R., Lamaziere, J. M. D. et al. (1998). Vitronectin expression and interaction with receptors in smooth muscle cells from human atherosclerotic plaque. *Arterioscl. Thromb. Vasc. Biol.*, *18*, 168-176.
- Dumont, E. A., Hofstra, L., van Heerde, W. L., van den Eijnde, S., Doevendans, P. A., DeMuinck, E. et al. (2000). Cardiomyocyte death induced by myocardial ischemia and reperfusion: measurement with recombinant human annexin-V in a mouse model. *Circulation*, *102*, 1564-1568.
- Dunphy, M. P., Freiman, A., Larson, S. M., & Strauss, H. W. (2005). Association of vascular 18F-FDG uptake with vascular calcification. *J. Nucl. Med.*, *46*, 1278-1284.
- Elmaleh, D. R., Fischman, A. J., Tawakol, A., Zhu, A., Shoup, T. M., Hoffmann, U. et al. (2006). Detection of inflamed atherosclerotic lesions with diadenosine-5',5''-P-1,P-4-tetraphosphate (AP(4)A) and positron-emission tomography. *Proc. Natl. Acad. Sci. U.S.A.*, *103*, 15992-15996.
- Elmaleh, D. R., Narula, J., Babich, J. W., Petrov, A., Fischman, A. J., Khaw, B. A. et al. (1998). Rapid noninvasive detection of experimental atherosclerotic lesions with novel 99mTc-labeled diadenosine tetraphosphates. *Proc. Natl. Acad. Sci. U.S.A.*, *95*, 691-695.
- van Engeland M., Nieland, L. J., Ramaekers, F. C., Schutte, B., & Reutelingsperger, C. P. (1998). Annexin V-affinity assay: a review on an apoptosis detection system based on phosphatidylserine exposure. *Cytometry*, *31*, 1-9.
- Eskola, O., Gronroos, T. J., Forsback, S., Tuomela, J., Komar, G., Bergman, J. et al. (2012). Tracer Level Electrophilic Synthesis and Pharmacokinetics of the Hypoxia Tracer [(18)F]EF5. *Mol. Imaging Biol.*, *14*, 205-212.
- Fan, J. & Watanabe, T. (2003). Inflammatory reactions in the pathogenesis of atherosclerosis. *J. Atheroscler. Thromb.*, *10*, 63-71.
- Farese, R. V., Jr., Véniant, M. M., Cham, C. M., Flynn, L. M., Pierotti, V., Loring, J. F. et al. (1996). Phenotypic analysis of mice expressing exclusively apolipoprotein B48 or apolipoprotein B100. *Proc. Natl. Acad. Sci. U.S.A.*, *93*, 6393-6398.
- Folco, E. J., Sheikine, Y., Rocha, V. Z., Christen, T., Shvartz, E., Sukhova, G. K. et al. (2011). Hypoxia but not inflammation augments glucose uptake in human macrophages: Implications for imaging atherosclerosis with 18fluorine-labeled 2-deoxy-D-glucose positron emission tomography. *J. Am. Coll. Cardiol.*, *58*, 603-614.
- Fujimoto, S., Hartung, D., Ohshima, S., Edwards, D. S., Zhou, J., Yalamanchili, P. et al. (2008). Molecular imaging of matrix metalloproteinase in atherosclerotic lesions: resolution with dietary modification and statin therapy. *J. Am. Coll. Cardiol.*, *52*, 1847-1857.
- Fuster, V., Badimon, L., Badimon, J. J., & Chesebro, J. H. (1992). The pathogenesis of coronary artery disease and the acute coronary syndromes. *N. Engl. J. Med.*, *326*, 242-250.
- Gaertner, F. C., Kessler, H., Wester, H. J., Schwaiger, M., & Beer, A. J. (2012). Radiolabelled RGD peptides for imaging and therapy. *Eur. J. Nucl. Med. Mol. Imaging*.

- Gaemperli, O., Shalhoub, J., Owen, D.R., Lamare, F., Johansson, S., Fouladi, N., et al. (2011). Imaging intraplaque inflammation in carotid atherosclerosis with ¹¹C-PK11195 positron emission tomography/computed tomography. *Eur. Heart J.*, Sep 19.
- Gimbrone, M. A., Jr. (1999). Vascular endothelium, hemodynamic forces, and atherogenesis. *Am.J.Pathol.*, 155, 1-5.
- Goldstein J. L., Brown M. S. Scriver C. R., Beaudet A. L., Sly W. S., Valle D. (1989). Familial hypercholesterolemia. *The Metabolic Basis of Inherited Diseases*. In: New York: McGraw-Hill, 1215–1250.
- Green, M. A. & Welch, M. J. (1989). Gallium Radiopharmaceutical Chemistry. *Nucl. Med. Biology*, 16, 435-&.
- Haider, N., Hartung, D., Fujimoto, S., Petrov, A., Kolodgie, F. D., Virmani, R. et al. (2009). Dual molecular imaging for targeting metalloproteinase activity and apoptosis in atherosclerosis: molecular imaging facilitates understanding of pathogenesis. *J. Nucl. Cardiol.*, 16, 753-762.
- Hamacher, K., Coenen, H. H., & Stocklin, G. (1986). Efficient Stereospecific Synthesis of No-Carrier-Added 2-[F-18]-Fluoro-2-Deoxy-D-Glucose Using Aminopolyether Supported Nucleophilic-Substitution. *J. Nucl. Med.*, 27, 235-238.
- Hansson, G. K. (2009). Inflammatory mechanisms in atherosclerosis. *J. Thromb. Haemost.*, 7 Suppl 1, 328-331.
- Hansson, G. K. & Libby, P. (2006). The immune response in atherosclerosis: a double-edged sword. *Nat. Rev. Immunol.*, 6, 508-519.
- Hardoff, R., Braegelman, F., Zanzonico, P., Herrold, E. M., Lees, R. S., Lees, A. M. et al. (1993). External imaging of atherosclerosis in rabbits using an ¹²³I-labeled synthetic peptide fragment. *J. Clin. Pharmacol.*, 33, 1039-1047.
- Hardoff, R., Zanzonico, P., Braegelman, F., Herrold, E. M., Lees, R. S., Lees, A. M. et al. (1995). Localization of (99m)Tc-Labeled ApoB Synthetic Peptide in Arterial Lesions of an Experimental Model of Spontaneous Atherosclerosis. *Am. J. Ther.*, 2, 88-99.
- Hartung, D., Petrov, A., Haider, N., Fujimoto, S., Blankenberg, F., Fujimoto, A. et al. (2007). Radiolabeled Monocyte Chemotactic Protein 1 for the detection of inflammation in experimental atherosclerosis. *J. Nucl. Med.*, 48, 1816-1821.
- Hartung, D., Sarai, M., Petrov, A., Kolodgie, F., Narula, N., Verjans, J. et al. (2005). Resolution of apoptosis in atherosclerotic plaque by dietary modification and statin therapy. *J.Nucl.Med.*, 46, 2051-2056.
- Heinonen, S. E., Leppänen, P., Kholova, I., Lumivuori, H., Häkkinen, S. K., Bosch, F. et al. (2007). Increased atherosclerotic lesion calcification in a novel mouse model combining insulin resistance, hyperglycemia, and hypercholesterolemia. *Circ. Res.*, 101, 1058-1067.
- Hellings, W. E., Peeters, W., Moll, F. L., & Pasterkamp, G. (2007). From vulnerable plaque to vulnerable patient: the search for biomarkers of plaque destabilization. *Trends Cardiovasc. Med.*, 17, 162-171.
- Hnatowich, D. J. (1977). Review of Radiopharmaceutical Development with Short-Lived Generator-Produced Radionuclides Other Than Tc-99M. *Int. J. Appl. Radiat. Isot.*, 28, 169-181.
- Hoffer, P. (1980). Gallium - Mechanisms. *J. Nucl. Med.*, 21, 282-285.
- Hoppela, E., Kankaanpää, M., Parkkola, R., Ikonen, T., Roine, S., Raitakari, O. et al. (2007). Imaging of human inflammatory plaques using [(11C)]PK11195 and [18F]FDG [abstract]. *J. Nucl. Cardiol.*, 14:2.
- Hoshiga, M., Alpers, C. E., Smith, L. L., Giachelli, C. M., & Schwartz, S. M. (1995). Alpha-v beta-3 integrin expression in normal and atherosclerotic artery. *Circ. Res.*, 77, 1129-1135.
- Hulten, L. M. & Levin, M. (2009). The role of hypoxia in atherosclerosis. *Curr. Opin. Lipidol.*, 20, 409-414.
- Indrevoll, B., Kindberg, G. M., Solbakken, M., Bjurgert, E., Johansen, J. H., Karlsen, H. et al. (2006). NC-100717: A versatile RGD peptide scaffold for angiogenesis imaging. *Bioorg. Med. Chem. Letters*, 16, 6190-6193.
- Ishibashi, S., Brown, M. S., Goldstein, J. L., Gerard, R. D., Hammer, R. E., & Herz, J. (1993). Hypercholesterolemia in low density lipoprotein receptor knockout mice and its reversal by adenovirus-mediated gene delivery. *J. Clin. Invest.*, 92, 883-893.
- Ishibashi, S., Herz, J., Maeda, N., Goldstein, J. L., & Brown, M. S. (1994). The two-receptor model of lipoprotein clearance: tests of the hypothesis in “knockout” mice lacking the low density lipoprotein receptor, apolipoprotein E, or both proteins. *Proc. Natl. Acad. Sci. U.S.A.*, 91, 4431-4435.
- Ishino, S., Kuge, Y., Takai, N., Tamaki, N., Strauss, H. W., Blankenberg, F. G. et al. (2007). 99mTc-Annexin A5 for noninvasive characterization of atherosclerotic lesions: imaging and histological studies in myocardial infarction-prone Watanabe

- heritable hyperlipidemic rabbits. *Eur. J. Nucl. Med. Mol. Imaging*, *34*, 889-899.
- Ishino, S., Mukai, T., Kuge, Y., Kume, N., Ogawa, M., Takai, N. et al. (2008). Targeting of lectinlike oxidized low-density lipoprotein receptor 1 (LOX-1) with ^{99m}Tc-labeled anti-LOX-1 antibody: potential agent for imaging of vulnerable plaque. *J. Nucl. Med.*, *49*, 1677-1685.
- Isobe, S., Tsimikas, S., Zhou, J., Fujimoto, S., Sarai, M., Branks, M. J. et al. (2006). Noninvasive imaging of atherosclerotic lesions in apolipoprotein E-deficient and low-density-lipoprotein receptor-deficient mice with annexin A5. *J. Nucl. Med.*, *47*, 1497-1505.
- Iuliano, L., Signore, A., Vallabajosula, S., Colavita, A. R., Camastra, C., Ronga, G. et al. (1996). Preparation and biodistribution of ^{99m}technetium labeled oxidized LDL in man. *Atherosclerosis*, *126*, 131-141.
- Jaffer, F. A., Libby, P., & Weissleder, R. (2006a). Molecular and cellular imaging of atherosclerosis: emerging applications. *J. Am. Coll. Cardiol.*, *47*, 1328-1338.
- Jaffer, F. A., Nahrendorf, M., Sosnovik, D., Kelly, K. A., Aikawa, E., & Weissleder, R. (2006b). Cellular imaging of inflammation in atherosclerosis using magnetofluorescent nanomaterials. *Mol. Imaging*, *5*, 85-92.
- Jeong, J. M., Hong, M. K., Chang, Y. S., Lee, Y. S., Kim, Y. J., Cheon, G. J. et al. (2008). Preparation of a promising angiogenesis PET imaging agent: ⁶⁸Ga-labeled c(RGDyK)-isothiocyanatobenzyl-1,4,7-triazacyclononane-1,4,7-triacetic acid and feasibility studies in mice. *J. Nucl. Med.*, *49*, 830-836.
- Jeziorska, M. & Woolley, D. E. (1999). Local neovascularization and cellular composition within vulnerable regions of atherosclerotic plaques of human carotid arteries. *J. Pathol.*, *188*, 189-196.
- Johnson, L. L., Schofield, L., Donahay, T., Narula, N., & Narula, J. (2005). ^{99m}Tc-annexin V imaging for in vivo detection of atherosclerotic lesions in porcine coronary arteries. *J. Nucl. Med.*, *46*, 1186-1193.
- Jones, H. A., Valind, S. O., Clark, I. C., Bolden, G. E., Krausz, T., Schofield, J. B. et al. (2002). Kinetics of lung macrophages monitored in vivo following particulate challenge in rabbits. *Toxicol. Appl. Pharmacol.*, *183*, 46-54.
- Jurrus, E. R. & Weiss, H. S. (1977). In vitro tissue oxygen tensions in the rabbit aortic arch. *Atherosclerosis*, *28*, 223-232.
- Kane, J. P. (1983). Apolipoprotein B: structural and metabolic heterogeneity. *Annu. Rev. Physiol.*, *45*, 637-650.
- Kato, K., Schober, O., Ikeda, M., Schäfers, M., Ishigaki, T., Kies, P. et al. (2009). Evaluation and comparison of ¹¹C-choline uptake and calcification in aortic and common carotid arterial walls with combined PET/CT. *Eur. J. Nucl. Med. Mol. Imaging*, *36*, 1622-1628.
- Keen, H. G., Dekker, B. A., Disley, L., Hastings, D., Lyons, S., Reader, A. J. et al. (2005). Imaging apoptosis in vivo using ¹²⁴I-annexin V and PET. *Nucl. Med. Biol.*, *32*, 395-402.
- Kietselaer, B. L., Reutelingsperger, C. P., Heidendal, G. A., Daemen, M. J., Mess, W. H., Hofstra, L. et al. (2004). Noninvasive detection of plaque instability with use of radiolabeled annexin A5 in patients with carotid-artery atherosclerosis. *N. Engl. J. Med.*, *350*, 1472-1473.
- Kim, T. N., Kim, S., Yang, S. J., Yoo, H. J., Seo, J. A., Kim, S. G. et al. (2010). Vascular inflammation in patients with impaired glucose tolerance and type 2 diabetes: analysis with ¹⁸F-fluorodeoxyglucose positron emission tomography. *Circ. Cardiovasc. Imaging*, *3*, 142-148.
- Kinlay, S., Libby, P., & Ganz, P. (2001). Endothelial function and coronary artery disease. *Curr. Opin. Lipidol.*, *12*, 383-389.
- Kircher, M. F., Grimm, J., Swirski, F. K., Libby, P., Gerszten, R. E., Allport, J. R. et al. (2008). Noninvasive in vivo imaging of monocyte trafficking to atherosclerotic lesions. *Circulation*, *117*, 388-395.
- Koch, C. J., Hahn, S. M., Rockwell, K., Covey, J. M., McKenna, W. G., & Evans, S. M. (2001). Pharmacokinetics of EF5 [2-(2-nitro-1-H-imidazol-1-yl)-N-(2,2,3,3,3-pentafluoropropyl) acetamide] in human patients: implications for hypoxia measurements in vivo by 2-nitroimidazoles. *Cancer Chemother. Pharmacol.*, *48*, 177-187.
- Kolodgie, F. D., Petrov, A., Virmani, R., Narula, N., Verjans, J. W., Weber, D. K. et al. (2003). Targeting of apoptotic macrophages and experimental atheroma with radiolabeled annexin V: a technique with potential for noninvasive imaging of vulnerable plaque. *Circulation*, *108*, 3134-3139.
- Koopman, G., Reutelingsperger, C. P., Kuijten, G. A., Keehnen, R. M., Pals, S. T., & van Oers, M. H. (1994). Annexin V for flow cytometric detection of phosphatidylserine expression on B cells undergoing apoptosis. *Blood*, *84*, 1415-1420.
- Krieger, M. & Herz, J. (1994). Structures and functions of multiligand lipoprotein receptors: macrophage

- scavenger receptors and LDL receptor-related protein (LRP). *Annu. Rev. Biochem.*, 63, 601-637.
- Kuge, Y., Takai, N., Ogawa, Y., Temma, T., Zhao, Y., Nishigori, K. et al. (2010). Imaging with radiolabelled anti-membrane type 1 matrix metalloproteinase (MT1-MMP) antibody: potentials for characterizing atherosclerotic plaques. *Eur. J. Nucl. Med. Mol. Imaging*, 37, 2093-2104.
- Laitinen, I., Marjamäki, P., Haaparanta, M., Nagren, K., Laine, J., Leppänen, P. et al. (2008). Uptake of [C-11]PK11195, a marker of inflammatory cells, into atherosclerotic plaques in mice. *Basic Clin. Pharmacol. Toxicol.*, 102, 48-49.
- Laitinen, I., Marjamäki, P., Haaparanta, M., Savisto, N., Laine, V. J., Soini, S. L. et al. (2006). Non-specific binding of [(18F)FDG to calcifications in atherosclerotic plaques: experimental study of mouse and human arteries. *Eur. J. Nucl. Med. Mol. Imaging*, 33, 1461-1467.
- Laitinen, I., Saraste, A., Weidl, E., Poethko, T., Weber, A. W., Nekolla, S. G. et al. (2009). Evaluation of alpha(v)beta(3) Integrin-Targeted Positron Emission Tomography Tracer F-18-Galacto-RGD for Imaging of Vascular Inflammation in Atherosclerotic Mice. *Circ. Cardiovasc. Imaging*, 2, 331-338.
- Laitinen, I. E. K., Luoto, P., Nagren, K., Marjamäki, P. M., Silvola, J. M. U., Hellberg, S. et al. (2010). Uptake of C-11-Choline in Mouse Atherosclerotic Plaques. *J. Nucl. Med.*, 51, 798-802.
- Langer, H. F., Haubner, R., Pichler, B. J., & Gawaz, M. (2008). Radionuclide imaging - A molecular key to the atherosclerotic plaque. *J. Am. Coll. Cardiol.*, 52, 1-12.
- Lankinen E, Saraste A, Nojonen T, Klen R, Teräs M, Kokko T, Kajander S, Pietilä M, Ukkonen J, Knuuti J. (2011) Coronary plaque imaging in patients with unstable angina pectoris using dual gated [18F]-FDG PET/CT. [abstract] *Eur. Heart J. Supp.* 13 (A), A2.
- Laufer, E. M., Winkens, H. M., Corsten, M. F., Reutelingsperger, C. P., Narula, J., & Hofstra, L. (2009). PET and SPECT imaging of apoptosis in vulnerable atherosclerotic plaques with radiolabeled Annexin A5. *Q. J. Nucl. Med. Mol. Imaging*, 53, 26-34.
- Laughlin, K. M., Evans, S. M., Jenkins, W. T., Tracy, M., Chan, C. Y., Lord, E. M. et al. (1996). Biodistribution of the nitroimidazole EF5 (2-[2-nitro-1H-imidazol-1-yl]-N-(2,2,3,3,3-pentafluoropropyl) acetamide) in mice bearing subcutaneous EMT6 tumors. *J. Pharmacol. Exp. Therapeut.*, 277, 1049-1057.
- Laurberg, J. M., Olsen, A. K., Hansen, S. B., Bottcher, M., Morrison, M., Ricketts, S. A. et al. (2007). Imaging of vulnerable atherosclerotic plaques with FDG-microPET: no FDG accumulation. *Atherosclerosis*, 192, 275-282.
- Lees, A. M., Lees, R. S., Schoen, F. J., Isaacsohn, J. L., Fischman, A. J., McKusick, K. A. et al. (1988). Imaging human atherosclerosis with 99mTc-labeled low density lipoproteins. *Arteriosclerosis*, 8, 461-470.
- Lees, R. S., Lees, A. M., & Strauss, H. W. (1983). External imaging of human atherosclerosis. *J. Nucl. Med.*, 24, 154-156.
- Ley, K. & Huo, Y. (2001). VCAM-1 is critical in atherosclerosis. *J. Clin. Invest*, 107, 1209-1210.
- Li, D., Patel, A. R., Klibanov, A. L., Kramer, C. M., Ruiz, M., Kang, B. Y. et al. (2010). Molecular imaging of atherosclerotic plaques targeted to oxidized LDL receptor LOX-1 by SPECT/CT and magnetic resonance. *Circ. Cardiovasc. Imaging*, 3, 464-472.
- Li, H., Cybulsky, M. I., Gimbrone, M. A., Jr., & Libby, P. (1993). An atherogenic diet rapidly induces VCAM-1, a cytokine-regulatable mononuclear leukocyte adhesion molecule, in rabbit aortic endothelium. *Arterioscler. Thromb.*, 13, 197-204.
- Li, Z. B., Cai, W., Cao, Q., Chen, K., Wu, Z., He, L. et al. (2007). (64)Cu-labeled tetrameric and octameric RGD peptides for small-animal PET of tumor alpha(v)beta(3) integrin expression. *J. Nucl. Med.*, 48, 1162-1171.
- Li, Z. B., Chen, K., & Chen, X. (2008). (68)Ga-labeled multimeric RGD peptides for microPET imaging of integrin alpha(v)beta(3) expression. *Eur. J. Nucl. Med. Mol. Imaging*, 35, 1100-1108.
- Libby, P. (2002). Inflammation in atherosclerosis. *Nature*, 420, 868-874.
- Libby, P. & Theroux, P. (2005). Pathophysiology of coronary artery disease. *Circulation*, 111, 3481-3488.
- Liu, Y., Abendschein, D., Woodard, G. E., Rossin, R., McCommis, K., Zheng, J. et al. (2010). Molecular imaging of atherosclerotic plaque with (64)Cu-labeled natriuretic peptide and PET. *J. Nucl. Med.*, 51, 85-91.
- Lusis, A. J. (2000). Atherosclerosis. *Nature*, 407, 233-241.
- Madjid, M., Zarrabi, A., Litovsky, S., Willerson, J. T., & Casscells, W. (2004). Finding vulnerable atherosclerotic plaques: is it worth the effort? *Arterioscler. Thromb. Vasc. Biol.*, 24, 1775-1782.
- Masteling, M. G., Zeebregts, C. J., Tio, R. A., Breek, J. C., Tietge, U. J., de Boer, J. F. et al. (2011).

- High-resolution imaging of human atherosclerotic carotid plaques with micro 18F-FDG PET scanning exploring plaque vulnerability. *J. Nucl. Cardiol.*, *18*, 1066-1075.
- Matter, C. M., Wyss, M. T., Meier, P., Spaeth, N., von Lukowicz, T., Weber, B. et al. (2005). F-18-choline images macrophages in atherosclerotic plaques. *Circulation*, *112*, U826.
- Matteson, E. L., Lowe, V. J., Prendergast, F. G., Crowson, C. S., Moder, K. G., Morgenstern, D. E. et al. (2009). Assessment of disease activity in rheumatoid arthritis using a novel folate targeted radiopharmaceutical FolateScan. *Clin. Exp. Rheumatol.*, *27*, 253-259.
- Menezes, L. J., Kotze, C. W., Agu, O., Richards, T., Brookes, J., Goh, V. J. et al. (2011). Investigating vulnerable atheroma using combined (18)F-FDG PET/CT angiography of carotid plaque with immunohistochemical validation. *J. Nucl. Med.*, *52*, 1698-1703.
- Minar, E., Ehringer, H., Dudczak, R., Schofl, R., Jung, M., Koppensteiner, R. et al. (1989). Indium-111-labeled platelet scintigraphy in carotid atherosclerosis. *Stroke*, *20*, 27-33.
- Moore K. J., & Tabas I. (2011). Macrophages in the pathogenesis of atherosclerosis. *Cell*, *145*, 341-355.
- Moriwaki, H., Matsumoto, M., Handa, N., Isaka, Y., Hashikawa, K., Oku, N. et al. (1995). Functional and anatomic evaluation of carotid atherothrombosis. A combined study of indium 111 platelet scintigraphy and B-mode ultrasonography. *Arterioscler. Thromb. Vasc. Biol.*, *15*, 2234-2240.
- Moulton, K. S., Vakili, K., Zurakowski, D., Soliman, M., Butterfield, C., Sylvain, E. et al. (2003). Inhibition of plaque neovascularization reduces macrophage accumulation and progression of advanced atherosclerosis. *Proc. Natl. Acad. Sci. U.S.A.*, *100*, 4736-4741.
- Murakami, Y., Takamatsu, H., Taki, J., Tatsumi, M., Noda, A., Ichise, R. et al. (2004). 18F-labelled annexin V: a PET tracer for apoptosis imaging. *Eur. J. Nucl. Med. Mol. Imaging*, *31*, 469-474.
- Murdoch, C., Muthana, M., & Lewis, C. E. (2005). Hypoxia regulates macrophage functions in inflammation. *J. Immunol.*, *175*, 6257-6263.
- Mäkinen, T. J., Lankinen, P., Pöyhönen, T., Jalava, J., Aro, H. T., & Roivainen, A. (2005). Comparison of F-18-FDG and Ga-68 PET imaging in the assessment of experimental osteomyelitis due to *Staphylococcus aureus*. *Eur. J. Nucl. Med. Mol. Imaging*, *32*, 1259-1268.
- Nahrendorf, M., Keliher, E., Marinelli, B., Leuschner, F., Robbins, C. S., Gerszten, R. E. et al. (2011). Detection of macrophages in aortic aneurysms by nanoparticle positron emission tomography-computed tomography. *Arterioscler. Thromb. Vasc. Biol.*, *31*, 750-757.
- Nahrendorf, M., Keliher, E., Panizzi, P., Zhang, H., Hembrador, S., Figueiredo, J. L. et al. (2009). 18F-4V for PET-CT imaging of VCAM-1 expression in atherosclerosis. *J. Am. Coll. Cardiol. Cardiovasc. Imaging*, *2*, 1213-1222.
- Nahrendorf, M., Zhang, H., Hembrador, S., Panizzi, P., Sosnovik, D. E., Aikawa, E. et al. (2008). Nanoparticle PET-CT imaging of macrophages in inflammatory atherosclerosis. *Circulation*, *117*, 379-387.
- Nakashima, Y., Plump, A. S., Raines, E. W., Breslow, J. L., & Ross, R. (1994). ApoE-deficient mice develop lesions of all phases of atherosclerosis throughout the arterial tree. *Arterioscler. Thromb.*, *14*, 133-140.
- Narula, J., Garg, P., Achenbach, S., Motoyama, S., Virmani, R., & Strauss, H. W. (2008). Arithmetic of vulnerable plaques for noninvasive imaging. *Nat. Clin. Prac. Cardiovasc. Med.*, *5*, S2-S10.
- Ogawa, M., Ishino, S., Mukai, T., Asano, D., Teramoto, N., Watabe, H. et al. (2004). (18) F-FDG accumulation in atherosclerotic plaques: immunohistochemical and PET imaging study. *J. Nucl. Med.*, *45*, 1245-1250.
- Ogawa, M., Nakamura, S., Saito, Y., Kosugi, M., & Magata, Y. (2012). What can be seen by 18F-FDG PET in atherosclerosis imaging? The effect of foam cell formation on 18F-FDG uptake to macrophages in vitro. *J. Nucl. Med.*, *53*, 55-58.
- Ohshima, S., Petrov, A., Fujimoto, S., Zhou, J., Azure, M., Edwards, D. S. et al. (2009). Molecular imaging of matrix metalloproteinase expression in atherosclerotic plaques of mice deficient in apolipoprotein e or low-density-lipoprotein receptor. *J. Nucl. Med.*, *50*, 612-617.
- Ohtsuki, K., Hayase, M., Akashi, K., Kapiwoda, S., & Strauss, H. W. (2001). Detection of monocyte chemoattractant protein-1 receptor expression in experimental atherosclerotic lesions: an autoradiographic study. *Circulation*, *104*, 203-208.
- Opalinska, M., Stompor, T., Pach, D., Mikolajczak, R., Fedak, D., Krzanowski, M. et al. (2012). Imaging of inflamed carotid artery atherosclerotic plaques with the use of (99m)Tc-HYNIC-IL-2 scintigraphy in end-stage renal disease patients. *Eur. J. Nucl. Med. Mol. Imaging*, *39*, 673-682.
- Oyen, W. J. G., Boerman, O. C., van der Laken, C. J., Claessens, R. A. M. J., van der Meer, J. W. M., &

- Corstens, F. H. M. (1996). The uptake mechanisms of inflammation- and infection-localizing agents. *Eur. J. Nucl. Med.*, *23*, 459-465.
- Packard, R. R., Maganto-Garcia, E., Gotsman, I., Tabas, I., Libby, P., & Lichtman, A. H. (2008). CD11c(+) dendritic cells maintain antigen processing, presentation capabilities, and CD4(+) T-cell priming efficacy under hypercholesterolemic conditions associated with atherosclerosis. *Circ. Res.*, *103*, 965-973.
- Parathath, S., Mick, S. L., Feig, J. E., Joaquin, V., Grauer, L., Habel, D. M. et al. (2011). Hypoxia is present in murine atherosclerotic plaques and has multiple adverse effects on macrophage lipid metabolism. *Circ. Res.*, *109*, 1141-1152.
- Paulhe, F., Racaud-Sultan, C., Ragab, A., Albiges-Rizo, C., Chap, H., Iberg, N. et al. (2001). Differential regulation of phosphoinositide metabolism by alpha(V)beta(3) and alpha(V)beta(5) integrins upon smooth muscle cell migration. *J. Biol. Chem.*, *276*, 41832-41840.
- Piedrahita, J. A., Zhang, S. H., Hagaman, J. R., Oliver, P. M., & Maeda, N. (1992). Generation of mice carrying a mutant apolipoprotein E gene inactivated by gene targeting in embryonic stem cells. *Proc. Natl. Acad. Sci. U.S.A.*, *89*, 4471-4475.
- Plump, A. S., Smith, J. D., Hayek, T., Aalto-Setälä, K., Walsh, A., Verstuyft, J. G. et al. (1992). Severe hypercholesterolemia and atherosclerosis in apolipoprotein E-deficient mice created by homologous recombination in ES cells. *Cell*, *71*, 343-353.
- Powell-Braxton, L., Véniant, M., Latvala, R. D., Hirano, K. I., Won, W. B., Ross, J. et al. (1998). A mouse model of human familial hypercholesterolemia: markedly elevated low density lipoprotein cholesterol levels and severe atherosclerosis on a low-fat chow diet. *Nat. Med.*, *4*, 934-938.
- Pugliese, F., Gaemperli, O., Kinderlerer, A.R., Lamare, F., Shalhoub, J., Davies, A.H., et al. (2010). Imaging of vascular inflammation with [11C]-PK11195 and positron emission tomography/computed tomography angiography. *J. Am. Coll. Cardiol.*, *17*, 653-661.
- Purcell-Huynh, D. A., Farese, R. V., Jr., Johnson, D. F., Flynn, L. M., Pierotti, V., Newland, D. L. et al. (1995). Transgenic mice expressing high levels of human apolipoprotein B develop severe atherosclerotic lesions in response to a high-fat diet. *J. Clin. Invest*, *95*, 2246-2257.
- Qin, G., Zhang, Y., Cao, W., An, R., Gao, Z., Li, G. et al. (2005). Molecular imaging of atherosclerotic plaques with technetium-99m-labelled antisense oligonucleotides. *Eur. J. Nucl. Med. Mol. Imaging*, *32*, 6-14.
- Razavian, M., Tavakoli, S., Zhang, J., Nie, L., Dobrucki, L. W., Sinusas, A. J. et al. (2011). Atherosclerosis plaque heterogeneity and response to therapy detected by in vivo molecular imaging of matrix metalloproteinase activation. *J. Nucl. Med.*, *52*, 1795-1802.
- Reddick, R. L., Zhang, S. H., & Maeda, N. (1994). Atherosclerosis in mice lacking apo E. Evaluation of lesional development and progression. *Arterioscler. Thromb.*, *14*, 141-147.
- Roger, V. L., Go, A. S., Lloyd-Jones, D. M., Benjamin, E. J., Berry, J. D., Borden, W. B. et al. (2012). Heart disease and stroke statistics--2012 update: a report from the american heart association. *Circulation*, *125*, e2-e220.
- Roivainen, A. & Yli-Kerttula, T. (2006). Whole-body distribution of (11)C-choline and uptake in knee synovitis. *Eur. J. Nucl. Med. Mol. Imaging*, *33*, 1372-1373.
- Rominger, A., Saam, T., Vogl, E., Ubleis, C., la, F. C., Forster, S. et al. (2010). In vivo imaging of macrophage activity in the coronary arteries using 68Ga-DOTATATE PET/CT: correlation with coronary calcium burden and risk factors. *J. Nucl. Med.*, *51*, 193-197.
- Rosen, J. M., Butler, S. P., Meinken, G. E., Wang, T. S., Ramakrishnan, R., Srivastava, S. C. et al. (1990). Indium-111-labeled LDL: a potential agent for imaging atherosclerotic disease and lipoprotein biodistribution. *J. Nucl. Med.*, *31*, 343-350.
- Rosenfeld, M. E., Polinsky, P., Virmani, R., Kauser, K., Rubanyi, G., & Schwartz, S. M. (2000). Advanced atherosclerotic lesions in the innominate artery of the ApoE knockout mouse. *Arterioscler. Thromb. Vasc. Biol.*, *20*, 2587-2592.
- Rudd, J. H., Myers, K. S., Bansilal, S., Machac, J., Woodward, M., Fuster, V. et al. (2009). Relationships among regional arterial inflammation, calcification, risk factors, and biomarkers: a prospective fluorodeoxyglucose positron-emission tomography/computed tomography imaging study. *Circ. Cardiovasc. Imaging*, *2*, 107-115.
- Rudd, J. H., Warburton, E. A., Fryer, T. D., Jones, H. A., Clark, J. C., Antoun, N. et al. (2002). Imaging atherosclerotic plaque inflammation with [18F]-fluorodeoxyglucose positron emission tomography. *Circulation*, *105*, 2708-2711.
- Ruehm, S. G., Corot, C., Vogt, P., Kolb, S., & Debatin, J. F. (2001). Magnetic resonance imaging of atherosclerotic plaque with ultrasmall

- superparamagnetic particles of iron oxide in hyperlipidemic rabbits. *Circulation*, 103, 415-422.
- Sadeghi, M. M., Krassilnikova, S., Zhang, J., Gharaei, A. A., Fassaei, H. R., Esmailzadeh, L. et al. (2004). Detection of injury-induced vascular remodeling by targeting activated alphavbeta3 integrin in vivo. *Circulation*, 110, 84-90.
- Saha, P., Modarai, B., Humphries, J., Mattock, K., Waltham, M., Burnand, K. G. et al. (2009). The monocyte/macrophage as a therapeutic target in atherosclerosis. *Curr. Opin. Pharmacol.*, 9, 109-118.
- Sarai, M., Hartung, D., Petrov, A., Zhou, J., Narula, N., Hofstra, L. et al. (2007). Broad and specific caspase inhibitor-induced acute repression of apoptosis in atherosclerotic lesions evaluated by radiolabeled annexin A5 imaging. *J. Am. Coll. Cardiol.*, 50, 2305-2312.
- Saraste, A., Nekolla, S. G., & Schwaiger, M. (2009). Cardiovascular molecular imaging: an overview. *Cardiovasc. Res.*, 83, 643-652.
- Sawamura, T., Kume, N., Aoyama, T., Moriwaki, H., Hoshikawa, H., Aiba, Y. et al. (1997). An endothelial receptor for oxidized low-density lipoprotein. *Nature*, 386, 73-77.
- Schäfers, M., Riemann, B., Kopka, K., Breyholz, H. J., Wagner, S., Schäfers, K. P. et al. (2004). Scintigraphic imaging of matrix metalloproteinase activity in the arterial wall in vivo. *Circulation*, 109, 2554-2559.
- Schäfers, M., Schober, O., & Hermann, S. (2010). Matrix-metalloproteinases as imaging targets for inflammatory activity in atherosclerotic plaques. *J. Nucl. Med.*, 51, 663-666.
- Schmitz, S. A., Coupland, S. E., Gust, R., Winterhalter, S., Wagner, S., Kresse, M. et al. (2000). Superparamagnetic iron oxide-enhanced MRI of atherosclerotic plaques in Watanabe hereditary hyperlipidemic rabbits. *Invest. Radiol.*, 35, 460-471.
- Shaw, P. X., Hörkkö, S., Tsimikas, S., Chang, M. K., Palinski, W., Silverman, G. J. et al. (2001a). Human-derived anti-oxidized LDL autoantibody blocks uptake of oxidized LDL by macrophages and localizes to atherosclerotic lesions in vivo. *Arterioscler. Thromb. Vasc. Biol.*, 21, 1333-1339.
- Shaw, S. K., Perkins, B. N., Lim, Y. C., Liu, Y., Nusrat, A., Schnell, F. J. et al. (2001b). Reduced expression of junctional adhesion molecule and platelet/endothelial cell adhesion molecule-1 (CD31) at human vascular endothelial junctions by cytokines tumor necrosis factor-alpha plus interferon-gamma. Does not reduce leukocyte transmigration under flow. *Am. J. Pathol.*, 159, 2281-2291.
- Sheikine, Y. & Akram, K. (2010). FDG-PET imaging of atherosclerosis: Do we know what we see? *Atherosclerosis*, 211, 371-380.
- Sluimer, J. C. & Daemen, M. J. (2009). Novel concepts in atherogenesis: angiogenesis and hypoxia in atherosclerosis. *J. Pathol.*, 218, 7-29.
- Sluimer, J. C., Gasc, J. M., van Wanroij, J. L., Kisters, N., Groeneweg, M., Gelpke, M. D. S. et al. (2008). Hypoxia, hypoxia-inducible transcription factor, and macrophages in human atherosclerotic plaques are correlated with intraplaque angiogenesis. *J. Am. Coll. Cardiol.*, 51, 1258-1265.
- Stary, H. C. (2000). Lipid and macrophage accumulations in arteries of children and the development of atherosclerosis. *Am. J. Clin. Nutr.*, 72, 1297S-1306S.
- Stefanadis, C., Toutouzas, K., Tsiamis, E., Pitsavos, C., Papadimitriou, L., & Toutouzas, P. (2001). Identification and stabilization of vulnerable atherosclerotic plaques: the role of coronary thermography and external heat delivery. *Indian Heart J.*, 53, 104-109.
- Sun, J., Sukhova, G. K., Wolters, P. J., Yang, M., Kitamoto, S., Libby, P. et al. (2007). Mast cells promote atherosclerosis by releasing proinflammatory cytokines. *Nat. Med.*, 13, 719-724.
- Tannock, L. R. & King, V. L. (2010). Animal models of atherosclerosis: more than mice. *Atherosclerosis*, 212, 32-33.
- Tatsumi, M., Cohade, C., Nakamoto, Y., & Wahl, R. L. (2003). Fluorodeoxyglucose uptake in the aortic wall at PET/CT: possible finding for active atherosclerosis. *Radiology*, 229, 831-837.
- Tawakol, A., Migrino, R. Q., Bashian, G. G., Bedri, S., Vermynen, D., Cury, R. C. et al. (2006). In vivo F-18-fluorodeoxyglucose positron emission tomography imaging provides a noninvasive measure of carotid plaque inflammation in patients. *J. Am. Coll. Cardiol.*, 48, 1818-1824.
- Tawakol, A., Migrino, R. Q., Hoffmann, U., Abbara, S., Houser, S., Gewirtz, H. et al. (2005). Noninvasive in vivo measurement of vascular inflammation with F-18 fluorodeoxyglucose positron emission tomography. *J. Nucl. Cardiol.*, 12, 294-301.
- Tekabe, Y., Li, Q., Luma, J., Weisenberger, D., Sedlar, M., Harja, E. et al. (2010). Noninvasive monitoring the biology of atherosclerotic plaque development with radiolabeled annexin V and matrix metalloproteinase inhibitor in spontaneous

- atherosclerotic mice. *J. Nucl. Cardiol.*, 17, 1073-1081.
- Tekabe, Y., Li, Q., Rosario, R., Sedlar, M., Majewski, S., Hudson, B. I. et al. (2008). Development of receptor for advanced glycation end products-directed imaging of atherosclerotic plaque in a murine model of spontaneous atherosclerosis. *Circ. Cardiovasc. Imaging*, 1, 212-219.
- Teräs M, Kokki T, Durand-Schaefer N, Noponen T, Pietilä M, Kiss J, Hoppela E, Sipilä H.T, Knuuti J. (2010) Dual-gated cardiac PET-clinical feasibility study. *Eur. J. Nucl. Med. Mol. Imaging.*, 37(3):505-516.
- Toretzky, J., Levenson, A., Weinberg, I. N., Tait, J. F., Uren, A., & Mease, R. C. (2004). Preparation of F-18 labeled annexin V: a potential PET radiopharmaceutical for imaging cell death. *Nucl. Med. Biol.*, 31, 747-752.
- Torzewski, M., Shaw, P. X., Han, K. R., Shortal, B., Lackner, K. J., Witztum, J. L. et al. (2004). Reduced in vivo aortic uptake of radiolabeled oxidation-specific antibodies reflects changes in plaque composition consistent with plaque stabilization. *Arterioscler. Thromb. Vasc. Biol.*, 24, 2307-2312.
- Tsimikas, S., Palinski, W., Halpern, S. E., Yeung, D. W., Curtiss, L. K., & Witztum, J. L. (1999). Radiolabeled MDA2, an oxidation-specific, monoclonal antibody, identifies native atherosclerotic lesions in vivo. *J. Nucl. Cardiol.*, 6, 41-53.
- Tsimikas, S., Shortal, B. P., Witztum, J. L., & Palinski, W. (2000). In vivo uptake of radiolabeled MDA2, an oxidation-specific monoclonal antibody, provides an accurate measure of atherosclerotic lesions rich in oxidized LDL and is highly sensitive to their regression. *Arterioscler. Thromb. Vasc. Biol.*, 20, 689-697.
- Turk, M. J., Breur, G. J., Widmer, W. R., Paulos, C. M., Xu, L. C., Grote, L. A. et al. (2002). Folate-targeted imaging of activated macrophages in rats with adjuvant-induced arthritis. *Arthritis Rheum.*, 46, 1947-1955.
- Ujula, T., Salomäki, S., Autio, A., Luoto, P., Tolvanen, T., Lehtikoinen, P. et al. (2010). Ga-68-Chloride PET Reveals Human Pancreatic Adenocarcinoma Xenografts in Rats-Comparison with FDG. *Mol. Imaging Biol.*, 12, 259-268.
- Véniant, M. M., Zlot, C. H., Walzem, R. L., Pierotti, V., Driscoll, R., Dichek, D. et al. (1998). Lipoprotein clearance mechanisms in LDL receptor-deficient "Apo-B48-only" and "Apo-B100-only" mice. *J. Clin. Invest.*, 102, 1559-1568.
- Virmani, R. (2007). Pathology of vulnerable plaque. *Int. J. Cardiol.*, 122, 8.
- Virmani, R., Kolodgie, F. D., Burke, A. P., Farb, A., & Schwartz, S. M. (2000). Lessons from sudden coronary death: a comprehensive morphological classification scheme for atherosclerotic lesions. *Arterioscler. Thromb. Vasc. Biol.*, 20, 1262-1275.
- Virmani, R., Kolodgie, F. D., Burke, A. P., Finn, A. V., Gold, H. K., Tulenko, T. N. et al. (2005). Atherosclerotic plaque progression and vulnerability to rupture: angiogenesis as a source of intraplaque hemorrhage. *Arterioscler. Thromb. Vasc. Biol.*, 25, 2054-2061.
- Waldeck, J., Häger, F., Hölte, C., Lanckohr, C., von Wallbrunn A., Torsello, G. et al. (2008). Fluorescence reflectance imaging of macrophage-rich atherosclerotic plaques using an alphavbeta3 integrin-targeted fluorochrome. *J. Nucl. Med.*, 49, 1845-1851.
- Williams, G. & Kolodny, G. M. (2008). Suppression of myocardial 18F-FDG uptake by preparing patients with a high-fat, low-carbohydrate diet. *AJR Am. J. Roentgenol.*, 190, W151-W156.
- Williams, G. & Kolodny, G. M. (2009). Retrospective study of coronary uptake of 18F-fluorodeoxyglucose in association with calcification and coronary artery disease: a preliminary study. *Nucl. Med. Commun.*, 30, 287-291.
- Williams, K. J. & Tabas, I. (1998). The response-to-retention hypothesis of atherogenesis reinforced. *Curr. Opin. Lipidol.*, 9, 471-474.
- Wilson, H. M., Barker, R. N., & Erwig, L. P. (2009). Macrophages: Promising Targets for the Treatment of Atherosclerosis. *Curr. Vasc. Pharmacol.*, 7, 234-243.
- Winter, P. M., Caruthers, S. D., Allen, J. S., Cai, K., Williams, T. A., Lanza, G. M. et al. (2010). Molecular imaging of angiogenic therapy in peripheral vascular disease with alphanubeta3-integrin-targeted nanoparticles. *Magn. Reson. Med.*, 64, 369-376.
- Worthley, S. G., Zhang, Z. Y., Machac, J., Helft, G., Tang, C., Liew, G. Y. et al. (2009). In vivo non-invasive serial monitoring of FDG-PET progression and regression in a rabbit model of atherosclerosis. *Int. J. Cardiovasc. Imaging*, 25, 251-257.
- Wykrzykowska, J., Lehman, S., Williams, G., Parker, J. A., Palmer, M. R., Varkey, S. et al. (2009). Imaging of Inflamed and Vulnerable Plaque in Coronary Arteries with F-18-FDG PET/CT in Patients with Suppression of Myocardial Uptake Using a Low-Carbohydrate, High-Fat Preparation. *J. Nucl. Med.*, 50, 563-568.
- Xia, W., Hilgenbrink, A. R., Matteson, E. L., Lockwood, M. B., Cheng, J. X., & Low, P. S.

- (2009). A functional folate receptor is induced during macrophage activation and can be used to target drugs to activated macrophages. *Blood*, *113*, 438-446.
- Young, S. G. (1990). Recent progress in understanding apolipoprotein B. *Circulation*, *82*, 1574-1594.
- Zemplenyi, T., Crawford, D. W., & Cole, M. A. (1989). Adaptation to Arterial-Wall Hypoxia Demonstrated In vivo with Oxygen Microcathodes. *Atherosclerosis*, *76*, 173-179.
- Zhang, Z., Machac, J., Helft, G., Worthley, S. G., Tang, C., Zaman, A. G. et al. (2006). Non-invasive imaging of atherosclerotic plaque macrophage in a rabbit model with F-18 FDG PET: a histopathological correlation. *BMC. Nucl. Med.*, *6*, 3.
- Zhao, Y., Kuge, Y., Zhao, S., Morita, K., Inubushi, M., Strauss, H. W. et al. (2007). Comparison of ^{99m}Tc-annexin A5 with ¹⁸F-FDG for the detection of atherosclerosis in ApoE^{-/-} mice. *Eur. J. Nucl. Med. Mol. Imaging*, *34*, 1747-1755.
- Zhao, Y., Zhao, S., Kuge, Y., Strauss, W. H., Blankenberg, F. G., & Tamaki, N. (2011). Localization of deoxyglucose and annexin A5 in experimental atheroma correlates with macrophage infiltration but not lipid deposition in the lesion. *Mol. Imaging Biol.*, *13*, 712-720.
- Ziemer, L. S., Evans, S. M., Kachur, A., Shuman, A. L., Cardi, C. A., Jenkins, W. T. et al. (2003). Noninvasive imaging of tumor hypoxia in rats using the 2-nitroimidazole F-18-EF5. *Eur. J. Nucl. Med. Mol. Imaging*, *30*, 259-266.